SANDIA REPORT
SAND2012-0519
Unlimited Release
Printed January 2012

Understanding and Predicting Metallic Whisker Growth and its Effects on Reliability: LDRD Final Report

Donald F. Susan, Joseph R. Michael, W. Graham Yelton, Bonnie B. McKenzie, Richard P. Grant, Jamin Pillars, and Mark A. Rodriguez

Prepared by
Sandia National Laboratories
Albuquerque, New Mexico 87185 and Livermore, California 94550

Sandia National Laboratories is a multi-program laboratory managed and operated by Sandia Corporation, a wholly owned subsidiary of Lockheed Martin Corporation, for the U.S. Department of Energy's National Nuclear Security Administration under contract DE-AC04-94AL85000.

Issued by Sandia National Laboratories, operated for the United States Department of Energy by Sandia Corporation.

Available to DOE and DOE contractors from
U.S. Department of Energy
Office of Scientific and Technical Information
P.O. Box 62
Oak Ridge, TN 37831

Telephone: (865) 576-8401
Facsimile: (865) 576-5728
E-Mail: reports@adonis.osti.gov
Online ordering: http://www.osti.gov/bridge

Available to the public from
U.S. Department of Commerce
National Technical Information Service
5285 Port Royal Rd.
Springfield, VA 22161

Telephone: (800) 553-6847
Facsimile: (703) 605-6900
E-Mail: orders@ntis.fedworld.gov
Online order: http://www.ntis.gov/help/ordermethods.asp?loc=7-4-0#online

SAND2012-0519
Unlimited Release
Printed January 2012

Understanding and Predicting Metallic Whisker Growth and its Effects on Reliability: LDRD Final Report

Donald F. Susan, Multiscale Metallurgical Science and Technology Dept.
Joseph R. Michael, Bonnie B. McKenzie, Richard P. Grant, and Mark A. Rodriguez
Materials Characterization Dept.
W. Graham Yelton and Jamin Pillars, Photonic Microsystems Technology Dept.
Sandia National Laboratories
P.O. Box 5800, Albuquerque, NM 87185-0886

Abstract

Tin (Sn) whiskers are conductive Sn filaments that grow from Sn-plated surfaces, such as surface finishes on electronic packages. The phenomenon of Sn whiskering has become a concern in recent years due to requirements for lead (Pb)-free soldering and surface finishes in commercial electronics. Pure Sn finishes are more prone to whisker growth than their Sn-Pb counterparts and high profile failures due to whisker formation (causing short circuits) in space applications have been documented.[1] At Sandia, Sn whiskers are of interest due to increased use of Pb-free commercial off-the-shelf (COTS) parts and possible future requirements for Pb-free solders and surface finishes in high-reliability microelectronics. Lead-free solders and surface finishes are currently being used or considered for several Sandia applications. Despite the long history of Sn whisker research and the recently renewed interest in this topic, a comprehensive understanding of whisker growth remains elusive. This report describes recent research on characterization of Sn whiskers with the aim of understanding the underlying whisker growth mechanism(s).

The report is divided into four sections and an Appendix. In Section 1, the Sn plating process is summarized. Specifically, the Sn plating parameters that were successful in producing samples with whiskers will be reviewed. In Section 2, the scanning electron microscopy (SEM) of Sn whiskers and time-lapse SEM studies of whisker growth will be discussed. This discussion includes the characterization of straight as well as kinked whiskers. In Section 3, a detailed discussion is given of SEM/EBSD (electron backscatter diffraction) techniques developed to determine the crystallography of Sn whiskers. In Section 4, these SEM/EBSD methods are employed to determine the crystallography of Sn whiskers, with a statistically significant number of whiskers analyzed. This is the largest study of Sn whisker crystallography ever reported. This section includes a review of previous literature on Sn whisker crystallography. The overall texture of the Sn films was also analyzed by EBSD. Finally, a short Appendix is included at the end of this report, in which the X-Ray diffraction (XRD) results are discussed and compared to the EBSD analyses of the overall textures of the Sn films. Sections 2, 3, and 4 have been or will be submitted as stand-alone papers in peer-reviewed technical journals. A bibliography of recent Sandia Sn whisker publications and presentations is included at the end of the report.

ACKNOWLEDGMENTS

The authors wish to thank Dr. Tom Buchheit and Dr. Charlie Robino for careful review of parts of this report. Michael Rye and Garry Bryant are gratefully acknowledged for expert FIB sample preparation. Special thanks to Alice Kilgo and Dr. Lisa Deibler for laser confocal scanning microscopy (LCSM). Thanks also to Mark Reece for preparation of the copper substrate materials. Several current and former students in Dept. 1725 performed Sn plating for this project including: Steve Limmer, Daniel Shore, Natalia Gurule, and Laura Montoya. For stimulating discussions about Sn whiskers, special thanks to Charlie Robino, Paul Vianco, Prof. Ed Webb (Lehigh University), Prof. Carol Handwerker (Purdue University), and Lyudmyla Panashchenko (Univ. Maryland). The support of Mike Hosking, the Laboratory Directed Research and Development program and its management, are also gratefully acknowledged.

CONTENTS

FIGURES

TABLES

ACRONYMS

BCT	body centered tetragonal
CA	chrono-amperometry
COTS	commercial off-the-shelf
CP	chrono-potentiometry
CV	cyclic voltometry
DC	direct current
DRX	dynamic recrystallization
EBSD	electron backscatter diffraction
FIB	focused ion beam
IMC	intermetallic compound
LCSM	laser confocal scanning microscopy
LOM	light optical microscopy
OM	orientation matrix
SAED	selected area electron diffraction
SEM	scanning electron microscopy
TEM	transmission electron microscopy
XRD	X-Ray diffraction

1. ELECTRODEPOSITION OF TIN: DC ELECTRODEPOSITION (GALVANOSTATIC VS. POTENTIOSTATIC)

Jamin Pillars, Graham Yelton

Tin was electrodeposited on tin and copper substrates using direct current application. Samples were plated with both a Galvanostatic and a Potentiostatic mode for whisker propensity comparison. After allowing time for incubation, the tin deposits were examined with microscopy for whiskering. Tin plated on copper samples showed high whisker densities, under specific plating parameters, using both a Galvanostatic and a Potentiostatic mode. Cyclic voltometry was performed and the results compared with a Pourbaix diagram to determine the reaction pathway for tin deposition in the alkaline plating system used. Samples of tin deposited on copper substrates were analyzed using X-ray diffraction (XRD) to determine the crystallographic orientations present. XRD analysis showed a 211 growth orientation preference for direct current deposited samples.

1.1 INTRODUCTION

With the phasing out of tin-lead alloy solders and coatings in electronics, pure tin's propensity to whisker has again become an active topic for research. To study tin whiskers, it is necessary to be able to produce samples that can reliably grow whiskers. This allows us to examine the driving forces and mechanisms involved in whiskering, as well as whisker growth tendencies and crystallographic orientation distributions of both whiskers and the tin film itself. Samples that are electrodeposited using direct current (DC) from an alkaline chemistry show a high level of whiskering. These samples also provide a comparison for samples produced with other techniques such as pulsing. DC samples can be deposited using two different modes: 1) Galvanostatic, where the current is constant and the potential varies, or 2) Potentiostatic, where the potential is constant and the current varies. In Galvanostatic mode the concentration gradient, or the slope of the concentration profile across the boundary layer, is constant. With mass diffusion being driven by the concentration gradient, the diffusion is constant. In Potentiostatic mode, the slope changes as the surface concentration is depleted over time. The change in the concentration gradient results in a change in the rate of mass diffusion to the electrode. Both methods are valuable to develop samples where whiskering is promoted for use in further experimentation. By examining the reaction pathway and characteristics of the alkaline system, insight can be gained as to the promotion or inhibition of tin whiskers.

1.2 EXPERIMENTAL PROCEDURE

An alkaline plating system was used because it displays a uniform current distribution across the substrate, providing for a more uniform deposit. The alkaline system has also shown a propensity to promote whiskering with DC deposition. The tin plating bath composition was kept constant throughout the experiments and consisted of 0.375M sodium stannate, 0.25M sodium hydroxide, 0.15M sodium acetate, and 0.0037M Sorbital. The pH for the bath was approximately

13-14. At this pH, a Pourbaix diagram was examined to note the species and reactions present as the potential is driven more negative. The system was then analyzed using cyclic voltometry to note for reduction and oxidation peaks that correspond to the Pourbaix diagram. Although some researchers employ the alkaline bath, most microelectronics applications use an acidic methane-sulfonate bath. The purpose of our investigation was not to replicate electronics applications, but rather to promote the growth of whiskers for further characterization.

To produce the deposits, a three-electrode closed cell was used. A Potentiostat PGZ301 was used with a Pt foil auxiliary electrode and a Hg/HgO in 0.1M KOH reference electrode (0.165 V vs. NHE). To avoid oxygen reacting with the bath chemistry, nitrogen gas was bubbled through deionized water and then flowed over the top of the closed cell. Two types of working electrodes were used: 1) a polycrystalline pure tin sheet and 2) a pure copper sheet electrode. A rotating disk electrode (RDE) was used with the rotation set at 1000 rpm to keep the Nernst boundary layer set at a maximum of approximately 10.9μm. The temperature for all experiments was constant at 70.0°C. The roughness of the substrates was also controlled by an alumina based polish and mechanically polishing the tin electrode down to a 50 nm particle size. The copper electrode was mechanically polished and then chemically polished using a 50/50 vol% ratio of nitric acid to sulfuric acid mixture.

The deposit samples were produced using both a Potentiostatic and a Galvanostatic mode. With the Potentiostatic mode (Chrono Amperometry) the samples were plated with constant potentials from -1500 mV to -2400 mV, over a range of times from 2.5 minutes to 70 minutes. Using the Galvanostatic mode (Chrono Potentiometry), samples were produced with constant current amplitudes from -0.4mA to -20.0mA over times ranging from 5 minutes to 120 minutes. After the samples were produced, they were allowed time for whiskers to nucleate, and then examined for whiskering.

1.3 RESULTS AND DISCUSSION

Using an alkaline bath, the tin is in a 4^+ oxidation state in solution. This can be compared to common acid systems where the oxidation state is 2^+ for tin cations in aqueous solution. The Pourbaix diagram in Fig. 1.1 represents the species and reactions expected in a pH 13-14 system as the potential is driven negatively. The overall reaction can then be broken down into a series of reactions based on the oxidation state of tin. As tin goes from a 4^+ to 2^+ oxidation state:

$$SnO_3^{2-} + 2e^- + 2H_2O \rightarrow HSnO_2^- + 3OH^- \qquad (1)$$

As tin goes from a 2^+ to 0 oxidation state and is deposited on the substrate:

$$HSnO_2^- + H_2O + 2e^- \rightarrow Sn + 6OH^- \qquad (2)$$

The overall reaction for the deposition of tin:

$$Sn(OH)_6^{2-} + 4e^- \rightarrow Sn + 6OH^- \qquad (3)$$

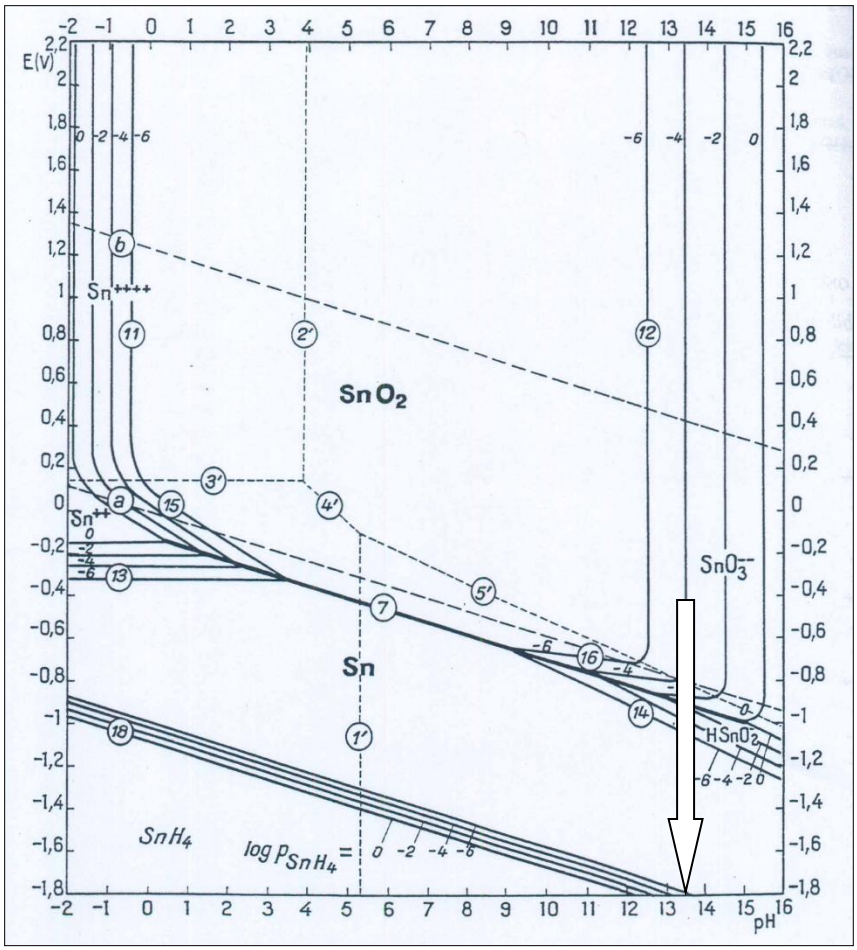

Figure 1.1 Pourbaix diagram for tin in water at 25°C.

It can also be seen from the Pourbaix diagram that SnH_4 gas is produced as the potential is driven into a very negative regime. This gas decomposes rapidly into its elements, creating an acidic environment at the electrode surface, and corrosion occurs on the substrate. At very negative current densities, using Galvanostatic mode, the current efficiency drops below 10% due to side reactions such as hydrogen evolution, the production of SnH_4, and water electrolysis. This is consistent with previous research showing a low current efficiency with an alkaline bath when compared to an acidic plating chemistry[1].

Cyclic voltometry (CV) was then performed on the plating bath for comparison to the Pourbaix diagram. The CV scan confirmed two oxidation peaks and two reduction peaks at potentials consistent with the transitions seen on the Pourbaix diagram (Fig. 1.2). These are numbered on the CV scan to correlate with the reactions mentioned previously. For the oxidation peaks, these reactions are reversed as tin goes from a 0 to 2^+ to 4^+ oxidation state.

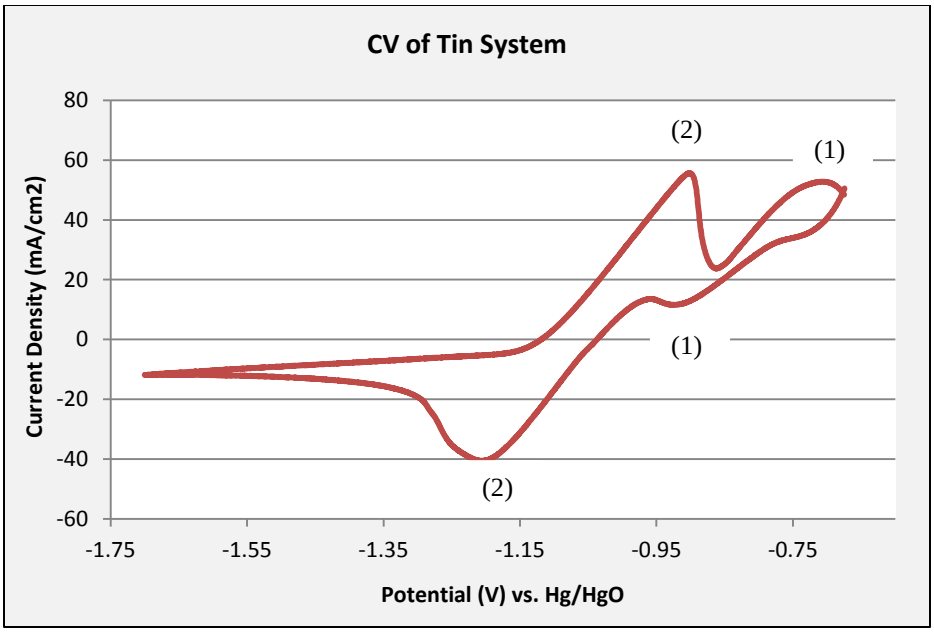

Figure 1.2. CV scan of alkaline tin plating bath showing two oxidation and reduction peaks.

Tin deposited on copper samples were examined for whiskering using microscopy. Both Galvanostatic and Potentiostatic methods showed favorable whiskering under certain plating parameters. This is demonstrated in Fig. 1.3. The depositions from Potentiostatic mode displayed significant whiskering when electroplated at -1900 mV for 10 minutes. At this potential and duration, the deposit thickness was about 1μm. The depositions from Galvanostatic mode showed a high whiskering density from two different plating parameters: 1) -20.0mA for 10 minutes and 2) -2.5 mA for 40 minutes. **Table 1.1** summarizes the sample plating conditions and whisker tendency. At -20.0mA for 10 minutes a deposit thickness of 1.5 – 4 μm was seen. The current efficiency at this current amplitude was very low at < 10%. This current amplitude also has the problem of SnH_4 production and corrosion at the cathode mentioned previously. At -2.5 mA for 40 minutes, a deposit thickness of approximately 2.4μm was measured. This equates to a current efficiency of 23% and while still low, is much better than the efficiency measured at the more negative current amplitude plating parameter. At a current of -2.5 mA, the problem of SnH_4 generation is removed and there is no corrosion at the cathode. This makes it the more desirable Galvanostatic method to produce tin samples likely to whisker.

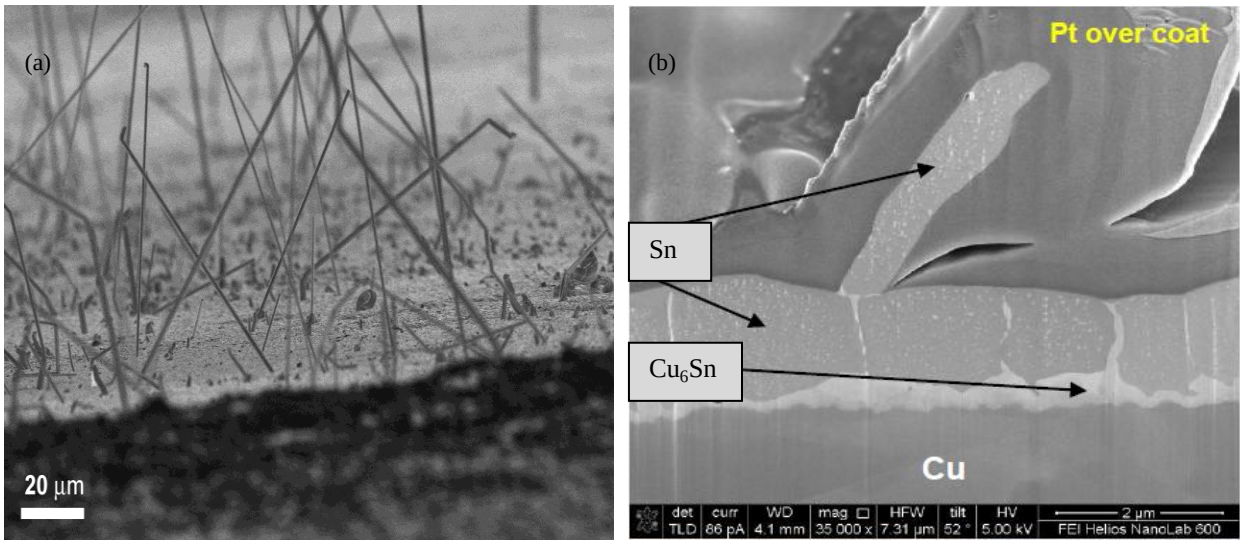

Figure 1.3. Images showing a) high whisker density on DC deposited tin. b) FIB cross section of whisker on tin deposit.

Samples of tin deposited on tin substrates were analyzed using X-ray diffraction (XRD). The XRD data was analyzed to determine a preferred crystallographic orientation of growth for both Galvanostatic and Potentiostatic methods of deposition. Both modes of deposition showed a strong preference for the 211 orientation regardless of the variance in plating parameters. This is illustrated in Fig. 1.4 where the dominant 211 peak can be seen with some smaller peaks (321) showing the secondary texture of the deposits. In Fig. 1.4, the XRD scans are compared to a baseline XRD scan of a random (powder) Sn specimen. Further details of XRD analysis will be discussed in Appendix A of this report. The DC deposit grain structure is shown in Figs. 1.3b and Fig. 1.5. The microstructure of the Sn deposits shows columnar grain boundaries essentially spanning the thickness of the film, although the grains themselves are equiaxed. This structure is sometimes referred to as a "bamboo" structure. The Cu_6Sn_5 layer at the base of the Sn film is very non-uniform. Note that some of the bright particles in the film are an artifact due to re-deposition of Sn and/or Cu_6Sn_5 during the FIB cut process. These deposits provide a good baseline for comparisons of orientations of pulse-plated samples with DC-plated samples. The grain structure of the DC samples can also be used for comparison with that of pulsed samples.

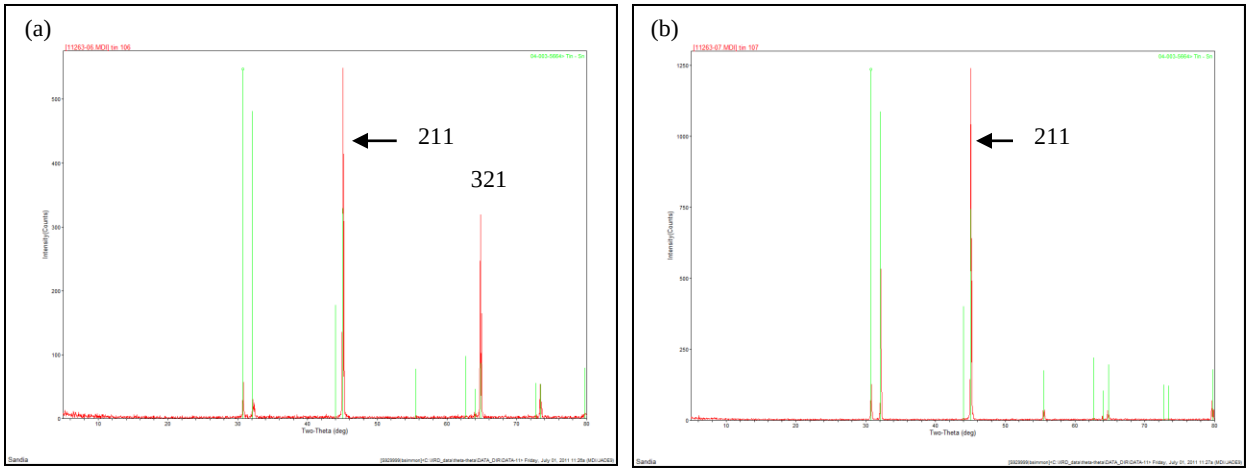

Figure 1.4. XRD results for (a) Potentiostatic mode at -2100mV for 5.3 minutes. (b) Galvanostatic mode at -3.0 mA for 8 minutes. Both modes showed a dominant 211 orientation.

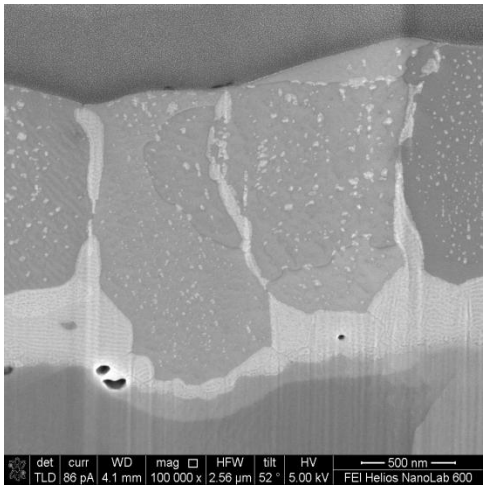

Figure 1.5. FIB Cross section depicting tin sample grain structure

1.4. CONCLUSIONS

The tin alkaline plating bath was shown to be consistent with the reaction pathway from the Pourbaix diagram by analysis with cyclic voltometry. Two oxidation peaks and two reduction peaks were seen correlating to the oxidation state transitions of tin as it is deposited. The tin deposited on copper samples, using both Galvanostatic and Potentiostatic methods, displayed good whisker densities under specific parameters. By identifying these parameters in an alkaline system, there is a high probability of producing samples that will whisker for performing further evaluations. This is a valuable tool for researchers examining the driving mechanism, whisker growth orientations, or other characteristics of tin whiskers. For tin deposited on tin, information was obtained regarding the preference for 211 growth using both Galvanostatic and

Potentiostatic methods for deposition. This provides a good baseline comparison tool for examining the growth orientations in pulsed electrodeposits.

1.5 ACKNOWLEDGEMENTS

- XRD: Mark Rodriguez (01822 Materials Characterization)
- FIB: Michael Rye and Garry Bryant (01822 Materials Characterization)
- Plating/electrochemical analysis: Natalia Gurule, Laura Montoya, Daniel Shore (01725 Photonic Microstructure Technology)
- LDRD # 130800

1.6 REFERENCES

1) Jiang, B., & Xian, A.-P. (2008). Whisker growth on tin finishes of differnet electrolytes. *Microelectronics Reliability* , 48: 105-110.

***Table 1.1 Plating parameters used with an alkaline stannate (sodium or potassium stannate) plating bath to produce Sn deposits that generated Sn whiskers.**

Plating mode	E (mV) or I (mA)	Time (min)	Temp. (˚C)	Agitation (rpm)	Approx. Thickness (um)	Whiskers ?
CP	-2.47mA	40	70	1000	2.4	Yes
CA	-1500mV	30	70	1000	1.8	Some
CP	-20.0mA	5	70	1000	2.2	Few
CP	-20.0mA	10	70	1000	4.4	Few
CP	-20.0mA	10	70	1000	1.5	Yes
CA	-2400mV	15	70	1000	1.5	Yes
CA	-1900mA	10	70	1000	0.68	Yes

CP = chrono potentiometry (constant current)
CA= chrono amperometry (constant voltage)

*** Note: many other plating parameters (not shown here) were utilized that *did not* produce whiskers.**

2. MORPHOLOGY AND GROWTH KINETICS OF STRAIGHT AND KINKED TIN WHISKERS

D.F. Susan, J.R. Michael, R.P. Grant, B.B. McKenzie, and W.G. Yelton

2.1 Abstract

Time-lapse in-situ SEM studies of Sn whisker growth were conducted to estimate growth kinetics and associated changes in whisker morphology. For straight whiskers, growth rates of 3 to 4 microns per day were measured at room temperature. The effect of the kink process on whisker growth was also characterized. Importantly, whisker kinks often coincide with a significant slowdown or complete stoppage in whisker growth, depending on the type of kink/bend the whisker undergoes. Two types of kinks were identified. In Type I kinks, the original growth segment orientation remains unchanged, there are no other changes in morphology or diameter, and growth often continues. In Type II kinks, the original segment changes orientation and it appears that the whisker bends over. Type II kinks often include changes in morphology and diameter at the base indicating grain boundary motion in the film. These processes at the whisker base eliminate the conditions suitable for long-term whisker growth. To estimate the errors in the whisker growth kinetic measurements, a technique is presented to correct for SEM projection effects. With this technique, the actual growth angles and lengths of a large number of whiskers were collected. Most whiskers grew at moderate or shallow angles with respect to the surface; few straight whiskers grew nearly normal to the surface. In addition, there is no simple correlation between growth angles and lengths for whiskers observed over an approximate 2-year period. It is hoped that the observations and data collected in this study will be useful for mechanistic models of the whisker growth process.

2.2 INTRODUCTION

Tin (Sn) whiskers have become a concern in recent years due to requirements for lead (Pb)-free soldering and surface finishes in commercial electronics. Pure Sn finishes are more prone to whisker growth than their Sn-Pb counterparts and high profile failures have been documented due to whiskers causing short circuits.[1] Compressive stress within the Sn film is generally agreed to drive Sn whisker growth. However, a full explanation of the whisker growth mechanism has yet to be developed.

Much has been learned about whiskers through scanning electron microscopy (SEM) and related techniques.[2,3] Along with traditional SEM methods, an efficient way to study growth kinetics is through time-lapse "in-situ" SEM imaging in which the same whiskers are followed during the growth process.[4-6] A difficulty lies in returning to the exact location of the whiskers after prolonged intervals. This can be accomplished with sophisticated indexed removable sample holders or by simply leaving the sample in the microscope chamber for long periods and using the automatic location memory available on most SEMs. This approach may be difficult in busy laboratories with multiple users, but it allows for simultaneous determination of growth kinetics and changes in whisker morphology or growth direction.

This paper presents an in-situ time-lapse microscopy study to determine Sn whisker growth kinetics. In particular, the effects of whisker kinking on the growth process will be discussed. Kinks in Sn whiskers have been observed for many years.[7-9] However, whisker kinks have not been studied in detail using in-situ techniques. The issues encountered with projected images of whiskers will also be discussed and the associated errors are estimated. After applying these corrections for image perspective, a summary of whisker growth angles, lengths, and other characteristics is presented.

2.3 EXPERIMENTAL PROCEDURE

Electroplated Sn coatings were deposited on commercially pure annealed Cu sheet substrates. The substrate thicknesses were either 2 or 3 mils (~50 or 75 microns) and the Sn coating thicknesses were in the 1-2 micron range. Prior to plating, the substrates were mechanically polished, followed by a chemical polish with a 50/50 volume% HNO_3/H_2SO_4 mixture. The Sn was plated from a 0.375M sodium stannate alkaline bath at pH~13 to 14 with 0.25M NaOH, 0.15M $NaCOOCH_3$, and with or without 0.0037M Sorbital additive. A rotating disk electrode setup was used at 1000 rpm and 70˚C. Plating was performed under various conditions, but those that favored Sn whisker growth were: -2 to -20mA in chrono-potentiometry mode (CP), or -1500 to -2400mV in chrono-amperometry mode (CA). A Pt foil auxiliary electrode and a Hg/HgO reference electrode were used and nitrogen was bubbled through the plating cell to avoid oxidation of the plating bath.

The Sn coated copper samples were stored under ambient conditions and periodically examined for whiskers by both light optical microscopy (LOM) and scanning electron microscopy (SEM). Time-lapse SEM imaging was performed using a Magellan 400 XHR SEM at 5kV accelerating voltage. Whisker growth was monitored with this technique for a period of about two weeks. Other SEM imaging, length measurement, and whisker angle determinations were performed on a Zeiss Supra 55VP SEM. Tin whisker lengths and growth angles were also characterized by laser confocal scanning microscopy (LCSM) on a Zeiss LSM 700. This method was used for direct comparison to SEM measurements on the same whiskers.

2.4 RESULTS AND DISCUSSION

2.4.1 Morphology and Growth Kinetics of Straight and Kinked Whiskers

Figure 2.1 displays time-lapse SEM photomicrographs of a tin whisker taken with a 45˚ sample tilt. The whisker tip morphology remains unchanged throughout the growth process with a so-called “cap grain”, indicating that growth occurs at the base of the whisker. The diameter of the whisker is approximately 1 micron, corresponding to the grain size of the Sn film. The whisker displays grooves along its length that are also typical of Sn whiskers seen in the literature.[10] It is presumed that the grooves are produced by the shape of the grains surrounding the whisker grain. As shown below (Fig. 2.5) the extrapolated incubation period (after Sn plating) for this whisker was approximately five days. Similar incubation periods have been reported by other researchers.[11] If whiskers are held under the electron beam for long periods or if the same location is repeatedly observed, slight beam damage can develop. This is shown by the arrows in

Fig. 2.1 as small voids along the length of the whisker. It is important not to interpret this artifact as a real morphological feature of the Sn whisker. The SEM photomicrographs in Fig. 2.1 are typical for a "straight" whisker.

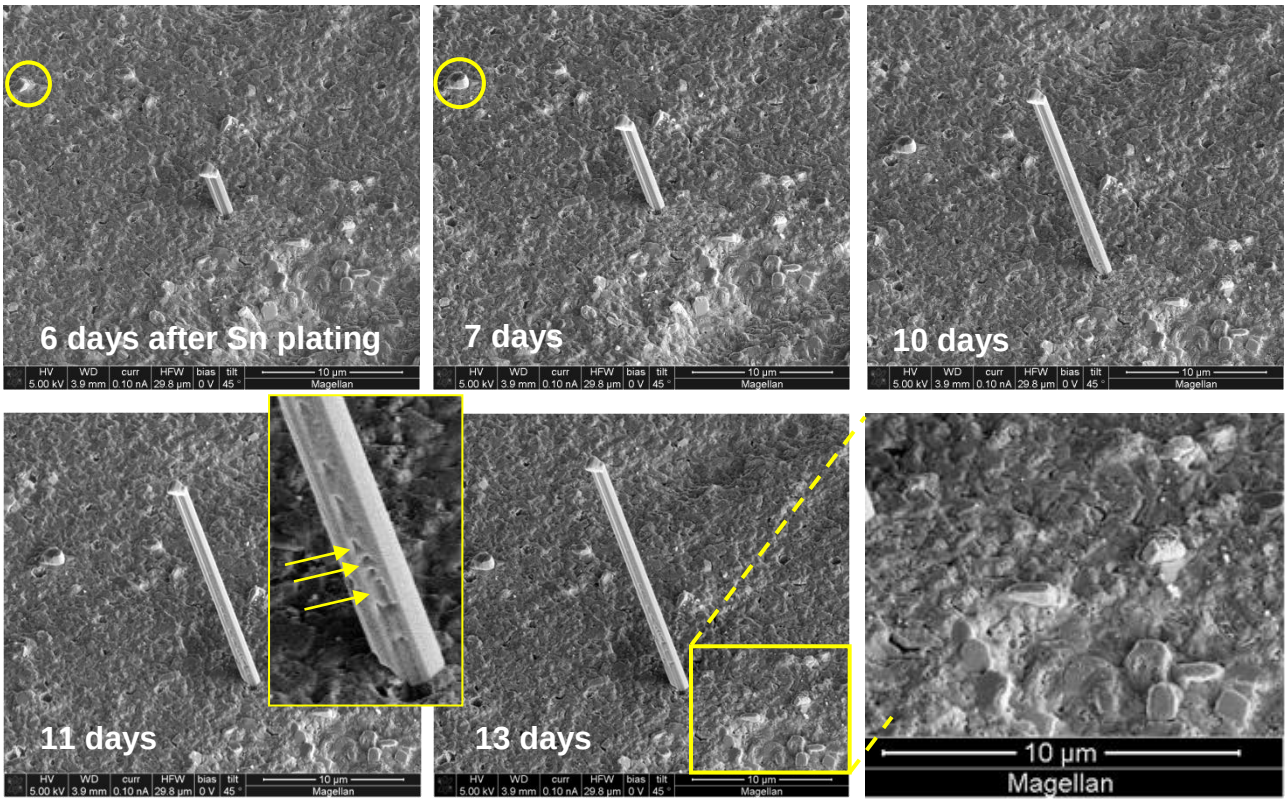

Figure 2.1. Time-lapse in-situ SEM photomicrographs of a straight tin whisker. Circles indicate a nucleated nearby growth with a change in orientation. Arrows indicate electron beam damage on the whisker surface. Bottom-right photo shows close-up of other popped grains/nucleated whiskers.

Another interesting feature in Fig. 2.1 is the occurrence of "popped grains". These are apparent Sn whiskers that nucleated, but did not grow to an appreciable length. The circles in Fig. 2.1 highlight a nucleated whisker that changes direction as it breaks through the surface and several other popped grains are visible in the bottom-right figure. While they are not a concern for electrical shorting, it may be important to include popped grains when studying the mechanisms of whisker nucleation and growth. Indeed, it appears that the nucleation of Sn whiskers is quite common in these samples – perhaps 1 in 100 grains. In contrast, inspection of many samples suggests the conditions suitable for long whiskers are much less common, perhaps 1 in 100,000 grains. However, the whisker density can vary widely depending on the exact plating conditions used, thickness of the Sn layer, etc. Figure 2.2 shows an example of a dense forest of whiskers. Therefore, while the ratio of long whiskers vs. nucleated/popped grains can be determined, it is difficult to make general statements about the overall whisker density without a controlled study aimed at this particular parameter.

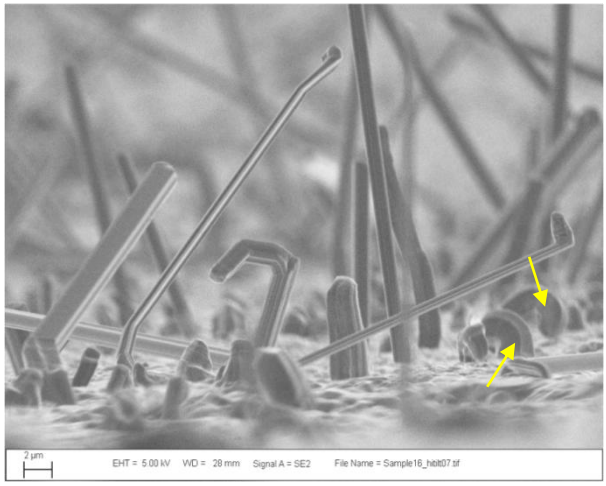

Figure 2.2. A dense forest of whiskers on a Sn-plated sample. Arrows indicate curved whiskers.

Many researchers have observed kinked or bent whiskers and several were characterized in the current study as well. Figure 2.3 displays time-lapse SEM photos of a whisker that changes growth direction. When this particular whisker kinked (at/near its base), the morphology and orientation of the original growth segment remained unchanged. This was labeled a Type I kink. Note in this study kinks are defined as sharply bent whiskers as opposed to curved whiskers like those shown by arrows in Fig. 2.2. Some whiskers with Type I kinks continued to grow at relatively fast rates after kinking. In addition, Type I kinks do not show morphological changes at their base and the apparent diameter of the whisker remains unchanged during growth. The whisker in Fig. 2.3 also shows a slight change in direction near its tip, indicating that this whisker also kinked very early in its growth process.

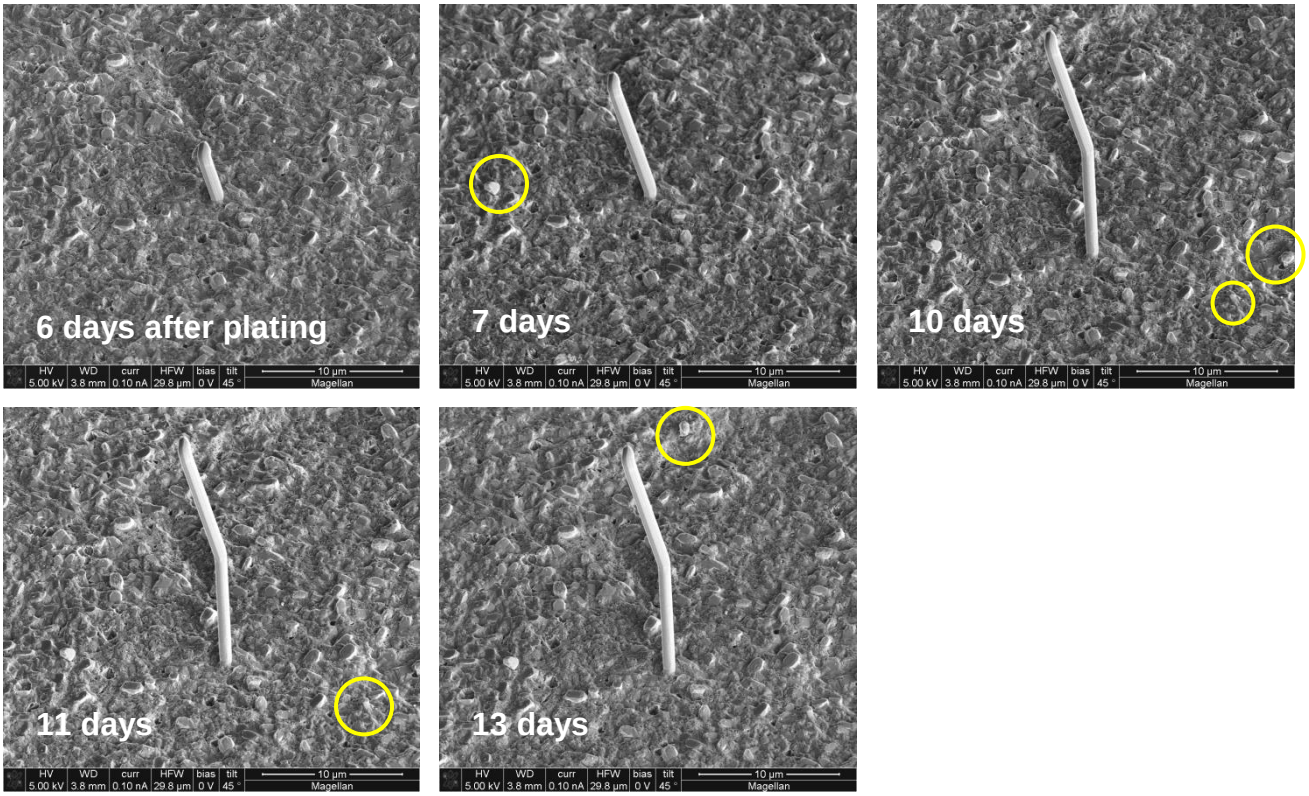

Figure 2.3. SEM time-lapse photos of a whisker with a Type I kink. The apparent orientation of the original segment remains unchanged after the kink. Circles indicate popped grains that nucleated during this sequence.

In contrast, Fig. 2.4 illustrates a Type II kinked whisker. Type II kinks/bends may not be as sharp as Type I kinks and they may show other accompanying changes in morphology. In Type II kinks the orientation of the original growth segment changes – the whiskers actually bend over. Type II kinks also often display a change in diameter associated with the kink process (bottom right, Fig. 2.4). This diameter change is caused by grain boundary movement near the base of the whisker. The change in diameter is gradual and, in Fig. 2.4, striations are observed around the whisker at this location. Importantly, without time-lapse observations, the whisker in Fig. 2.4 would probably not have been identified as a whisker that changed direction during growth. The most significant aspect of Type II kinks, however, is that they are associated with a significant slowdown or complete stoppage in whisker growth (Fig. 2.5 below). Thus, the grain boundary motion at the base of the whisker also eliminates the local crystallographic (and/or diffusional) conditions that were favorable for Sn whisker growth. This stoppage in growth may account for the frequent observations of whiskers with kinks near their base.[10] In the extreme, grain boundary motion at the base of a whisker can result in a transition from whiskers to hillock formation.[4,12,13] For limited grain boundary motion – perhaps the incorporation of a single extra grain into the whisker – the result is only a change in orientation of the whisker and cessation of growth in many cases.

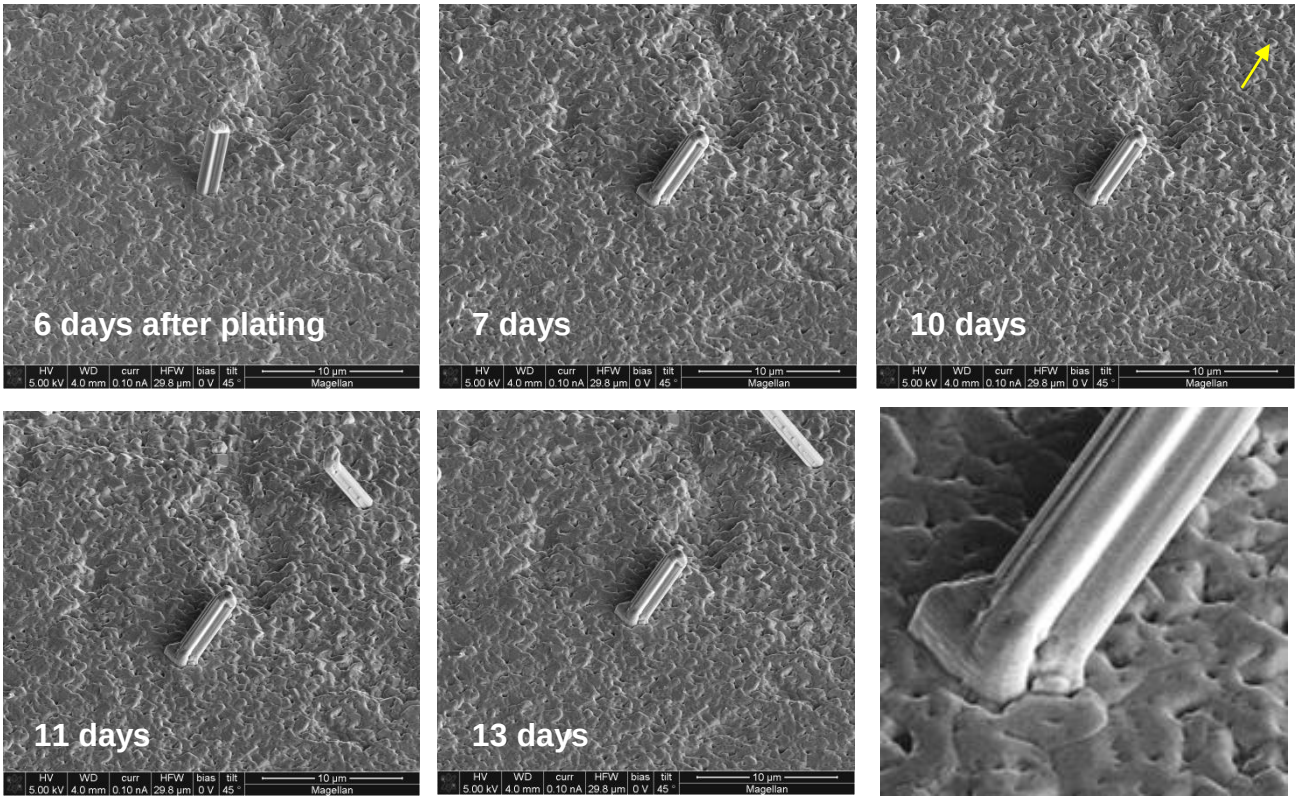

Figure 2.4. Time-lapse SEM photos of a whisker that kinks and then stops growing. Note another whisker nucleated between 10 and 11 days. Bottom-right photo close-up view of the base of the whisker. The arrow indicates the nucleation point of a whisker that begins growing between 10 and 11 days.

The results of whisker growth measurements of 23 straight and kinked whiskers are shown in Fig. 2.5. The times at which the kinks were observed are noted by ovals in Fig. 2.5b. For straight whiskers, an average growth rate of about 2.7 microns per day (~3.1 x 10^{-5} μm/sec) was determined, with the rate tapering off slightly over time. The highest growth rate was about 4 microns per day (~4.6 x 10^{-5} μm/sec). The highest observed rate may be a more accurate value due to the SEM projection effect, in which the apparent whisker length will always be less than or equal to its actual length. That is, the angle of the whisker with respect to the substrate surface is unknown in photomicrographs like those in Figs. 1-4, which causes errors in length measurements. Even with these errors, it is believed that the growth rate measurements are reasonable order-of-magnitude estimates, with the projection effect contributing to the scatter toward lower growth rates. The SEM imaging effects and an estimation of measurement errors will be discussed in detail later.

Figure 2.5b shows the results for kinked whiskers. The times at which kinks were first observed are noted in the plot. The kink process almost always results in a significant reduction in growth rate or complete termination of growth -- when whiskers stop growing the SEM photos appear completely unchanged. Again, the SEM projection effect could produce changes in measured growth rates, but based on the predominance of this observation, it is apparent that the kink process does result in growth stoppage for many whiskers. If the underlying process and

crystallography for kinks could be determined, it may be useful for understanding the conditions that govern whisker growth. Note, however, that the kink process is not *necessary* for whiskers to stop growing – some whiskers stopped growing without any apparent change in growth direction.

The kink processes can be very complex. Whiskers can display multiple kinks of multiple types. Figure 2.6 exhibits a whisker with two kinks – a Type I kink followed by a Type II kink. Such behavior presents a challenge for explaining the whisker growth process and even for simply measuring whisker lengths. One possible scenario for the Type I kink process is shown schematically in Fig. 2.7. In this two-dimensional scenario, it is assumed that the grain boundaries at the whisker base form a chevron "V" shape. This morphology has been observed with focused ion beam (FIB) cuts by several researchers.[14] It is further assumed that Sn is added to the whisker base at one grain boundary and the other grain boundary is able to slide. The simplest case is if growth is parallel to boundary B and normal to boundary A. This is a simplification since, for three-dimensional whiskers, Sn atoms are added to the whisker at more than one grain boundary simultaneously. A steady state in the rates of Sn addition and sliding at each boundary must be achieved for straight whisker growth. Also note that whiskers are surrounded by several other grains. As shown in Fig. 2.7, during a Type I kink the situation flips so that the previous sliding boundary now becomes the location of Sn addition. The result is a kink and change in growth direction (Fig. 2.7). In this simple two-dimensional model with two neighboring grains, the angle of the kink will depend on the angle between these two grain boundaries at the base of the whisker. The orientation (here, in two-dimensions) of the original whisker segment is maintained.

Whiskers are usually single crystals as shown by EBSD measurements (Fig. 2.8). The single crystal is preserved on either side of a kink – the EBSD patterns do not change as the electron beam moves from one side of the kink to the other. If the crystallographic growth directions can be determined, then the possible kink angles will be limited to the angles between crystalline directions in Sn.[7] For example, a whisker growing in a <100> direction can continue to grow as a single crystal in an <010> direction with a 90˚ kink such as the one shown in Fig. 2.8. A 90˚ kink is possible for whiskers growing at acute angles from the surface (Fig. 2.7), but not for a whisker growing perpendicular from the substrate. The situation for a Type II kink is more complex and involves the movement of one or more grain boundaries at the base of the whisker. As the whisker grain grows into an adjacent grain, there is a simultaneous change in growth direction. This can be achieved by a rotation of the crystal in order to maintain the previous crystallographic growth direction or by a change in the crystallographic growth direction itself. In either case, the original whisker segment will be rotated. Such rotation was predicted by Frolov et al. using molecular dynamics simulation of hillock growth.[15] As discussed in that reference, sideways growth of a hillock due to grain boundary movement at its base, coupled with different Sn accretion rates at the base and still some pinning of grain boundaries "might lead to whiskers that appear to change direction".[15] This rotation mechanism is different than the Type I true kink process described previously. Clearly, more work is needed to understand complex Type II kinks.

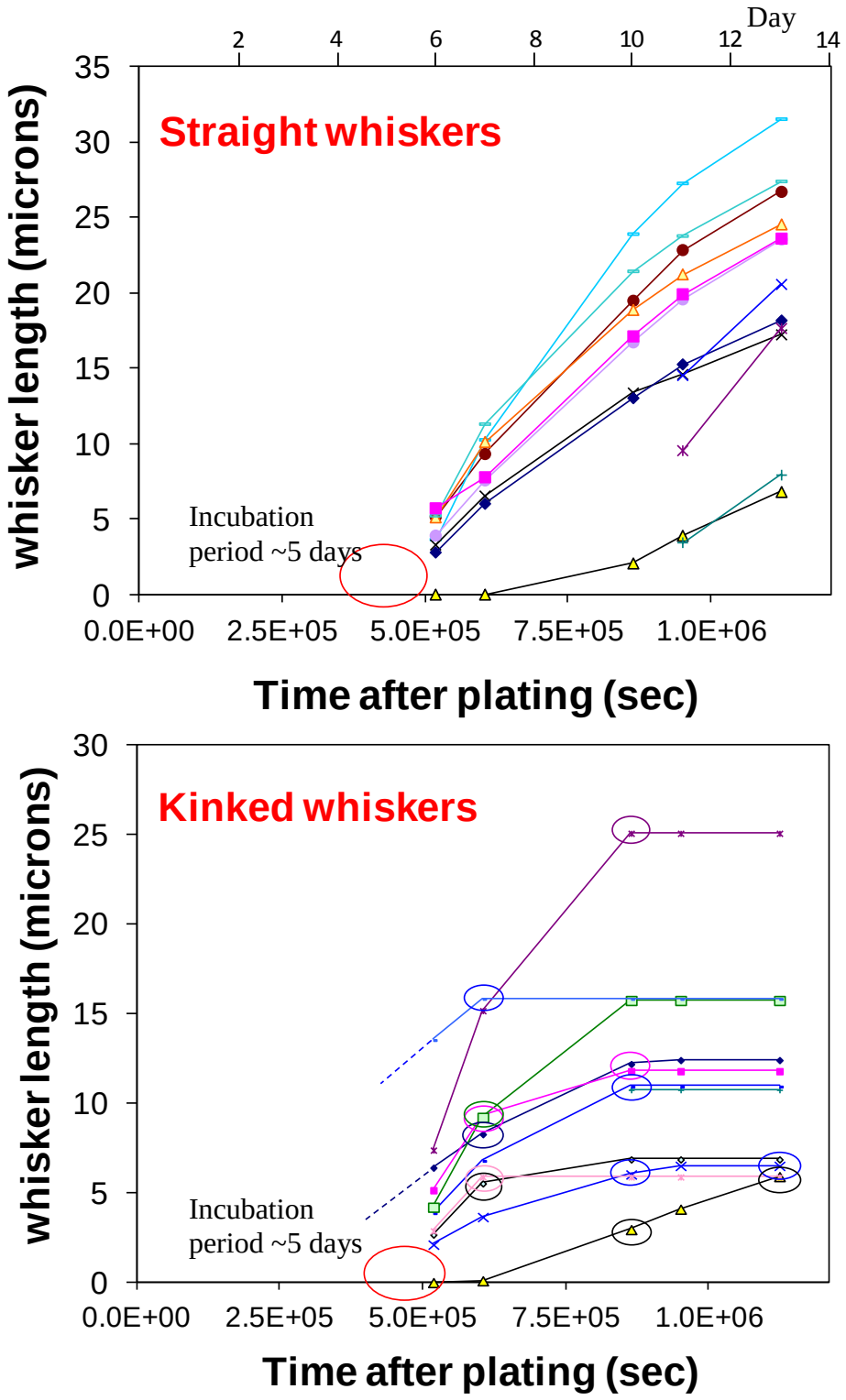

Figure 2.5. a) Whisker growth kinetics for straight whiskers. b) Whisker growth kinetics for kinked whiskers. The times when kinks were observed are indicated.

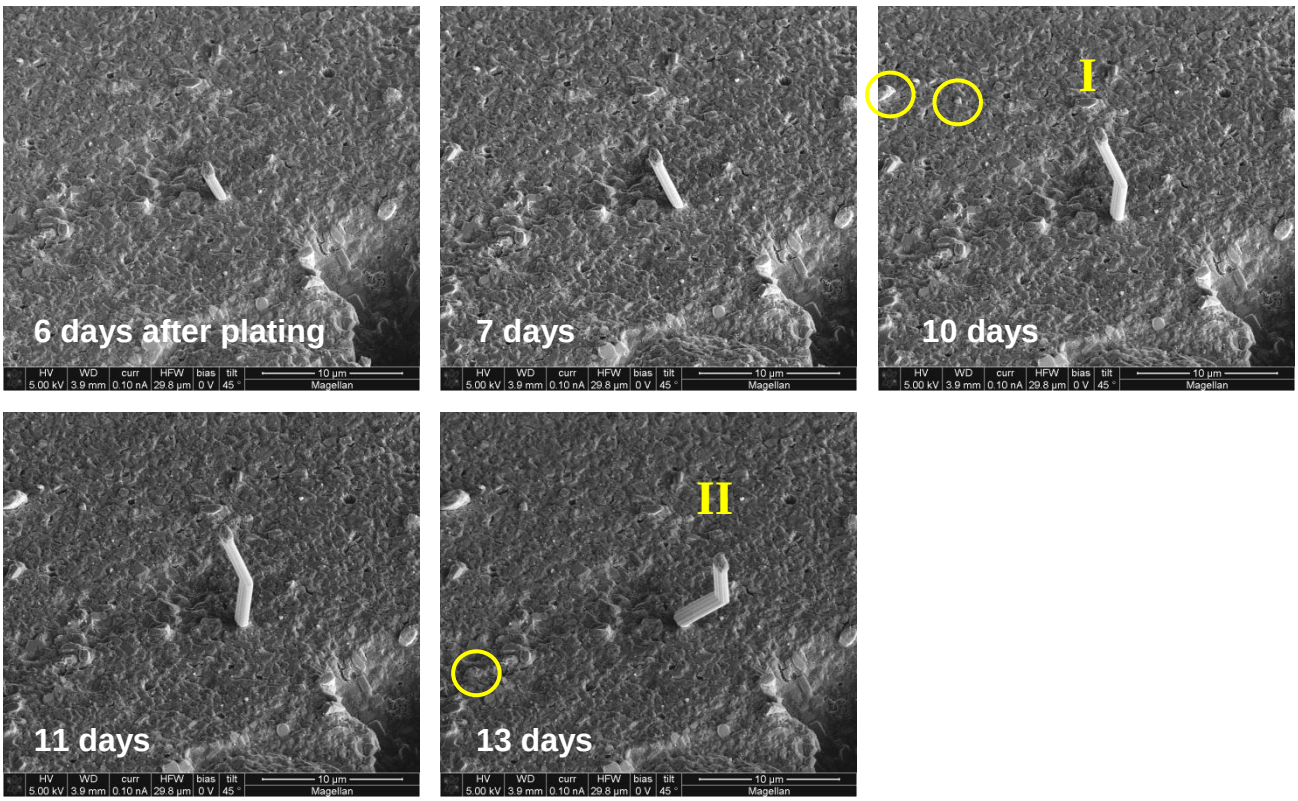

Figure 2.6. Complex whisker growth showing a Type I kink followed by a Type II kink/bend. Circles indicate nucleated whiskers that show up but do not grow appreciably during this sequence.

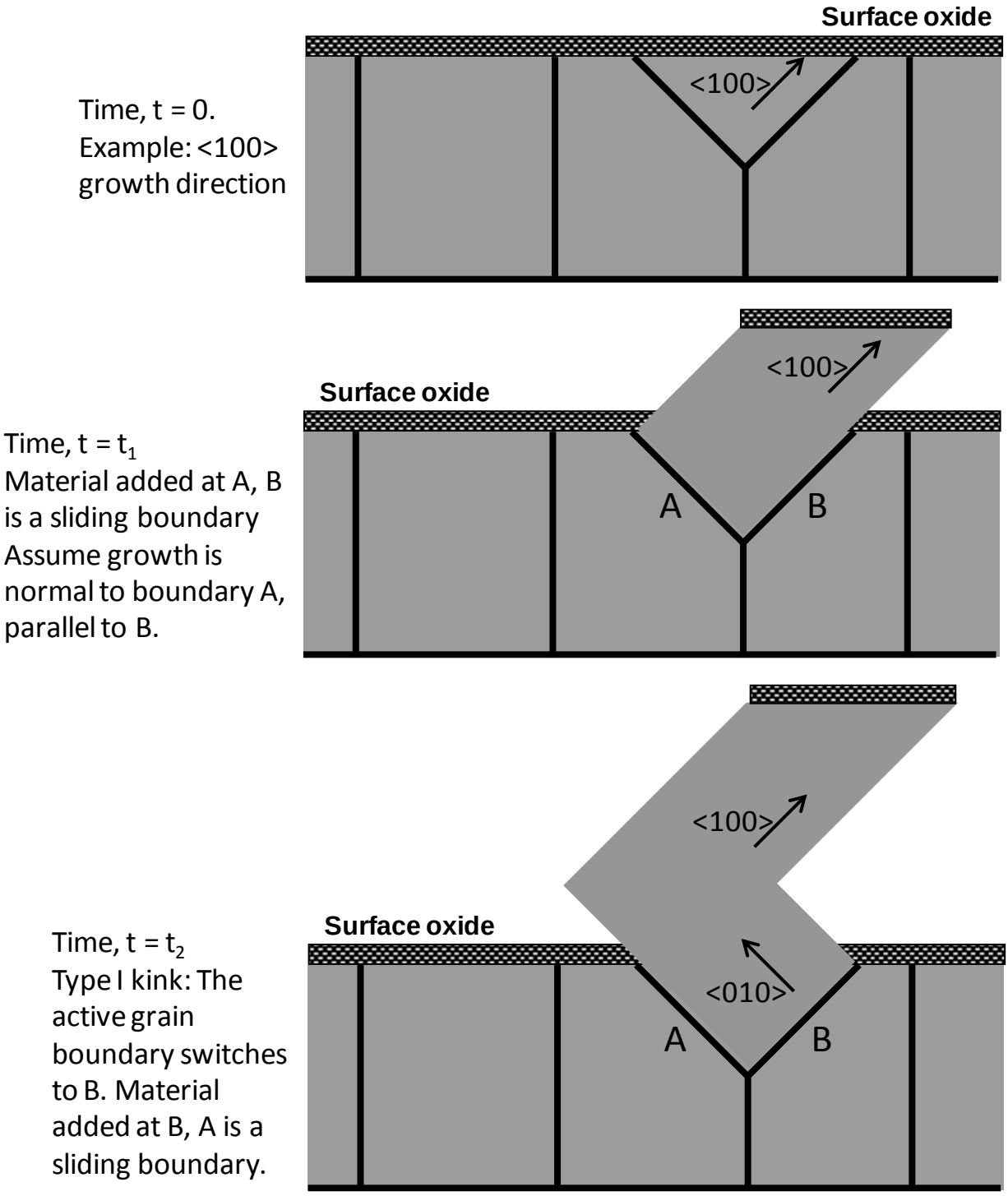

Figure 2.7. Schematic diagram of Type I kink process.

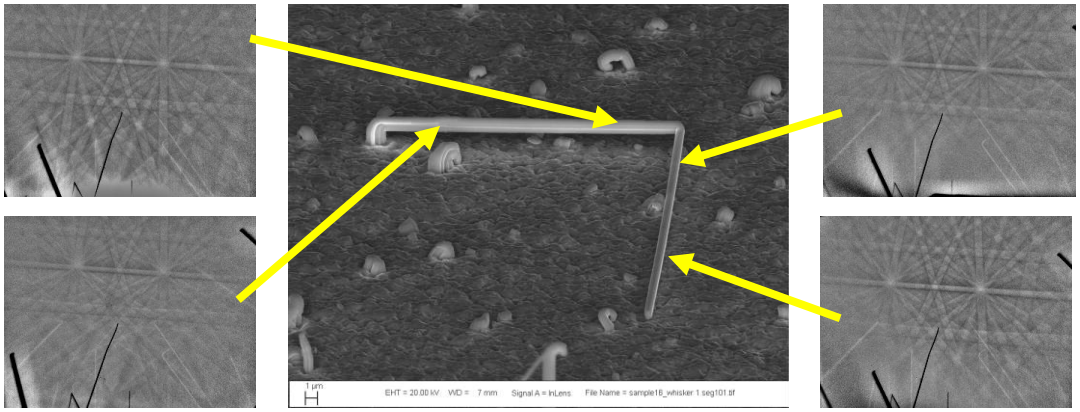

Figure 2.8. A kinked Sn whisker. The EBSD patterns remain unchanged showing that the whisker is single crystal (same crystallographic orientation throughout).

2.4.2. SEM Projection Effect and Estimates of Measurement Error

As mentioned previously, the fastest growth rates in Fig. 2.5a are probably the most accurate, with the scatter toward lower growth rates possibly attributed to the SEM projection effect. To estimate the measurement errors in Fig. 2.5 it is necessary to determine actual whisker lengths using two different SEM tilts. Through geometry (parallax), the actual whisker growth angle and the correct length can be determined.[16-18] The following describes one approach to obtaining accurate whisker lengths and growth angles. First, the sample is rotated so the whisker is aligned with the tilt axis of the SEM. The projected length of the whisker is measured (Fig. 2.9). Next, the distance from the whisker tip to a reference point on the sample surface is measured (apparent z_1). The sample is then tilted a known angle. The whisker will appear to change orientation (unless it is lying perfectly flat on the surface). The distance from the whisker tip to the same reference point is measured again (apparent z_2). The following equations are used to determine the *actual* z-height of the whisker tip above the surface.[19]

$$\text{Parallax} = P = z_1 - z_2$$

$$\text{Actual z-height} \approx P/(\sin(\alpha/2)),$$

where α is the SEM tilt angle. Now the parameters x and z in a right triangle are known and the actual whisker length and the growth angle with respect to the surface are simply calculated from geometry. This procedure was performed for 155 whiskers from five different samples (unfortunately after the time-lapse SEM study was complete) and Fig. 2.10 shows that many whiskers grow at shallow angles with respect to the surface (large angles with respect to surface normal). Many whiskers grow at angles of 45-60˚ with respect to normal, or 30-45˚ with respect to the sample surface. For whiskers measured with a single SEM tilt, the growth angles of the whiskers relative to the viewing direction will determine the error in length measurements. Figure 2.11a shows a comparison of the apparent and calculated whisker lengths determined for a subset of whiskers from three samples. In this study, the worst absolute errors were 45 to 50 microns for long whiskers oriented at a high angle with respect to the surface. The largest relative error was about 80%, which happened to be from a whisker with actual length of 10.7

microns and an apparent length of only 1.7 microns, again due to its high growth angle. The apparent lengths are always shorter than the actual (calculated) lengths, as expected. The simple functional relationship of length measurement error vs. whisker growth angle is shown in Fig. 2.11b with the data points from the three samples. Due to their shallow growth angles, most errors were in the 0 to 40% range. In the extreme, whiskers growing nearly normal to the surface and viewed with zero tilt will appear to have almost no apparent length and the measurement error increases dramatically. The results in Fig. 2.11 can be used to estimate typical errors to be expected if whisker lengths are measured at a single tilt. Note that the results presented above in Fig. 2.5 were obtained with a 45˚ SEM tilt, so whiskers with a 45˚ growth angle will have the minimum measurement error.

For comparison to Fig. 2.5, the lengths of eight whiskers from the time-lapse study were plotted together with the data shown in Fig. 2.11a. The eight whiskers represent the major portion of the scatter in length and, thus, the scatter in growth rates in Fig. 2.5. As shown in Fig. 2.12, the data were plotted two different ways. In the first case, it was assumed that the shorter whiskers correspond to an "apparent" length. All of the other whisker lengths are then plotted with that same apparent length. All of the whisker lengths are within the vertical scatter band obtained from measurements of apparent and actual lengths of other whiskers using the two-tilt technique. In the second case, it is assumed that the longest measured lengths from Fig. 2.5 correspond to an "actual" whisker length. The data from the other seven whiskers are then plotted with that same actual length. Again, the scatter from the eight whiskers lies within the horizontal scatter band obtained from measurements of other whiskers with multiple SEM tilts. The results in Fig. 2.12 indicate that it is at least possible that the scatter in Fig. 2.5 is due primarily from the projection effect when lengths are measured on whiskers at unknown angles. More work would be required, with in-situ time-lapse measurement of whiskers with multiple tilt views of each whisker, to obtain more accurate whisker growth kinetics and the range/scatter of those kinetics.

The error estimation discussed above only accounts for errors due to the unknown angle of the whisker with respect to the surface, i.e., the elevation angle. The rotational orientation (azimuth) is accounted for by rotating the whisker to align with the tilt axis of the SEM (Figs. 9-11). An additional error is present in Fig. 2.5, and other studies in the literature, due to the rotational orientation of the whisker relative to the viewing direction. In our in-situ growth study, whiskers were rotated to a favorable angle for viewing so this error should be minimal. Few studies of whisker growth actually correct for SEM perspective effects and, in fact, tin whisker standards do not specify measurements at more than one tilt. The JESD22-A121A document does recommend that whiskers be "positioned perpendicular to the viewing direction for measurement".[20] This approach will also minimize errors but requires that the sample be tilted until the maximum apparent whisker length is obtained. The tilt angle required will be different for each straight whisker and each segment of a kinked whisker.

All of the whisker lengths and growth angles in the present study were obtained from straight whiskers. It should be recognized that a major concern with whiskers is the distance required for electrical shorting between two conductors. Therefore, the distance of the whisker tip from the sample surface is of interest, not necessarily the combined length of kinked segments. For whisker growth mechanism studies, however, the full length is important. To minimize error, it is recommended that two SEM tilts be used to measure whisker lengths.[16-18] With the method described above, this would require a sample rotation, whisker measurement, sample tilt, and another measurement for each data point (for example, in a plot of growth rate such as Fig. 2.5).

To accurately measure the combined lengths of the segments of a kinked whisker, the tilt and measure technique must be repeated for each whisker segment. As such, the accurate measurement of the lengths of kinked whiskers, as well as the kink angles, requires extensive SEM analysis time.

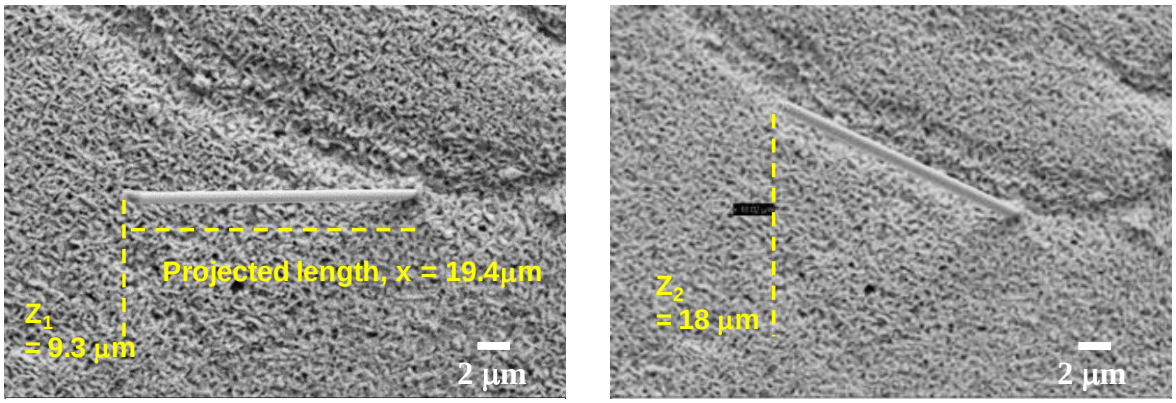

Figure 2.9. SEM photos showing procedure for measuring whisker length and growth angle. The whisker is oriented along the tilt axis (x-axis for our SEM). Left: 0˚ tilt, Right: 10˚ tilt. The actual z-height is 50 μm, the whisker length is 53.6 μm, and the growth angle is 69˚ wrt surface.

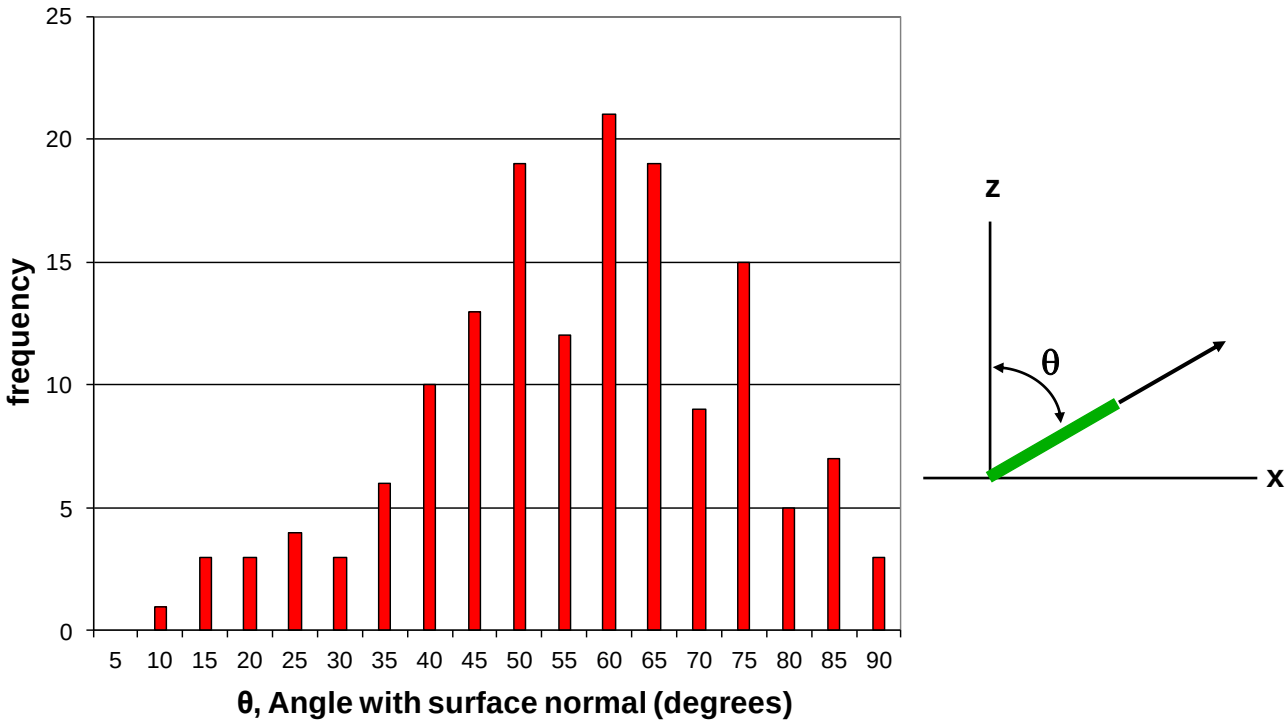

Figure 2.10. Summary histogram of whisker growth angles for 155 whiskers from 5 samples. The data was obtained from straight (non-kinked) whiskers only.

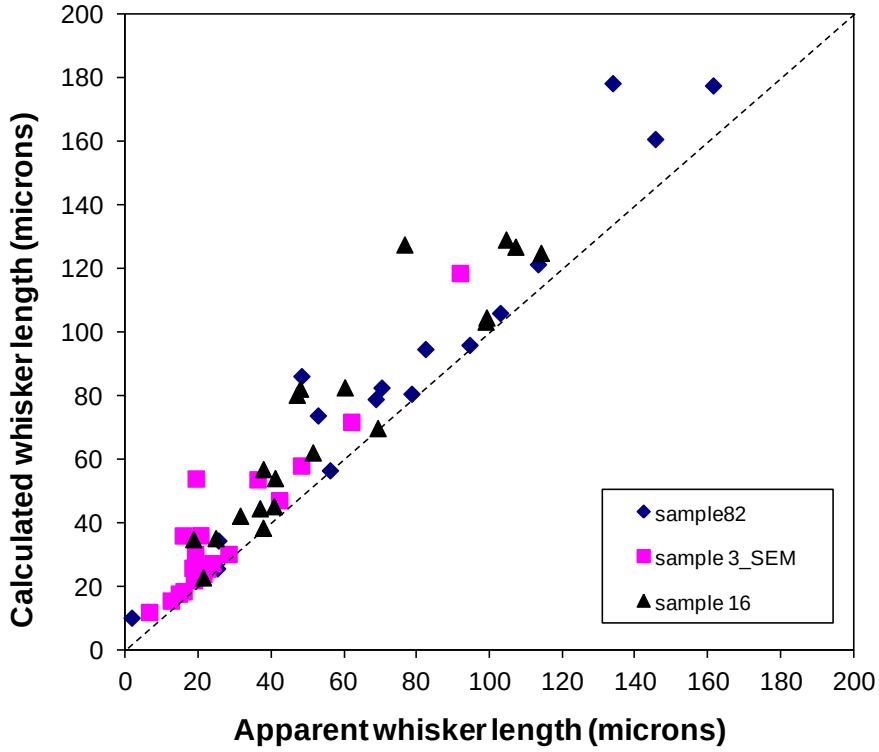

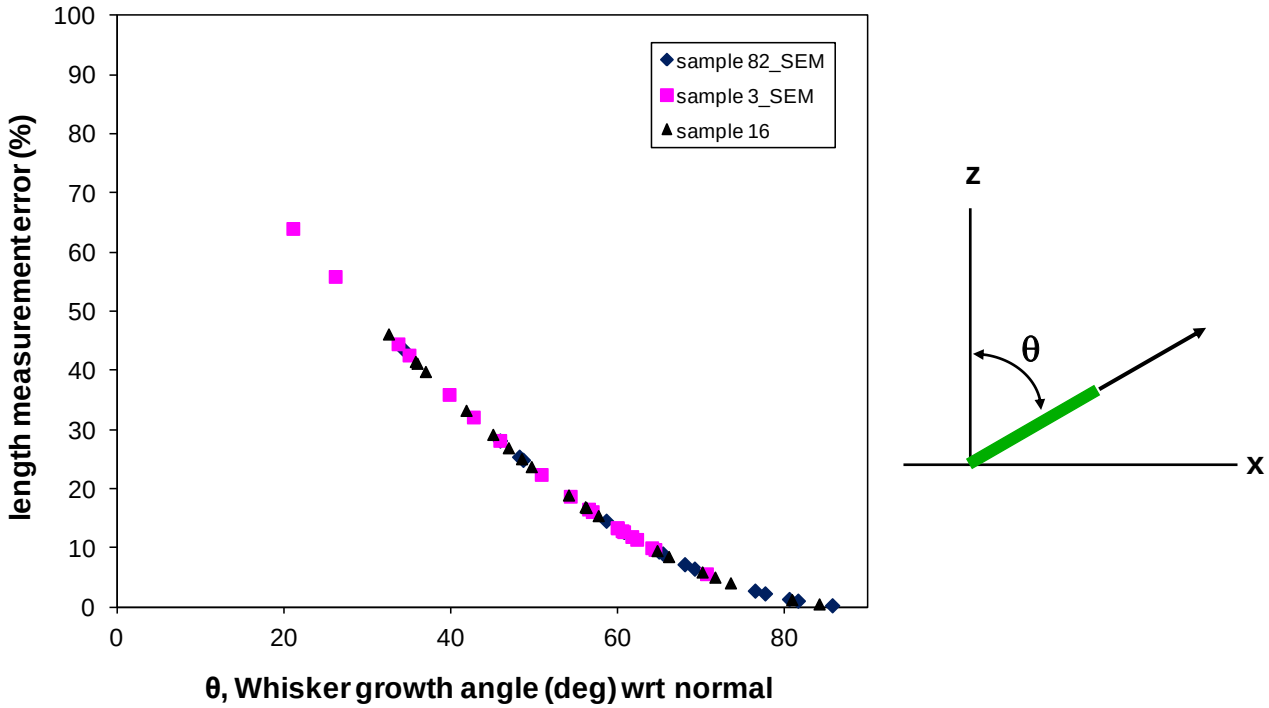

Figure 2.11. a) Comparison of apparent (projected) whisker lengths and whisker lengths obtained with the SEM tilt technique described in the text. b) Error in whisker length measurements as a function of the growth angle.

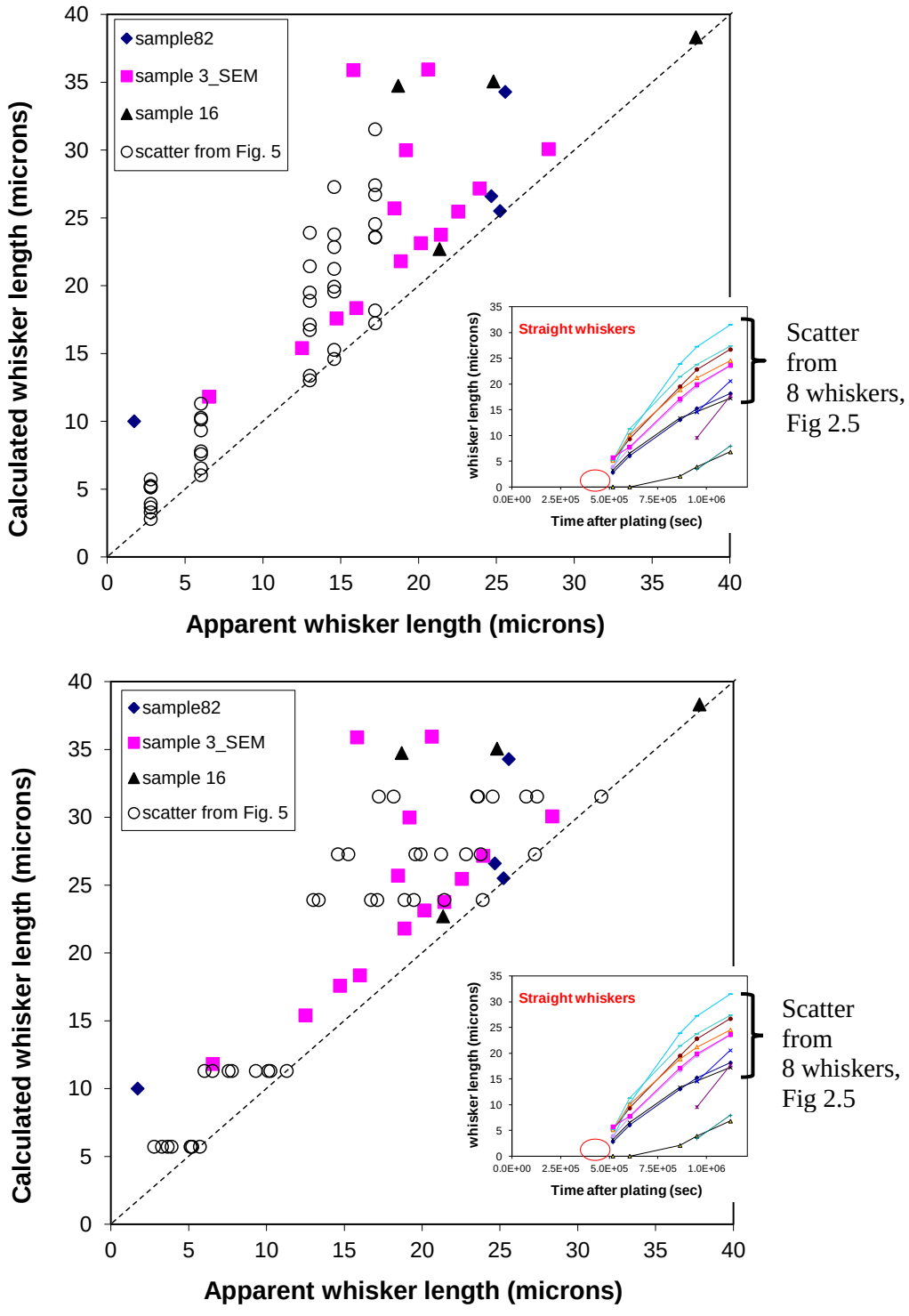

Figure 2.12. Whisker lengths from eight straight whiskers from Fig. 2.5 plotted together with data from Fig. 2.11 above. See text for assumptions made for plotting Fig. 2.5 data. The scatter from the eight whiskers is within the scatter obtained from other whiskers with known actual lengths.

As a further check on the SEM analysis techniques described above, whiskers were measured using laser confocal scanning microscopy (LCSM). This is an optical microscopy technique that provides the ability to accurately obtain z-heights and other topographic information. The LCSM constructs an image from a z-stack of image slices (can be hundreds) using only the features in focus at each particular image plane. Figure 2.13 shows an LCSM photomicrograph and a topographic representation of a Sn whisker. The LCSM software requires alignment of markers exactly along the whisker length to produce the topographic information in Fig. 2.13b. If the marker alignment is not exact, some data dropout can occur but relatively accurate determinations of growth angles and lengths are still produced. LCSM was performed on six selected whiskers that were also characterized by SEM. Figure 2.14 displays a comparison of the two techniques. The length data were comparable for both cases, which provides support for the accuracy of the SEM tilt-and-measure process described previously. Both projected lengths (distance x in Figs. 9a and 13b) and actual whisker lengths are compared in Fig. 2.14a. For angle measurements, more scatter was found between the two techniques (Fig. 2.14b). This is possibly due to difficulties in determining the exact whisker origin (intersection of the whisker with the substrate) using LCSM. The benefit of LCSM is faster analysis speed compared to SEM, especially if kinked whisker lengths and kink angles are to be measured. A disadvantage of LCSM is that crystallographic information cannot be obtained, unlike that which can be determined by SEM with electron backscatter diffraction (Fig. 2.8). In addition, only longer whiskers can be characterized due to resolution limitations with LCSM. More work is needed to further develop LSCM for both straight and kinked whiskers.

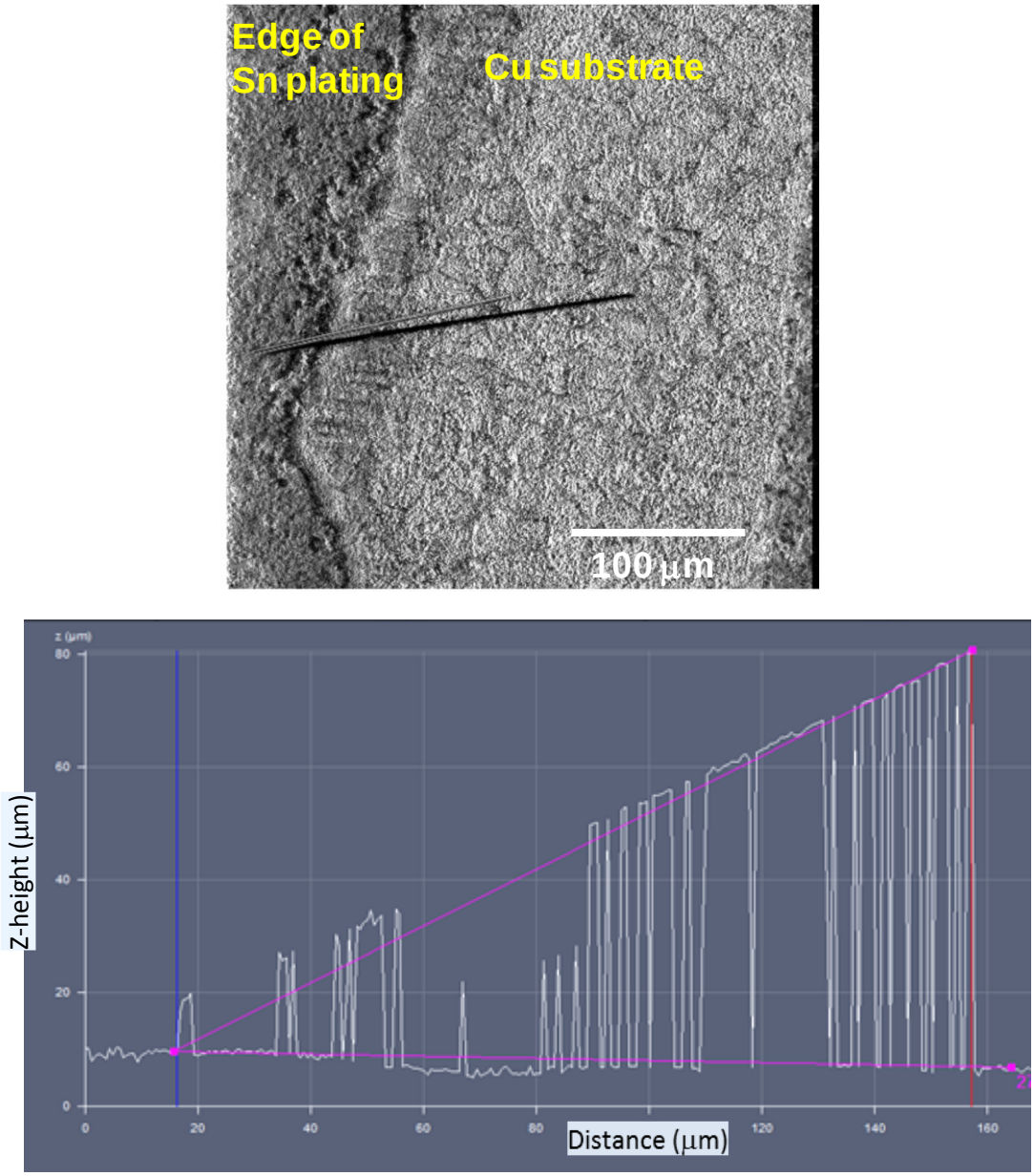

Figure 2.13. a) LCSM photomicrograph of a Sn whisker. Both a whisker and its "shadow" are visible in this image. b) Topographic information obtained from the Sn whisker using LCSM.

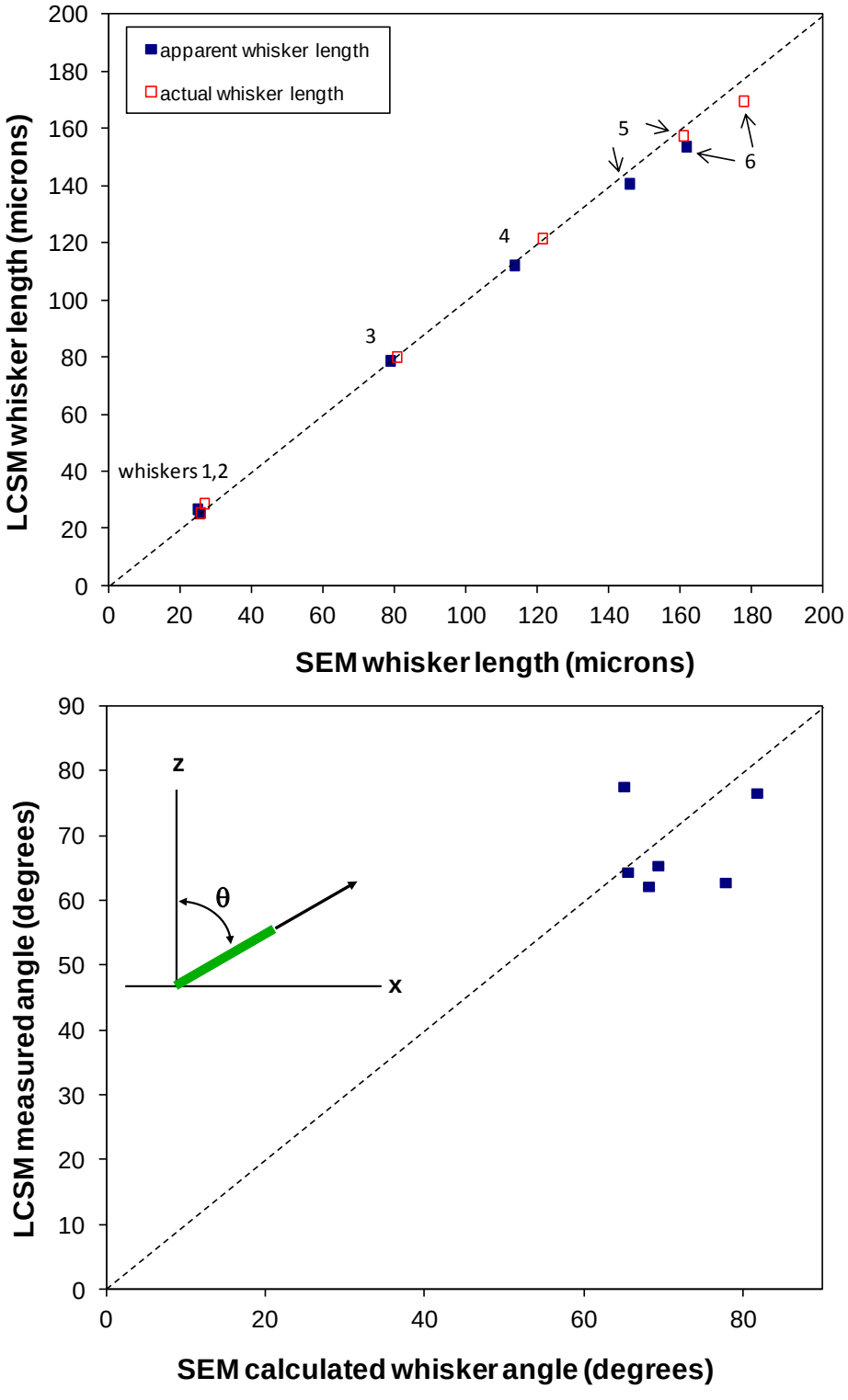

Figure 2.14. a) Comparison of LCSM measured whisker lengths and those determined by SEM tilt-and-measure technique for the same whiskers. b) Whisker growth angles for the same whiskers obtained by LCSM and SEM.

2.4.3. No Apparent Relationship between Growth Angle and Whisker Length

Based on the analysis of whisker lengths and growth angles at multiple SEM tilts, a summary of approximately 150 straight whiskers was compiled. The whiskers were from several samples, observed at various times after Sn deposition, but all within about 2 years of plating. Figure 2.15a shows there is no correlation between whisker lengths and growth angles. Like Fig. 2.10 above, the plot also shows the lack of whiskers growing at high angles from the surface. The broad distribution of whisker lengths is probably not due to a broad range of growth rates, but rather from the following factors: a) whiskers nucleate with different incubation times (Fig. 2.4), b) whiskers stop growing at various times (Fig. 2.5), and/or c) whiskers stop growing and then re-start growth later. A careful in-situ time lapse study of many whiskers over a long time period, with corrections for SEM projection effects, would be required to determine the *distribution* of growth rates on individual samples. If there are varying growth rates, one possible contributor could be different crystallographic growth directions.

A similarly broad distribution of whisker lengths was found by Panashchenko for 2-year-old samples.[17,18] Panashchenko also corrected the length measurements for the SEM projection effect. The whisker length distribution was found to be approximately log-normal and the results are plotted in Fig. 2.15b. While the distributions from the present study and that of Panashchenko are both broad, there are differences for longer whiskers; Panashchenko found some whiskers as long as 1000 μm or more. The span of whisker lengths shown in Fig. 2.15b can be used as a quantitative basis for probabilistic failure models of shorting between adjacent conductors.[21] However, more work is needed to determine how whisker length distributions evolve as a function of time. Such models should also account for kinked whiskers. If kinked whiskers are included, the effective lengths and angles measured directly from the whisker tip to the substrate will be different and will include more "growth angles" close to perpendicular from the surface. In one respect, however, the lack of correlation between whisker lengths and growth angles actually decreases the complexity involved in modeling shorting failures.

With regard to whisker growth mechanisms, it is unclear how the results of the present work will relate to existing theories. While the compressive stress or stress gradients are considered to be the drivers for whisker growth, whether or not a grain will form a whisker needs to be addressed at the local scale. Several factors could be responsible for the localization of whiskers to certain grains:

1) Very localized stress (strain) gradients as proposed by Choi et al.[22]
2) Heterogeneous nucleation at stochastic sites could be responsible for the initiation of whiskers (popped grains). The sustained growth of long whiskers could then occur at certain grains with favorable microstructural conditions such as a stable grain boundary configuration at the base. The correct conditions of strain and strain rate were proposed by Vianco and Rejent (dynamic recrystallization).[23,24]
3) Whiskers could grow from certain grains with lower yield strength, i.e. low resistance to plastic deformation, due to the anisotropic nature of Sn.[25]

4) Whiskers could be the result of a favorable grain orientation for fast diffusion, in this case due to the anisotropy of *diffusion* in Sn [26], or a local surrounding network of grain boundaries that provide an anomalously fast diffusion path.

5) Alternatively, whisker sites could be the result of the opposite effect of diffusion anisotropy, namely "bottlenecks" of material that build up at specific sites because a local diffusion path is anomalously slow.

In any of these localized scenarios, it appears that crystallography would play an important role – the whisker grain orientation, the orientations of the surrounding grains, and the grain boundaries between them – must have the correct characteristics for whiskers to grow.

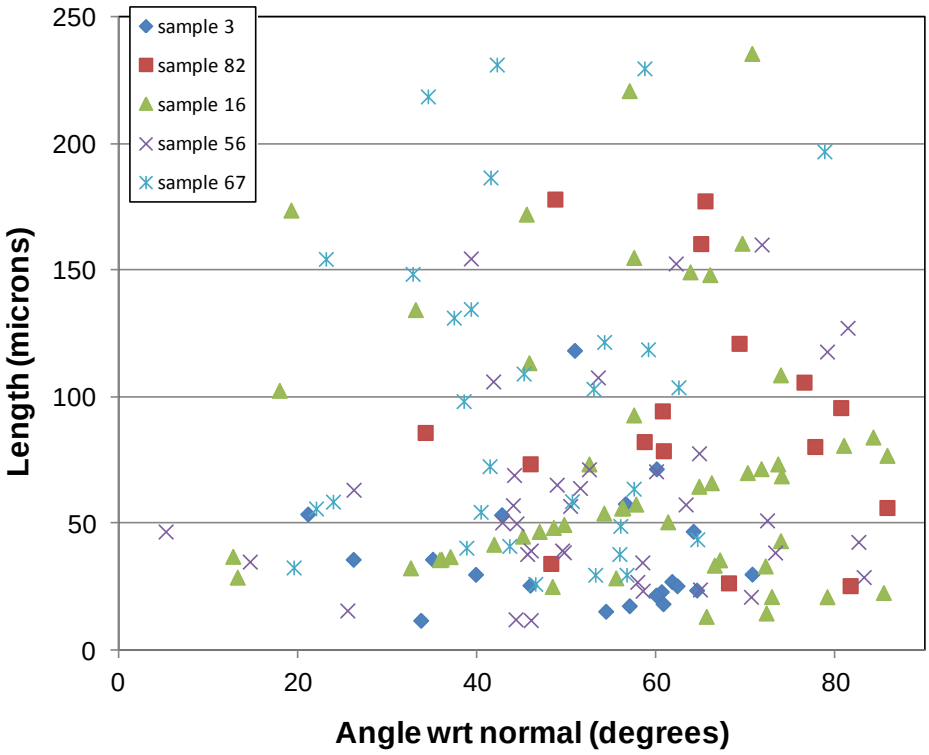

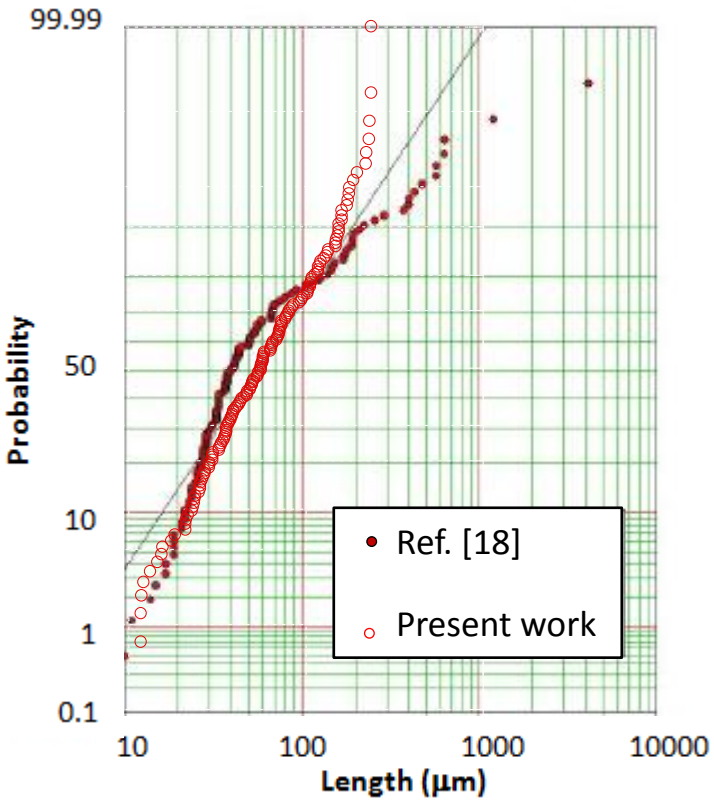

Figure 2.15. a) Plot showing no correlation between whisker lengths and their growth angles. b) Probability plot of whisker length distributions obtained from samples approximately 2 years old. The length distributions are similar for the present study (open symbols) and results from Panashchenko (closed symbols). [18]

2.5 CONCLUSIONS

A time-lapse in-situ SEM study of Sn whisker growth was conducted to estimate growth kinetics and associated changes in whisker morphology. A technique to correct for SEM projection effects was discussed and the magnitude of measurement errors was estimated for uncorrected SEM observations. With these techniques, the actual growth angles and lengths of a large number of whiskers were collected. The following points were compiled from this work:

1. For straight whiskers, growth rates of 3 to 4 microns per day were determined at room temperature. Since the growth angles were unknown, the SEM projection effect contributes to the scatter in the measured growth rates. In this study, the whiskers displayed an incubation time of about five days. For kinked whiskers, the kink process often coincides with a significant slowdown or complete stop in whisker growth.

2. Two types of whisker kinks were discussed. In Type I kinks, the original growth segment orientation remains unchanged, there are no other changes in morphology or diameter, and growth often continues. In Type II kinks, the original segment changes orientation and it appears that the whisker bends over. Type II kinks often show changes in morphology and diameter at the base indicating grain boundary motion in the film. These changes at the whisker base eliminate the conditions suitable for long-term whisker growth.

3. A technique was described using two SEM tilts to correct for image projection effects. Such techniques must be used to obtain accurate measurements of whisker lengths and growth angles for studies of the whisker growth mechanism. Based on this approach, it was determined that many whiskers grow at moderate or shallow angles with respect to the surface. Few straight whiskers grow nearly normal to the surface. For general inspection purposes, the results of this study can be used to estimate typical errors if whisker lengths are only measured with a single SEM tilt.

4. There is no simple correlation between growth angles and lengths for whiskers observed over an approximate 2-year period. In addition, the distribution of lengths is broad. The broad distribution may be due to differences in the incubation periods and growth periods of individual whiskers, in addition to the actual spread in individual growth rates.

2.6 ACKNOWLEDGEMENTS

Special thanks to Alice Kilgo for laser confocal microscopy analysis. Jamin Pillars is acknowledged for Sn plating and Mark Reece for substrate preparation. Thanks also to Dr. C.V. Robino for insightful review of the manuscript.

* Sandia National Laboratories is a multi-program laboratory managed and operated by Sandia Corporation, a wholly owned subsidiary of Lockheed Martin Corporation, for the U.S. Department of Energy's National Nuclear Security Administration.

2.7 REFERENCES

[1] NASA Goddard Space Flight Center Tin Whisker Homepage, website http://nepp.nasa.gov/whisker/
[2] D.F. Susan, J.R. Michael, R.P. Grant, and W.G. Yelton, *Microscopy and Microanalysis, Vol. 16, Suppl. 2*, pp 792-793, Cambridge Univ. Press, 2010.
[3] J.R. Michael, B.B. McKenzie, and D.F. Susan, *Microscopy and Microanalysis, Vol. 17, Suppl. 2*, pp 392-393, Cambridge University Press, 2011.
[4] N. Jadhav, E. Buchovecky, E. Chason, and A. Bower, *JOM*, 62, (7), pp 30-37, 2010.
[5] K.N. Tu and J.C.M. Li, *Mat. Sci. Eng. A*, A409, pp 131-139, 2005.
[6] L. Reinbold, N. Jadhav, E. Chason, and K.S. Kumar, *J. Mater. Res.*, 24, (12), pp 3583-3589, 2009.
[7] G.S. Baker, *Acta Met.*, Vol. 5, pp 353-357, 1957.
[8] N. Furuta, *Japan J. Appl. Phys.*, Vol. 4, pp 155-156, 1965.
[9] P.W. Levy and O.F. Kammerer, *J. Appl. Phys.*, Vol. 26, pp 1182-1183, 1955.
[10] J.B. Lebret and M.G. Norton, *J. Mater. Res.*, 18, (3), pp 585-593, 2003.
[11] J.W. Osenbach, J.M. DeLucca, B.D. Potteiger, A. Amin, and F.A. Baiocchi, *J. Mater. Sci: Mater. Electron*, Vol. 18, pp 283-305, 2007.
[12] P. Sarobol, A.E. Pedigo, P. Su, J.E. Blendell, and C.A. Handwerker, *IEEE Trans. Elect. Pack. Manuf.*, 33, (3), pp 159-164, 2010.
[13] W.J. Boettinger, C.E. Johnson, L.A. Bendersky, K.-W. Moon, M.E. Williams, and G.R. Stafford, *Acta Mat.*, Vol. 53, pp 5033-5050, 2005.
[14] G.T. Galyon and L. Palmer, *IEEE Trans. Elect. Pack. Manuf.*, 28, (1), pp 17-30, 2005.
[15] T. Frolov, W.J. Boettinger, and Y. Mishin, *Acta Mat.*, Vol. 58, pp 5471-5480, 2010.
[16] B.-Z. Lee and D.N. Lee, *Acta Mat.*, 46, (10), pp 3701-3714, 1998.
[17] L. Panashchenko and M. Osterman, *IEEE Elect. Comp. Tech. Conf.*, pp 1037-1043, 2009.
[18] L. Panashchenko, M.S. Thesis, Univ. Maryland, 2009.
[19] J.I. Goldstein et al., Scanning Electron Microscopy and X-Ray Microanalysis, 2nd Ed., pp 260-267, Plenum Press, 1992.
[20] JESD22-A121A, JEDEC Standard No. 22-A121A, JEDEC Solid State Technology Assoc., 2008.
[21] S. Meschter, P. Snugovsky, J. Kennedy, S. McKeown, J. Keeping, and E. Kosiba, *5th Int. Symposium on Tin Whiskers*, CALCE and Univ. of Maryland, 2011.
[22] W.J.Choi, T.Y. Lee, K.N. Tu, N. Tamura, R.S. Celestre, A.A. MacDowell, Y.Y. Bong, and Luu Nguyen, *Acta Mat.*, Vol. 51, pp 6253-6261, 2003.
[23] P.T. Vianco and J.R. Rejent, *J. Elect. Mat.*, Vol. 38, pp. 1815 – 1825, 2009.
[24] P.T. Vianco and J.R. Rejent, *J. Elect. Mat.*, Vol. 38, pp. 1826 – 1837, 2009.
[25] E.J. Buchovecky, N. Du, and A.F. Bower, *Appl. Phys. Lett.*, Vol. 94, p 191904, 2009.
[26] M.S. Sellers, A.J. Schultz, C. Basaran, and D.A. Kofke, *Phys. Rev. B*, Vol. 81, p 134111, 2010.

3. APPLICATION OF ELECTRON BACKSCATTER DIFFRACTION TO THE CRYSTALLOGRAPHIC CHARACTERIZATION OF TIN WHISKERS

J. R. Michael, B. B. McKenzie and D. F. Susan

3.1 Abstract

Understanding the growth of whiskers or high aspect ratio features on substrates can be aided when the crystallography of the feature is determined. This study has evaluated three methods that utilize electron backscatter diffraction (EBSD) for the determination of crystallographic growth direction of an individual whisker. EBSD has traditionally been a technique applied to planar, polished samples and thus the use of EBSD for out-of-surface features is more difficult and requires additional steps. One of the methods requires the whiskers to be removed from the substrate resulting in the loss of valuable physical growth relationships between the whisker and the substrate. The other two techniques do not suffer this disadvantage and provide the physical growth information as well as the crystallographic growth directions. The final choice of method depends on the information required. The accuracy and the advantages and disadvantages of each method are discussed.

3.2 INTRODUCTION

The crystallographic characterization of micrometer or nanometer-sized whiskers, filaments or rods is important to help explain their peculiar shape and unique properties. For whiskers growing from a substrate, full crystallographic characterization of whiskers includes the crystallographic axis of growth and the physical angle of the whisker with respect to the sample surface normal. These parameters may be useful in quantitative models for the prediction of whisker growth mechanisms. A topic of recent research interest is the development of tin whiskers (beta tin is body centered tetragonal, a= 0.582 nm and c=0.318 nm) on lead-free solders and surface finishes where the Sn-whiskers may grow to lengths that cause failure through shorting of closely spaced electrical conductors (Boettinger et al., 2005). Figure 3.1 is an example of whiskers that grew from a pure Sn electroplated coating. Note that there are many whiskers and they grow to a range of lengths and at a variety of angles from the sample surface.

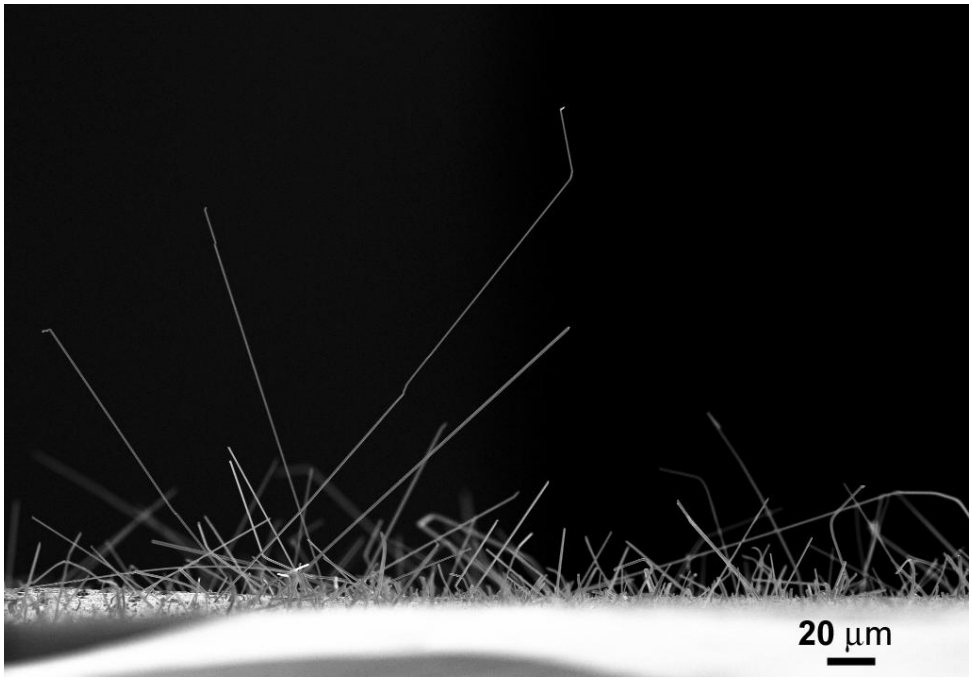

Figure 3.1. SEM image of Sn whiskers that grew from electroplated Sn on a Cu substrate. Note the variety of physical growth angles of the whiskers with respect to the substrate.

The traditional method of studying the crystallography of whiskers or high-aspect ratio particles is transmission electron microscopy (TEM). In these studies the whisker is removed from the substrate and mounted on a suitable thin support film for TEM examination through selected area electron diffraction (SAED). The growth axis of the whisker is then determined by aligning the whisker axis with one of the primary image directions in the microscope (x or y) and then from the SAED pattern determining the crystallographic direction that corresponds to the long axis of the whisker. The main disadvantage to this technique is that the whisker is removed from the surface and the relationship of the growth direction of the whisker with respect to the original sample surface is lost (Luborsky et al., 1963);(Morris and Bonfield, 1974). TEM also requires the diameter of the whisker to be small so that it is electron transparent. With some larger whiskers, only the very edges of the whisker may be imaged in the TEM. Thus, it is difficult to draw conclusions about the entire whisker thickness.

Electron backscatter diffraction (EBSD) in the scanning electron microscope (SEM) has become a common technique used to investigate the crystallographic orientation or the texture of crystalline materials. EBSD has been shown to be useful in the study of whiskers, nano-rods and nano-wires. EBSD has been used to characterize the growth direction of whiskers of GaN nanowires by suspending the wires in a liquid and then dispersing the liquid containing the nano-wires onto a suitable substrate and allowing the liquid to evaporate (Motayed et al., 2006); (Long et al., 2007); (Motayed et al., 2007). It has also been used to characterize the growth axis of Sn-whiskers (Hutchinson et al., 2004). This approach suffers the same disadvantage as the previously discussed TEM approach as the relationship with the growth substrate cannot be determined. However, larger diameter whiskers can be easily studied.

In this paper we will discuss three methods that use EBSD for characterizing whisker growth on substrates. One of the three methods requires the whiskers to be removed from the growth substrate. The other two techniques allow the whisker to be studied in-situ, so that the crystallographic growth axis and the physical angle that the whisker makes with respect to the sample surface are determined. These latter two techniques provide significantly more information that is useful for isolating whisker growth mechanisms. This paper will introduce these three techniques and demonstrate their use through the analysis of whiskers formed on Sn electroplated surfaces.

3.3 MATERIALS AND METHODS

EBSD was carried out in a Zeiss Supra55VP field emission SEM. The SEM was equipped with an Oxford/HKL Nordlys II EBSD detector and the patterns were analyzed with Oxford/HKL Channel 5 software. The SEM was operated at 15 or 20 kV and with a beam current of 5nA. The accelerating voltage was selected to optimize the pattern quality as higher quality patterns could be obtained from thinner whiskers at lower voltages. Each of the techniques discussed here for the crystallographic analysis of whiskers requires the sample to be imaged with no tilt and then tilted to a high angle (~70º) for analysis. The requirement to view the sample at multiple tilts does not allow for the use of a pre-tilted sample holder. In addition, imaging of a whisker while still attached to the substrate at two tilt angles, allows for accurate measurement of whisker length and the physical growth angle with respect to the substrate.

Sample mounting varied depending on the characterization method that was to be used. One technique requires the whiskers to be removed from the substrate. In this study a TEM grid with an attached thin carbon support film was simply rubbed over the sample surface with whiskers. Some of the whiskers lie flat and adhere to the carbon film. The TEM grid with the support and the whiskers is then mounted on a standard SEM stub for EBSD analysis. Alternative methods did not require the whiskers to be removed from the substrates so these test coupons were mounted on standard SEM sample stubs for EBSD characterization.

EBSD of whiskers can be more challenging than comparable analyses of polished samples. One of the main issues is the acquisition of the flat-field image that is used to enhance the contrast in the EBSD patterns. The most difficult case for flat-field collection is for whiskers removed from the substrate and mounted on a thin carbon support film. In this case the copper grid is useful for the flat field acquisition, although this is not as good as using a flat field image obtained from the actual whisker material as the intensity distribution depends on the atomic number of the target material. When the whiskers are not removed from the substrate, the shadowing caused by nearby whiskers can be an issue and these shadows can be mistaken by the automatic band recognition software and this may result in patterns that cannot be indexed automatically or incorrect pattern indexing. When this happens the bands must be carefully selected manually to ensure that whisker shadows are not mistaken for bands in the patterns.

Crystallographic analysis of whiskers is best done by single point analysis and not in mapping mode where the beam is scanned over the sample pixel-by-pixel. Care must be taken in collecting patterns from individual free standing whiskers as the angle of the whisker with

respect to the tilt angle of the sample varies. It is generally possible to obtain patterns from whiskers by carefully varying the beam position on the whisker surface until the EBSD pattern is optimized. The electron beam was placed on various points along a whisker and EBSD patterns were collected at each point. Identical patterns along the whisker axis indicated that each whisker was a single crystal. Once the whisker was determined to be a single crystal, a pattern was collected and indexed. The orientation information for each indexed pattern was stored.

Once the EBSD patterns are indexed, the data is visualized using pole figures (actually stereographic projections showing *directions*, not poles) or inverse pole figures (again, showing *directions*) depending on how the data was collected. Alternatively, the orientation matrix is used to quantitatively determine the whisker orientation. The orientation matrix is a 3 x 3 matrix where the columns are made of the direction cosines that are the angles the primary unit axes of the crystal unit cell make with the sample coordinate system. In the orientation matrix the columns represent the directions with respect to the X, Y, or Z directions respectively. Additional matrix transformations may be required. (Young and Lytton, 1972); (Bunge, 1982).

3.4 DISCUSSION OF EBSD METHODS FOR ANALYZING WHISKERS

3.4.1 Method 1 - Whiskers removed from substrate

A straightforward way to obtain information about the growth axis of the whisker is to remove it from the substrate. This can be done in a number of ways as discussed previously (Hutchinson, 2004); (Motayed et al., 2006); (Long et al., 2007); (Motayed et al., 2007). The sample with the whiskers was imaged at normal incidence and rotation of the sample stage allowed the long axis of the whisker to be carefully aligned with the tilt axis of the SEM. The sample must then be tilted to the high tilt required for EBSD as shown in Figure 3.2 where the sample is tilted to 70º. This sample manipulation is easier if the SEM is equipped with some form of eucentric tilting so that the whisker of interest is not lost during sample tilting. It is often difficult to ensure that the whisker is perfectly flat on the substrate so this can introduce some errors into the growth axis determination. Accuracy of the whisker axis determination depends on how accurately the whisker is aligned with the tilt axis of the SEM and the way the whisker lies on the support material. The accuracy of absolute orientations determined by EBSD is dependent on the sample fixturing, but typical accuracy of about 1º is relatively easy to achieve.

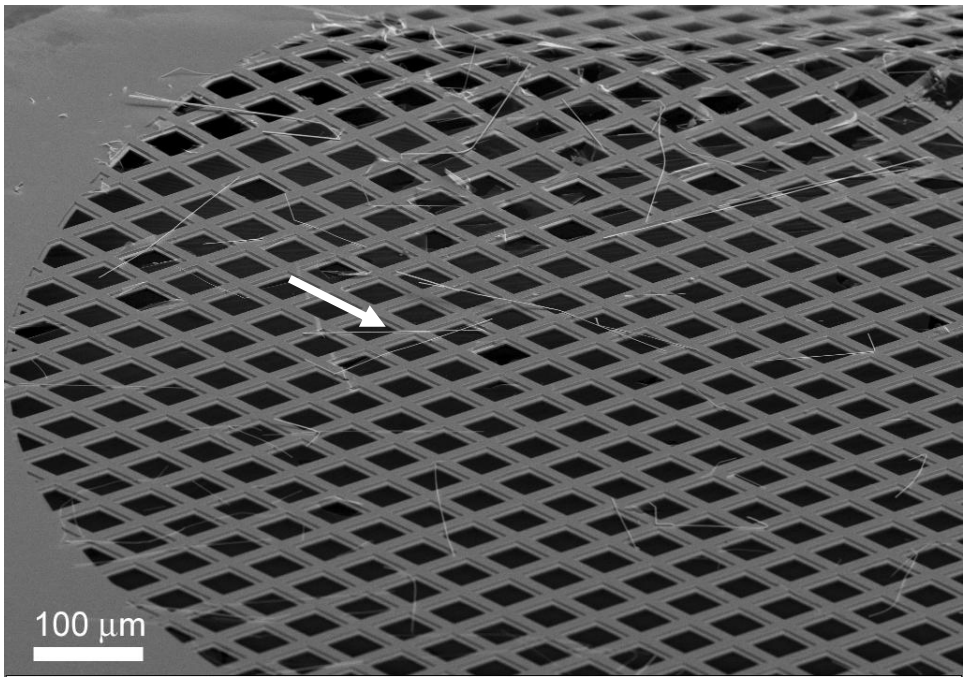

Figure 3.2. SEM image of Sn whiskers mounted on a carbon coated TEM support grid. The arrowed whisker is oriented correctly for EBSD.

Once the sample is tilted, EBSD patterns can then be acquired from the whisker and the pattern is indexed. Figure 3.3 shows a schematic construction of the stereogram for this geometry. The alignment of the whisker growth axis allows a much easier interpretation of the resulting orientation as the growth axis of the whisker must lie in the inverse pole figure plotted with respect to the x-direction. There are two possible ways to obtain the growth direction of the whisker, one using stereograms or inverse pole figures and one by inspection of the orientation matrix produced by the EBSD pattern indexing software. If the whisker is aligned with the tilt axis, the simplest approach to determining the crystallographic growth axis is to plot an inverse pole figure that corresponds to the tilt axis direction. Thus, if the tilt axis corresponds to the x-axis of the EBSD system, the inverse pole figure with respect to the x-axis should be plotted. The position of the direction plotted in the inverse pole figure indicates the long axis (or the growth axis) of the whisker. One can also plot stereographic projections for a variety of specific crystallographic directions. A quantitative method is to examine the orientation matrix and select the row or the column of the matrix that represents the direction of the whisker long axis.

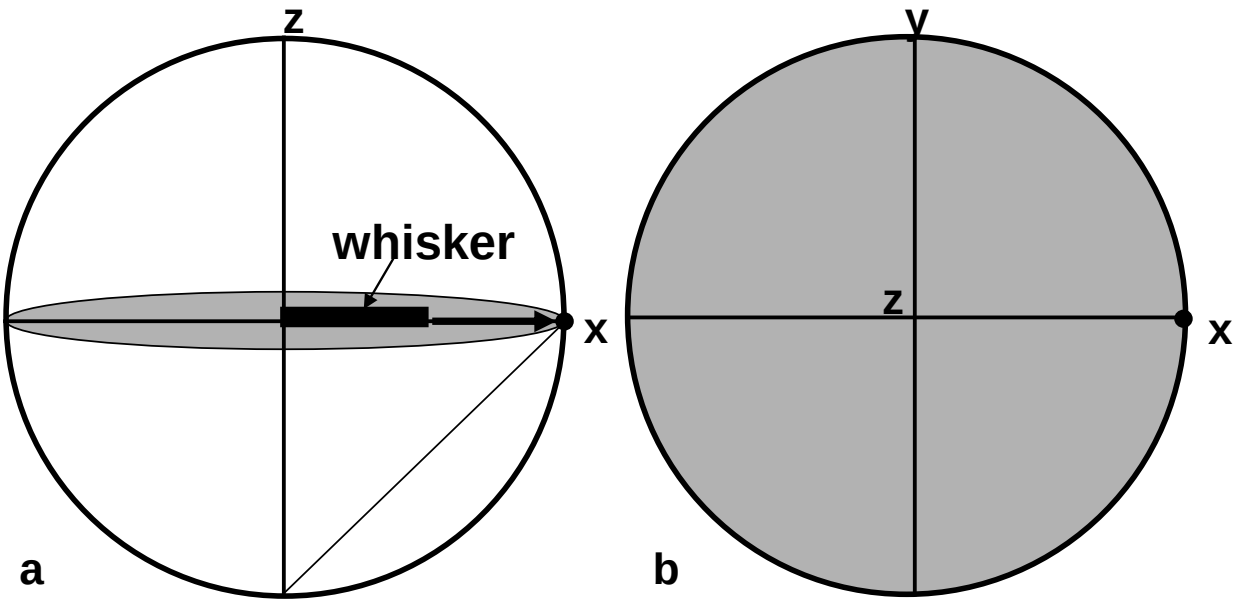

Figure 3.3. Schematic diagram of whisker orientation for Method I a) geometry of whisker on a TEM grid, b) corresponding stereographic projection.

Figure 3.4 is an inverse pole figure with respect to the x-direction (in the case of the Zeiss SEM this is parallel to the tilt axis) with crystallographic directions from the whisker shown in Figure 3.2 plotted. Note that two patterns from different positions on the whisker were collected. It is immediately apparent that the growth direction of the whisker is near <001>. A matrix that describes the crystallographic directions associated with the SEM stage axes for the whisker shown in Figure 3.2 is:

$$\begin{array}{c} \\ u \\ v \\ w \end{array} \begin{array}{c} \begin{array}{ccc} X & Y & Z \end{array} \\ \begin{bmatrix} -0.0162 & 0.1386 & 0.1002 \\ 0.0086 & -.5813 & 0.8121 \\ 0.3137 & 0.1056 & 0.0045 \end{bmatrix} \end{array}$$

As the whisker long axis coincides with the x-axis of the microscope (the first column of this matrix), inspection of the orientation matrix shows that the growth axis <uvw> is <-162 86 3137> which is 6.1º from <001>. This is the same result obtained from the inverse pole figure shown in Figure 3.4. This matrix is not orthogonal as it describes the crystallographic direction <uvw> for a non-cubic unit cell. Note that the deviation from <001> is due to the errors in the physical orientation of the whisker on the support film within the SEM.

The advantage of this method is mostly speed and ease of visualization of the growth direction as many whiskers can be analyzed in a short period of time and the data can be presented without any further mathematical operations. This technique only requires the whisker to be aligned when the sample is normal to the electron beam, which also allows a direct measurement of the

whisker length. As Figure 3.4 demonstrates, the whisker axis is easy to identify and visualize using inverse pole figures. Disadvantages of this technique are mainly related to the fact that the whiskers must be removed from the native growth substrate for analysis resulting in bent whiskers and inaccurate physical orientation of the whiskers on the support film. This of course causes any relationship with the growth surface to be lost and also thin whiskers may be bent or mechanically damaged during removal to the whisker support.

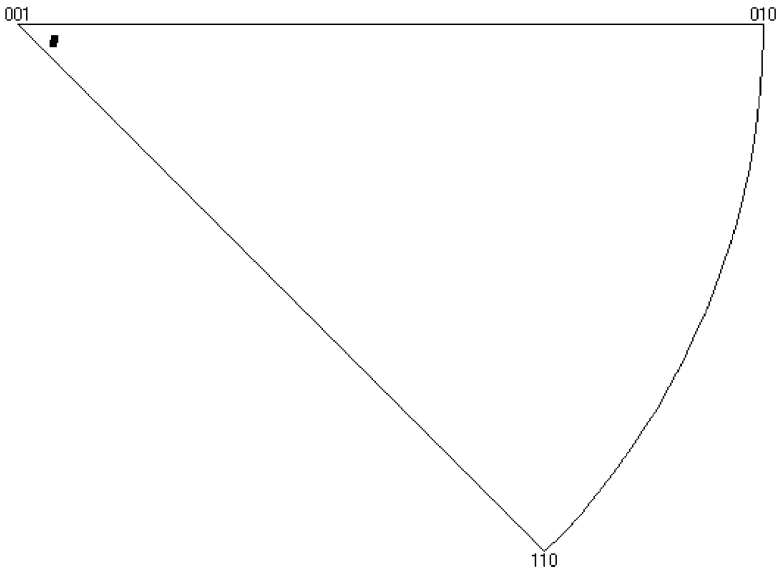

Figure 3.4. Inverse pole figure (with directions plotted, not poles) with respect to the tilt axis of the SEM. Two EBSD orientation measurements of the whisker from Figure 3.2 are shown. Note that the orientations are close to the <001> direction.

3.4.2 Methods II and III - Whiskers Examined in-situ on Substrate

Method II

There are two methods that are used to determine the growth axis of whiskers that have not been removed from the substrate. The selection of either of these methods depends on the details of the information needed and the way that information is to be displayed. Method II relies simply on the known whisker spatial orientation (the long axis of the whisker aligned with a known direction in the SEM) and inspection of a variety of stereographic projections to determine the growth axis and the angle of the whisker with respect to the normal to the surface. In this method, the projected length of the whisker is aligned with the direction parallel to the tilt axis of the SEM stage, identical to method I, except that the projected whisker length is used, as the whiskers attached to the substrate are generally inclined with respect to the substrate. The sample is then tilted to the appropriate angle for EBSD and patterns are then acquired from the whisker and indexed. Stereogram construction for method II is shown in Figure 3.5. As a result of aligning the projected long axis of the whisker with the X-axis of the SEM stage, the whisker growth axis is located on the equator of the stereogram and the angle of the whisker with respect to the surface normal is measured from the center of the stereogram to the plotted direction that represents the whisker growth axis. The angle with respect to the sample surface (90-θ) is

measured from the x-direction, the far right side of the stereogram. A variety of stereographic projections that represent expected growth axes is needed and must be carefully inspected to ensure that the whisker growth axis was correctly identified. Whiskers with high index or irrational growth directions may be difficult to characterize with method II as the appropriate stereogram may not have been plotted. Sn whiskers used to demonstrate this method are shown in Figure 3.6. Figure 3.6a is an image of the whiskers with the electron beam normal to the sample surface and the whiskers aligned with the tilt axis of the SEM. Figure 3.6b is an image of the same whiskers after tilting to 70^{o} for the acquisition of EBSD patterns. EBSD patterns are obtained from the whiskers and then indexed. Stereograms for <100> and <001> are shown in Figure 3.6c where the growth directions are indicated and as expected they fall on the equator of the stereographic projection. The number of points on each stereogram is due to multiplicity and the fact that axes for both whiskers are shown on the stereograms. The angle of the whisker with respect to the sample surface can be determined by measuring the angle from the x-direction to the specific plotted direction that falls on the equator of the pole figure. Thus, in this case there are two whiskers analyzed and the whiskers have <001> and <100> growth directions for whiskers 1 and 2 respectively. It is perhaps surprising that two nearby whiskers with nearly the same physical angle with respect to the surface have grown with different crystallographic orientations.

The use of this method is limited to whiskers that have predictable low index growth directions. For whiskers with higher index or random growth directions it would be quite difficult to plot a sufficient number of stereographic projections to allow the correct direction to be identified. This method also suffers in comparison with the other methods discussed in this paper in that inverse pole figures cannot be used directly to view the growth directions of the whiskers.

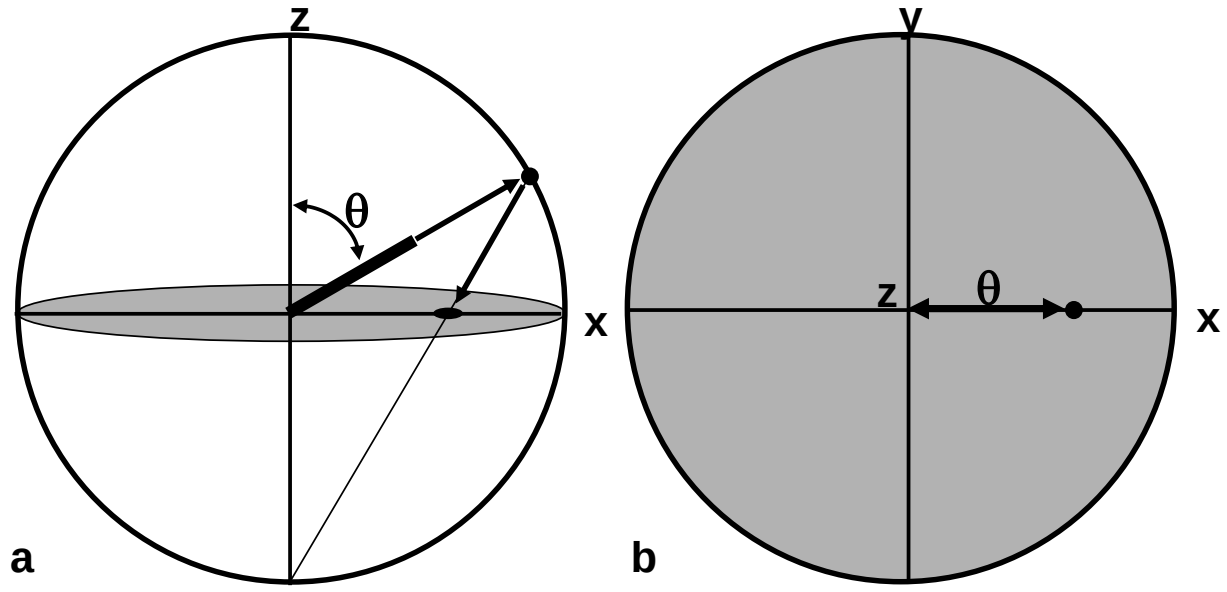

Figure 3.5. Schematic of whisker orientation for method II a) geometry of whisker intact on the growth substrate and b) corresponding stereographic projection construction of directions.

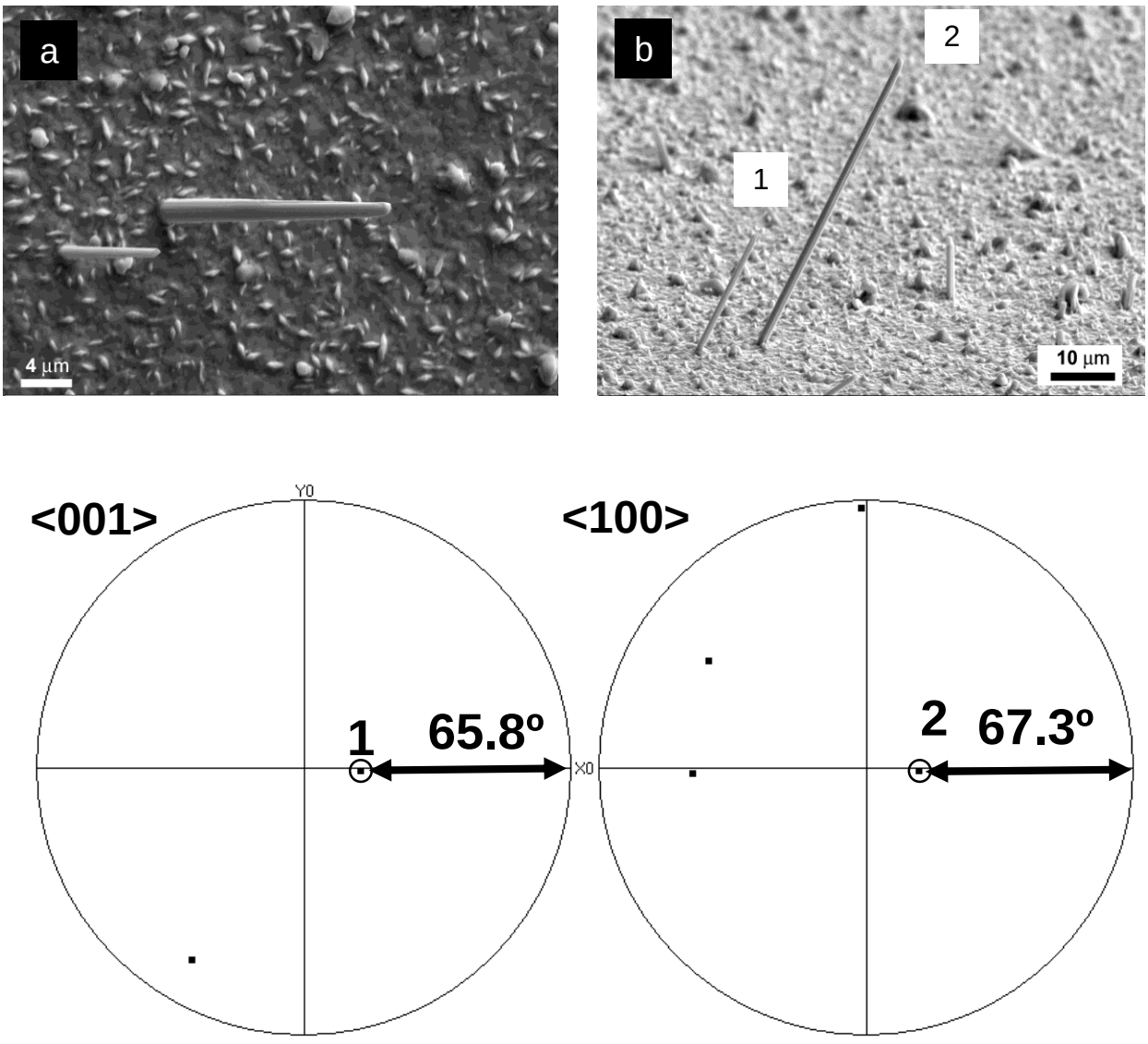

Figure 3.6. Orientation of Sn whiskers determined using method II a) SEM image of two Sn whiskers aligned with their projected length parallel to the tilt axis of the SEM. b) Same two whiskers after tilting to 70º c) <001> and <100> stereograms show the growth axis of the whiskers labeled 1 and 2 in figure 3.6b. Multiple directions are a result of plotting both whiskers on both stereograms and multiplicity of directions.

Method III

The most quantitative method that can be used to determine the growth axis of the whisker combines the previous in-situ method with a quantitative measurement of the angle of the whisker with respect to the surface normal and then the use of this measured angle to rotate the

orientation matrix so that the growth direction coincides with one of the primary axes of the pole figure. Tilting the sample results in an apparent motion of the tip of the whisker with respect to the sample substrate, or parallax, and this motion is used to measure the height of the whisker tip above the substrate surface. The measurement of the whisker length and the apparent distance from the tip of the whisker to the sample surface allow the angle of the whisker with respect to the surface normal to be measured independently of the crystallography. Figure 3.7 shows a schematic of the geometry used to calculate both the true whisker length and the angle of the whisker with respect to the sample surface when the whisker projection is aligned along the tilt axis of the SEM. Others have reported on tilting techniques to measure feature heights in the SEM, but the alignment of the long axis of the whisker with the tilt axis greatly simplifies the crystallographic visualization and the calculation of the whisker length and physical growth angle (Goldstein et al., 2003) ; (Panashchenko and Osterman, 2009). The whisker of interest is imaged with the electron beam normal to the substrate surface as before. The projected length of the whisker (view 1 of length *ab* in Figure 3.7) is measured and recorded. The sample is tilted to the appropriate angle for EBSD (ω in Figure 3.7) and an EBSD pattern is recorded and indexed. The apparent distance (view 2 of length *cb* in Figure 3.7) from the whisker tip in the tilted condition to a horizontal line through the whisker base is recorded. The actual whisker length (distance *ad* in Figure 3.7) is then given by geometry to be:

$$length = ad = \sqrt{ab^2 + \left(\frac{cb}{\sin(\omega)}\right)^2} \qquad 3.1$$

The angle (θ in Figure 3.7) that the whisker makes with respect to the sample surface is given by:

$$angle = \theta = ArcTan\left(\frac{\frac{cb}{\sin(\omega)}}{ab}\right) \qquad 3.2$$

Figure 3.8 shows the whiskers from Figure 3.6 with the required measurements superimposed on the images. The projected length of the whisker is aligned with the horizontal, which coincides with the tilt axis of the SEM. The projected length of the whisker is 21.56 μm. The displacement of the tip of the whisker with respect to the base after tilting is measured as shown to be 43.5 μm. The length of the whisker is then:

$$length = \sqrt{21.56^2 + \left(\frac{43.5}{\sin(70)}\right)^2} = 51.1\mu m$$

The angle of the whisker with respect to the surface normal is then:

$$90 - \theta = 90 - ArcTan\frac{43.5\mu m}{21.56\mu m} = 26.4°$$

It is now possible to plot a variety of stereographic projections for different crystallographic directions to determine which direction falls on the equator of the stereogram with an angle from the surface normal of 26.4º or 63.6 º from the surface. This method is more definitive than the in-situ method (Method II) discussed previously because the angle of the growth axis with respect to the x or z axis of the stereogram is known. However, a variety of stereographic projections must still be plotted in order to select the correct growth direction.

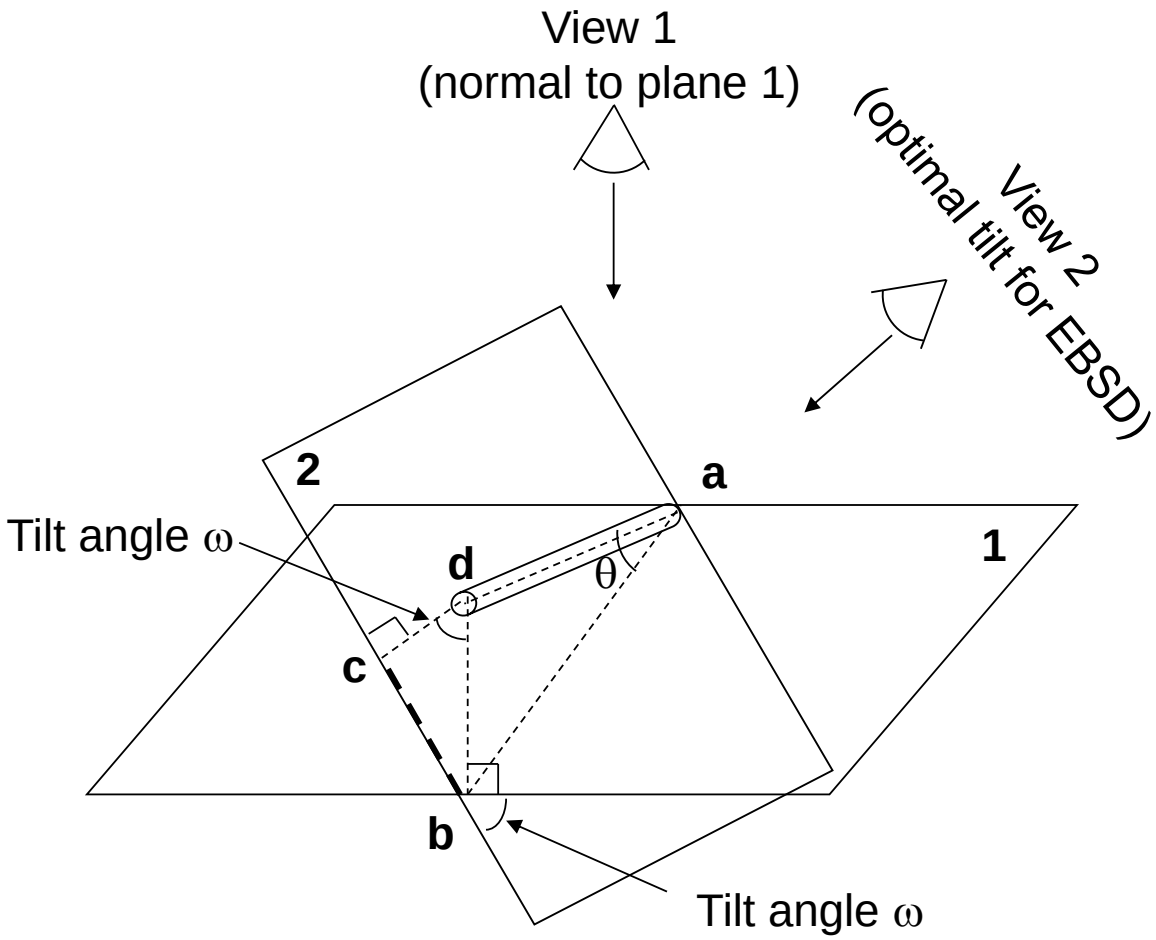

Figure 3.7. Schematic diagram of the geometry and the views of a whisker in the untilted and tilted conditions. View 1 is for the untilted whisker and view 2 is once the whisker is tilted for EBSD. Refer to the text for how the whisker length and angle from the substrate are determined.

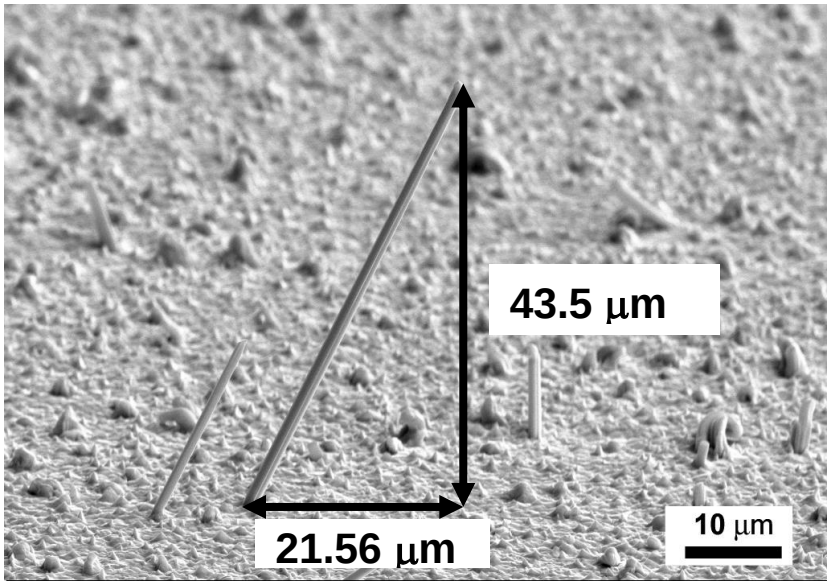

Figure 3.8. Measurements of a Sn whisker after tilting required for the calculation of the true whisker length and the growth angle with respect to the substrate.

A more quantitative result can be obtained from the orientation matrix (OM) that is calculated by indexing the EBSD pattern. The columns of the orientation matrix represent crystallographic directions with respect to the x, y and z frame of reference for the microscope where x is a direction parallel to the tilt axis of the stage and z is the direction that represents the surface normal. If the sample crystallography is cubic, then the orientation matrix may be used directly. For samples with non-cubic crystallography, the orientation matrix must be presented in ortho-normal space. This is accomplished by multiplying the orientation matrix by the transformation matrix given by (Young and Lytton, 1972):

$$T = \begin{bmatrix} a & b\cos\gamma & c\cos\beta \\ 0 & b\sin\gamma & c(\cos\alpha - \cos\beta\cos\gamma)/\sin\gamma \\ 0 & 0 & c(1+2\cos\alpha\cos\beta\cos\gamma - \cos^2\alpha - \cos^2\beta - \cos^2\gamma)^{1/2}/\sin\gamma \end{bmatrix} \quad 3.3$$

Where a, b, c are the unit cell lengths and α, β and γ are the angles between the unit cell axes. Note that for crystals with orthogonal axes (cubic, tetragonal and orthorhombic) the above matrix reduces to:

$$T = \begin{bmatrix} a & 0 & 0 \\ 0 & b & 0 \\ 0 & 0 & c \end{bmatrix} \quad \text{(For tetragonal structures, a=b}\neq\text{c)} \quad 3.4$$

Thus, the transformation to ortho-normal coordinates is given by:

$$OMortho = T * OM \qquad 3.5$$

To accurately determine the growth axis of a whisker, a rotation matrix is applied to the orientation matrix to bring a selected axis in coincidence with the microscope frame of reference. In this work, the projected length of the whisker was aligned with the tilt axis (or the x-axis) of the microscope. A rotation about the y-direction by the angle of the whisker with respect to the surface normal will bring the growth axis direction in coincidence with the z-direction or the surface normal. This rotation is accomplished by a matrix multiplication of the orientation matrix by the rotation matrix corresponding to a rotation about the y-axis or (Young and Lytton, 1972):

$$OMrot = OMortho \begin{bmatrix} \cos\theta & 0 & -\sin\theta \\ 0 & 1 & 0 \\ \sin\theta & 0 & \cos\theta \end{bmatrix} \qquad 3.6$$

Where θ is the angle of the whisker with respect to the surface normal, OMortho is the ortho-normal matrix calculated from the OM and OMrot is the rotated ortho-normal orientation matrix. The crystallographic growth direction of the whisker is then represented by the third column of the matrix. OMrot must be multiplied by the inverse of the transformation matrix to allow the growth direction to be represented as direction indices with respect to the given unit cell.

The larger whisker shown in Figure 3.8 will be used to demonstrate this technique. As shown the use of parallax measurement determined that the whisker growth direction is 63.6 º from the sample surface and this measurement compares well with the measurement from the <100> stereogram shown in Figure 3.6c of 67.3 º. If we follow the steps outlined above to rotate the OM so that the growth direction is aligned with the sample normal (or Z direction in this case) we obtain the directions <uvw> parallel to the x, y and z axes of the SEM stage as shown in the non-orthonormal matrix :

$$\begin{array}{c} \quad X \qquad\quad Y \qquad\quad Z \\ \begin{array}{c} u \\ v \\ w \end{array} \begin{bmatrix} 0.0127 & 0.033 & 0.1713 \\ 0.1453 & -0.0912 & -0.009 \\ 0.1667 & 0.2673 & -0.0175 \end{bmatrix} \end{array}$$

Thus, the exact growth direction is given by the third column of the OM or <1713 -9 -175> which is 4.3º from <100>. After rotation in this manner the results can be plotted on an inverse pole figure with respect to the z-direction to show the growth axes of the whiskers analyzed.

Figure 3.9a is an inverse pole figure with respect to the z-direction (sample normal) for the rotated OM for the whisker shown in Figure 3.8. Note that the point on the inverse pole figure plot falls close to the <100> direction (note that in tetragonal systems that <100> is equivalent to <010>) as was calculated by rotating the orientation matrix. Note that the growth axis near <100> is the same result that was shown in Figure 3.6c, where the angle of the whisker with respect to the surface was not measured.

Sn whiskers have been shown to grow from grains embedded in the plated layer and there is no grain boundary between the grain and the whisker. Thus, with this technique we are also able to associate the crystallographic growth direction of the whisker with the crystallographic surface normal of the parent grain and this direction is obtained from the original orientation matrix of the whisker before mathematical rotation. Figure 3.9b is an inverse pole figure with respect to the z-direction (surface normal) for the whisker shown in Figure 3.8. This technique now allows a direct comparison of the crystallographic growth axis, the angle of the whisker with respect to the surface normal and the orientation of the parent grain to be determined for a large number of whiskers.

The main disadvantage to this technique is the time required to obtain the projected length of the whisker and then the measurement of the whisker parameters when tilted. The sample manipulations required to achieve this are time consuming and extremely difficult if a non-eucentric SEM stage is used. Due to this constraint, only about 40 whiskers can be analyzed in this manner in 8 hours. This technique is the only one that provides quantitative measurements of the growth axis and the angle of the whisker with respect to the sample substrate. Thus, if the relationship with the substrate is important or thought to be important, measurement of the angle of the whisker followed by rotation of the OM is the most quantitative method and is recommended.

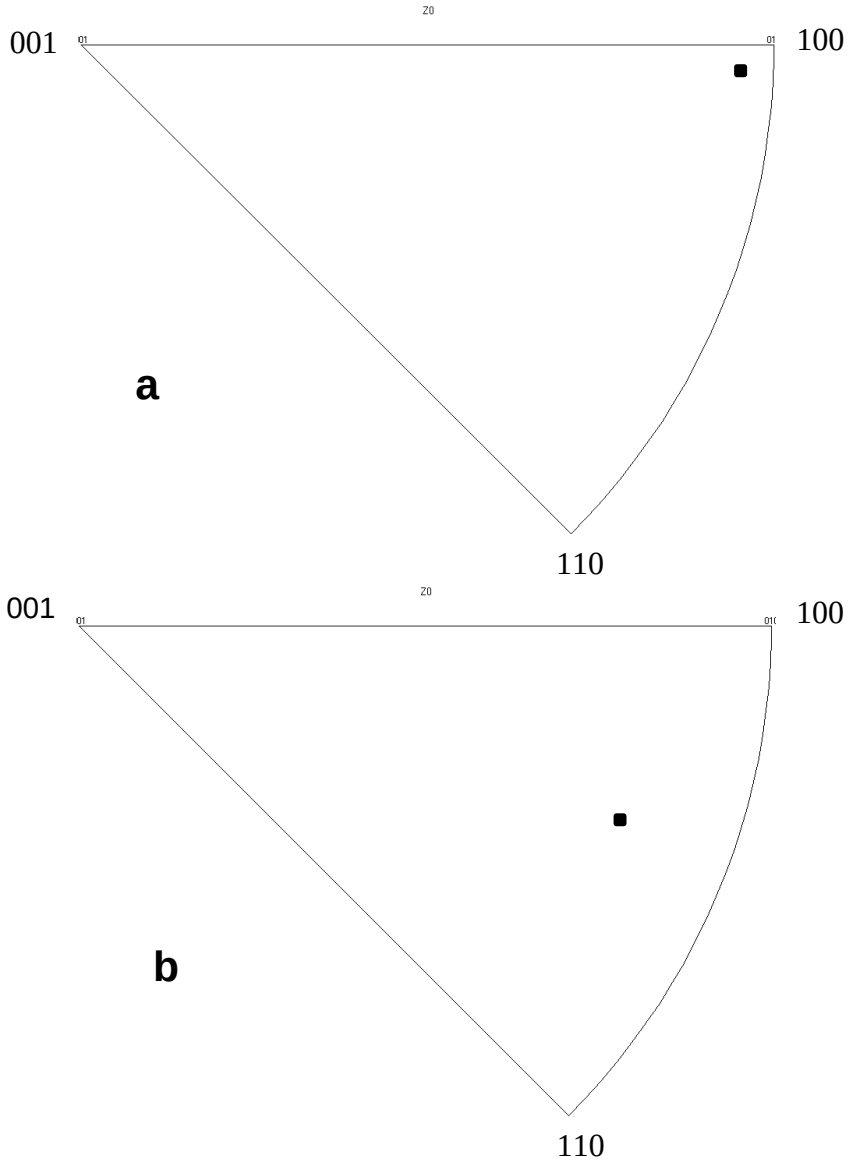

Figure 3.9. Inverse pole figures (with directions plotted, not poles) for the whisker shown in Figure 3.8. a) Inverse pole figure for the rotated orientation matrix for the whisker shown in Figure 3.8 plotted with respect to the whisker growth direction. The growth axis is shown as close to the <010> direction. b) Inverse pole figure with respect to the surface normal before matrix rotation.

3.5 SUMMARY

This paper has described three methods to determine the growth axis of whiskers using EBSD and these techniques have been demonstrated using Sn single crystal whiskers that were grown on pure Sn electroplating. The simplest and quickest method involves removal of the whiskers from the substrate and mounting them on a suitable support. The whisker is then rotated and tilted within the SEM and an EBSD pattern is collected and analyzed. The whisker orientation is then determined from an inverse pole figure or the whisker axis can be determined more exactly from the corresponding orientation matrix. This method has proven to be fast and reliable, but one has to keep in mind that whisker damage may occur during removal and that all information about the physical relationship of the whisker to the substrate is lost.

The most accurate method that does not lose the physical relationship of the whisker to the substrate is method III. Here the projected whisker length is aligned with the tilt axis of the SEM. Following tilting, additional measurements are obtained so that the angle of the whisker with respect to the substrate can be calculated. At the same tilt angle EBSD patterns from the whisker are obtained and indexed to yield an orientation matrix. Matrix rotations are then used to rotate the orientation matrix so that the whisker axis corresponds to one of the primary axes (x, y, z) which in the example shown here was the z-axis. This method has numerous advantages as it is quantitative, the results can be shown on an inverse pole figure (as plotted directions), and finally the relationship of the whisker with respect to the substrate is maintained. The main disadvantage to this technique is that it is time consuming. However, if the relationship of the whisker to the substrate is important, this method is the only one to provide that information.

3.6 ACKNOWLEDGEMENTS

The authors would like to thank Graham Yelton of Sandia National Laboratories for the electroplated samples. Sandia National Laboratories is a multi-program laboratory operated by Sandia Corporation, a wholly owned subsidiary of Lockheed Martin Company, for the U.S. Department of Energy's National Nuclear Security Administration under contract DE-AC04-94AL85000.

3.7 REFERENCES

Boettinger, W. J., Johnson, C. E., Bendersky, L. A., Moon, K.-W., Williams, M. E., and Stafford, G. R.(2005). Whisker and Hillock Formation on Sn, Sn-Cu and Sn-Pb electrodeposits, *Acta Mat*. **53**, 5033-5050.

Bunge, H. –J. (1982) *Texture Analysis in Materials Science*, pp 3-19, Butterworths, Boston.

Goldstein, J. I., Newbury, D. E., Joy, D. C., Lyman, C. E., Echlin, P., Lifshin, E., Sawyer, L. and Michael, J. R.(2003). *Scanning Electron Microscopy and X-Ray Microanalysis*, pp 217-220. Kluwer Academic/Plenum Publishers, New York.

Hutchinson, B., Oliver, J., Nylen, M. and Hagstrom, J.(2004). Whisker growth from Tin coatings, *Materials Science Forum*, **467-470**, 465-470.

Long, J. P., Simpkins, B. S., Rowenhurst D. J. and Pehrsson, P. E.(2007). Far-field imaging of optical second-harmonic generation single GaN nanowires, *Nano Lett*. **7**, 831-836.

Luborsky F. E., Koch, E. F. and Morelock, C. R. (1963). Crystallographic orientation and oxidation of submicron Whiskers of iron, iron-cobalt and cobalt, Journal of Applied Physics **34**, 2905-2909.

Morris, R. B. and Bonfield, W.(1974). The crystallography of alpha-tin whiskers, Scripta. Met. **8**, 231-236.

Motayed, A., Daydov, A. V., Vaidin, M., Levin, I., Melngailis, J., He, M. and Mohammad, S. N.(2006). Fabrication of GaN-based nanoscale device structures utilizing focused ion beam induced Pt deposition, *J. Appl. Phys*. **100**, 024306-1.

Motayed, A., Vaidin, M., Daydov, A. V., Melngailis, J., He, M. and Mohammad, S. N.(2007). Diameter dependent transport properties of gallium nitride nanowire field effect transistors, *Appl. Phys. Lett*. **90**, 043104-1.

Panashchenko, L. and Osterman, M. (2009). Examination of Nickel Underlayer as a Tin Whisker Mitigator, IEEE 59th Electronic Components and Technology Conference **1-4**, 1037-1043.

Young, C. T. and Lytton, J. L.(1972). Computer generation and identification of Kikuchi patterns, J. Appl. Phys. **43**, 1408-1417.

4. THE CRYSTALLOGRAPHY OF SN WHISKERS

J.R. Michael, B.B. McKenzie, and D.F. Susan

4.1 Abstract

The crystallography of tin whiskers was studied using electron backscatter diffraction (EBSD). A statistical sampling of ~140 whiskers was performed on several Sn-plated copper specimens using techniques previously developed.[1] The analysis showed that the whiskers are single crystals and the major crystallographic growth directions were determined to be the following low index directions in beta Sn (tetragonal crystal structure): <001>, <100>, <101>, and <111>. No simple relationship was found between the crystallography of a whisker and the orientation of the grain from which it had grown. As a result, there is no simple relationship between the physical growth angle of the whisker (with respect to the substrate) and its crystallography. The overall textures of the Sn films in this study were also determined by both EBSD and x-ray diffraction (XRD). No simple relationship was found between the predominant crystallographic whisker growth directions and the film texture. Although the films were not highly textured, the whiskers generally grew from grains that did not correspond to the major textures in the film. Kinked whiskers are also single crystals with the kink angles corresponding to the possible angles between the crystallographic directions in Sn. Whiskers can kink and continue growing in an equivalent crystallographic direction (homogeneous kink) or they can grow in a different crystallographic direction after the kink (heterogeneous kink). Only a few kinked whiskers were analyzed and they were mostly of the heterogeneous type. The literature on the crystallography of Sn whiskers was reviewed in light of the results of the present study.

4.2 BACKGROUND

Recent efforts to reduce lead (Pb) in microelectronics have increased the use of pure tin (Sn) finishes that may be prone to the formation of whiskers. The whiskers can grow to lengths that can cause shorting of closely spaced electrical conductors.[2] As part of many characterization studies of Sn whiskers, authors have examined their crystallography using EBSD, transmission electron microscopy (TEM), and other techniques (Table 4.1). A review of the literature pertaining to Sn whisker crystallography is presented in the following section.

In previous work, SEM/EBSD methods were developed to accurately determine the crystallography of whiskers, their physical growth angle, and the crystallography of the "parent grain" from which the whisker is growing (the parent grain is the "whisker grain"). Details of the techniques are given in Reference [1]. The method employed here involves aligning the projected whisker length with the tilt axis of the SEM. Following tilting, additional measurements are obtained so that the angle of the whisker with respect to the substrate can be calculated. At the same tilt angle, EBSD patterns from the whisker are obtained and indexed to yield an orientation matrix. Matrix rotations are then used to rotate the orientation matrix so that the whisker axis corresponds to one of the primary axes (x, y, z), for example the z-axis parallel to the SEM column. This rotate-tilt-EBSD procedure was repeated for over 140 "straight" (not kinked) Sn whiskers. The objective was to determine a statistically meaningful sampling of Sn

whisker crystallography. Kinked Sn whiskers were also examined. The individual straight segments of a few kinked whiskers were analyzed in the same way as described above. The kink angles were correlated to the possible angles between crystallographic directions in beta Sn (beta tin is body centered tetragonal, a= 0.582 nm and c=0.318 nm).

4.2.1 Review of Literature on Tin Whisker Crystallography

Table 4.1 contains a list of references that reported at least some crystallographic information on Sn whiskers. Before discussing some of the individual investigations, a few general comments will be made concerning these previous studies. First, most studies reported the analysis of a few Sn whiskers, with the maximum number analyzed in any one investigation being ~26. In general, this is because the techniques used at the time were very labor intensive and time consuming, e.g., TEM analysis or XRD of individual whiskers. For many papers the main objective was not whisker crystallography – it was simply reported as part of a TEM or SEM/EBSD analysis of other whisker characteristics. Hence, many authors report the crystallography of only one, two, or three whiskers. There are likely many other papers, not reported here, that contain incidental crystallographic information on Sn whiskers.

Second, most researchers report only the crystallographic growth directions of the whiskers themselves. In a few cases, XRD was also performed to determine the overall texture of the Sn film. There are many other references where XRD textures were determined for films growing whiskers, but they did not specifically report individual whisker crystallography so they are not included here. Only two other reports were found in which the crystallography of the "parent" Sn grain was determined. The parent grain is the same grain as the whisker itself, that is, there are no grain boundaries separating the part of the whisker above the Sn surface and the grain within the Sn film from which it is growing. In contrast to the whisker itself (for which the growth direction is usually reported), the crystallography of the parent grain can be thought of as the orientation of the grain, with respect to the surface normal, that would be reported if no whisker was present. Therefore, the determination of this parent grain crystallography is equivalent to determining the orientation of the whisker with respect to the surface normal of the film. The parent grain information is useful for comparison to the Sn film texture. In part, the reason why this information is not more widely reported is that whisker removal from the substrate was commonly part of the analysis techniques. With whisker removal, any information from individual whiskers relative to the substrate is lost.

Third, many researchers report low index growth directions such as <100>, <101>,<001>, etc. However, there are a few reports of other, higher index, crystallographic growth directions such as <123>, <211>, and others. One of the objectives of the present work is to determine the crystallographic growth directions for a larger number of whiskers to eliminate some of the ambiguity that arises when surveying the previous work.

Table 4.1. Sn whisker crystallography references.

Whisker Growth Direction	"Parent" whisker grain orientation	number of whiskers analyzed	Film Texture (Primary, secondary, tertiary)	Reference
<100>, <101>, <001>		13		Treuting and Arnold, 1957 [3]
<001>, <100>, <101>, <111>		~12		Smith and Rundle, 1958 [4]
<100>, <001>, <101>, <123>, <111>		?		Ellis et al., 1958 [5]
<111>, <101>, <211>		4		Powell and Skove, 1963 [6]
<001>, <100>, <101>, <111>		8		Ellis, 1966 [7]
<101>, <100>, <012>		3		Ellis, 1967 [8]
<100>, <210>, <101>, <001>, <110>		~20-30		Morris and Bonfield, 1974 (removal technique, TEM) (squeeze method) [9]
<100>	(220), (420), (620) (420), (501), (321) calculated	5 (crystallography) 25 (growth angle)	(200) (0.5 A/dm2) (220) (3.5 A/dm2)	Lee and Lee, 1998 [10]
<001>		1+		Sheng et al., 2002 [11]

<001>	<210>	1+	<321>	Choi et al., 2003 [12]
<110>, <103>, <321>		3?		Lebret and Norton, 2003 (sputter deposited Sn) [13]
<001>, <100>, <101>, <111>, <123> (2)		11	(111) weak	Hutchinson et al., 2004 (removal method) [14]
<110>, <111>, <100>		>26	(552), <001>, (110), (112), (102) (all are weak textures)	Frye, Galyon, and Palmer, 2007 [15]
<001>		1		Chiu and Lin, 2009 [16]
<001>		1		Cheng and Vianco, 2010 (hillock) [17]

Early studies of Sn whiskers employed X-Ray diffraction techniques.[3-8] In the 1950s, Treuting and Arnold [3] determined that Sn whiskers grew with low-index crystallographic directions. They analyzed several "spontaneous" whisker types (Sn, Cd, Zn) as well as whiskers grown from vapor and generally found low-index growth directions for all whisker types. Smith and Rundle [4] studied Sn whiskers, specifically, using XRD analysis and found the same low-index directions. Of note, the authors commented that these low-index directions are not all equally close-packed in terms of their atomic structure. Thus, by the end of the 1950s the preference for low index growth directions was already established, albeit for a relatively small number of whiskers.

In the following years, Ellis et al. analyzed Sn, Cd, and Zn whiskers with X-Ray methods, including individual segments of a kinked Sn whisker.[5,7,8] They found low index growth directions and noted the absence of the <110> direction. Interestingly, they made reference to the easy glide directions for plastic flow in tin which are similar, i.e., low-index directions with the absence of <110>. However, the <100> direction was also not listed as an easy glide direction. Ellis reported that the whiskers were predominantly single crystals and these studies were the first to mention other higher-index growth directions such as <123> and <012>.

Later publications on Sn whisker crystallography employed TEM analysis, most notably the investigations by Morris and Bonfield [9] and Lebret and Norton [13]. Morris and Bonfield were

the first to examine a relatively large number of whiskers. They reported mainly low index growth directions, although the <210> direction was also well represented. Using the standard triangle of the stereographic projection for tin, they showed that not all whiskers were perfectly oriented in the low-index directions – some displayed slight deviations from the exact low-index orientation. They also noted some small crystallites and the presence of low angle boundaries in some whiskers (0.5° misorientation). Lebret and Norton, in a more recent TEM study, reported other growth directions including some higher-index orientations. They also showed that whiskers could nucleate on more than one grain and subsequently grow together, resulting in the grooves frequently observed along the lengths of whiskers. Note that both of these TEM studies were the only ones to report the <110> growth direction.

Lee and Lee also utilized TEM to examine a small number of whiskers and found only the <100> growth direction.[10] In that study, Lee and Lee also performed XRD analysis of the Sn film texture and attempted to correlate the whisker growth directions to the film texture. However, the resulting "parent grain" orientations were calculated with the assumption of a <100> whisker growth direction and a perfectly textured film, i.e., the orientations determined in the texture analysis were assumed to be present at the base of the whiskers and all adjacent grains. The work by Lee and Lee was also the first to measure the physical growth angles of whiskers in-situ using multiple SEM tilts to correct for the SEM image projection effect. They found growth angles between 45 and 67 degrees with respect to the substrate, depending on the current density used to deposit the films.

Recent analyses of Sn whisker crystallography have used the more recently developed technique of electron backscatter diffraction (EBSD).[14,15] Hutchinson et al. presented a thorough analysis of eleven whiskers that indicated low-index growth directions were dominant. They reported two whiskers with a <123> growth direction. The EBSD analysis was performed on whiskers removed from the substrate. The films had a weak (111) texture which suggested high angle grain boundaries at the base of whiskers although this was not confirmed for individual whiskers due to the removal technique. Frye, Galyon, and Palmer also used EBSD to analyze 26 whiskers. They reported low index growth directions which, interestingly, included the <110> direction. They also reported data on film texture, obtained by EBSD, which showed a large variety of crystallographic textures.

In summary, the majority of Sn whisker crystallography work has shown that low-index growth directions are preferred. There are other growth directions reported and it seems that these higher index directions are less common, although a thorough sampling of many whiskers has not been performed. The absence of the <110> growth direction was noted by some authors while a few others have observed <110>. Some correlation has been made to the easy glide directions in Sn corresponding to the low-index directions. Due to its tetragonal structure, tin is known to be anisotropic in other properties as well, most notably diffusion rates. For example, the c-axis <001> displays different diffusion rates compared to the a-axis <100> direction.[18] Only a few studies have determined both the overall film texture and the orientation of the whisker parent grains. The factors that determine the particular crystallographic growth direction of a whisker are unknown and, in particular, the relationship of the growth direction to the orientation of surrounding grains (grain boundary characteristics at the base of the whisker) has not been studied in detail.

Table 4.2. References pertaining to kinks in Sn whiskers.

Whisker Growth Direction	Kink angles (deg)	Kink Crystallography	# of kinks analyzed	Reference
	30, 60 (most frequent)		~76	Levy and Kammerer, 1955 [19]
	90, 28, 61, 41, 48 (most frequent)	(Most likely) Several possible 90 deg, <100>/<101> <001>/<101> <101>/<111> <100>/<111>	~300	Baker, 1957 [20]
	30, 15, 60			Furuta, 1965 [21]
<012>, <101>, <100>	18.9, 28.6 (calculated, present authors)	<012>/<101>/<100>	2	Ellis, 1967 [8]
<110>, <103>, <321>	27, 45 estimates	Possibly <100>/<110> (45°) <100>/<101> (28.6°)	2	Lebret and Norton, 2003 (sputter deposited Sn) [13]

Some researchers in Table 4.1 analyzed kinked whiskers as part of the general analysis of crystallography, but kinks were not the main focus. Table 4.2 lists the references in which kinked whiskers were a major topic. Levy and Kammerer [19] measured kink angles of several spiral shaped whiskers produced by squeezing together two Sn-plated samples. Many kink angles were determined to be close to 30 and 60 degrees. A twinning mechanism was considered. However, twin boundaries have not generally been observed in whiskers. Baker [20] carefully measured

kink angles and successfully correlated a number of angles (28, 41, 61°, etc.) to the possible angles between crystallographic directions in Sn. This work provided good insight into the crystallography of Sn whiskers and kinks without actually analyzing the crystallography directly. With the exception of one whisker analyzed by Ellis [8], no one has confirmed Baker's assertion by measuring both the kink angles and independently determining the crystallography of the straight segments of kinked whiskers.

Ellis[8] analyzed the crystallography of multiple segments of a kinked whisker. The kinked whisker was a single crystal, with each segment having a different crystallographic growth direction. Based on the directions reported by Ellis, the kink angles can be calculated and are given in Table 4.2.[20,22] The calculated angles agree well with the photomicrograph of the kinked whisker in Ref 8. Lebret and Norton [13] estimated kink angles of 45 and 27 degrees from SEM images. However, the measurement of kink angles from SEM images can be misleading. They suggested that the kinks could correspond to <110/<110> and <100>/<101> kinks, respectively. They determined <110> growth directions in their work but they only referred to the other directions as possibilities based on other references. Therefore, the kink angles and growth directions of the kinked whiskers in Lebret and Norton's study, while possible, must be considered unconfirmed.

Furuta [21] used time-lapse optical microscopy to described two different kink types. In one type, the whisker undergoes repeated kinks and each segment remains in the same plane while the growth direction at the base changes. In the second type, the whisker bends over and subsequent segments are non-coplanar. The growth direction of new segments at the base remain relatively the same. This second type of kink/bend often involves a twist as well as bending.

To summarize, although fewer studies have involved kinked whiskers, much has been learned about them through careful analyses of kink angles. In particular, Baker's work showed good correlation between measured kink angles and the angles between directions in tin. Having said that, the research to date has involved measurement of kink angles and correlation to the possible kink types without independent measurement of the crystallography of the whisker segments.

4.3 EXPERIMENTAL PROCEDURE

Electroplated Sn coatings were deposited on commercially pure annealed Cu sheet substrates. The Sn coating thicknesses were in the 1-2 micron range. The Sn was plated from an alkaline stannate bath with a rotating disk electrode setup at 1000 rpm and 70˚C. Details of the plating procedure are given elsewhere.[23] The Sn coated copper samples were stored under ambient conditions and periodically observed for whiskers by both light optical microscopy (LOM) and scanning electron microscopy (SEM). SEM imaging, length measurement, and growth angle determinations were performed on a Zeiss Supra 55VP SEM. EBSD was performed on the same instrument equipped with an Oxford/HKL Nordlyss II EBSD detector and the patterns were analyzed with Oxford/HKL Channel 5 software. The SEM was operated at 15 or 20 kV and with a beam current of 5nA. The accelerating voltage was selected to optimize the pattern quality as higher quality patterns could be obtained from thinner whiskers at lower voltages. EBSD required tilting the sample to a high angle (~70º) for analysis. The crystallography of whiskers was determined by the technique described briefly above and discussed in detail elsewhere.[1]

For kinked whiskers, the kink angles were measured either from 1) kinked whiskers removed from the substrate and found to be *lying flat* on a sample holder grid, or 2) kinked whiskers still attached to the substrate and found by SEM to be lying flat on the substrate surface. In either case, it was important for the whiskers to be lying in a known plane for accurate measurement of the kink angles. The crystallography of the individual segments was measured by the same process described elsewhere.[1]

In addition to analysis of individual whiskers, EBSD was also used to determine the overall texture of the Sn films. This method necessitated "cleaning" of the surface of the sample using a focused ion beam (FIB) instrument. Removal of a small amount of material from the surface allowed for better EBSD pattern quality to be produced over large areas. EBSD crystal orientation data were obtained from about 2000 grains within the Sn film with this technique. In addition, X-ray diffraction was also used for Sn film texture determination. XRD was performed (without FIB cleaning) using a Siemens model D500 θ-θ diffractometer equipped with a sealed-tube (Cu Kα) source, fixed (1^o) slits, a diffracted-beam graphite monochromator, and a scintillation detector. Generator settings were 40kV and 30mA. Scan parameters were 20-80^o 2θ angular range, a 0.04^o step-size, and 4 second count-time.

4.4 RESULTS AND DISCUSSION

Figure 4.1 shows SEM photomicrographs of typical straight and kinked Sn whiskers analyzed in this work. The kinked whisker actually displays two kinks, one of which is very close to the substrate. The whisker diameters are ~1 micron, on the order of the grain size of the Sn film. Other short whiskers can be observed in Fig. 4.1, along with some Sn grains that appear to be nucleated whiskers that did not grow to any appreciable length.

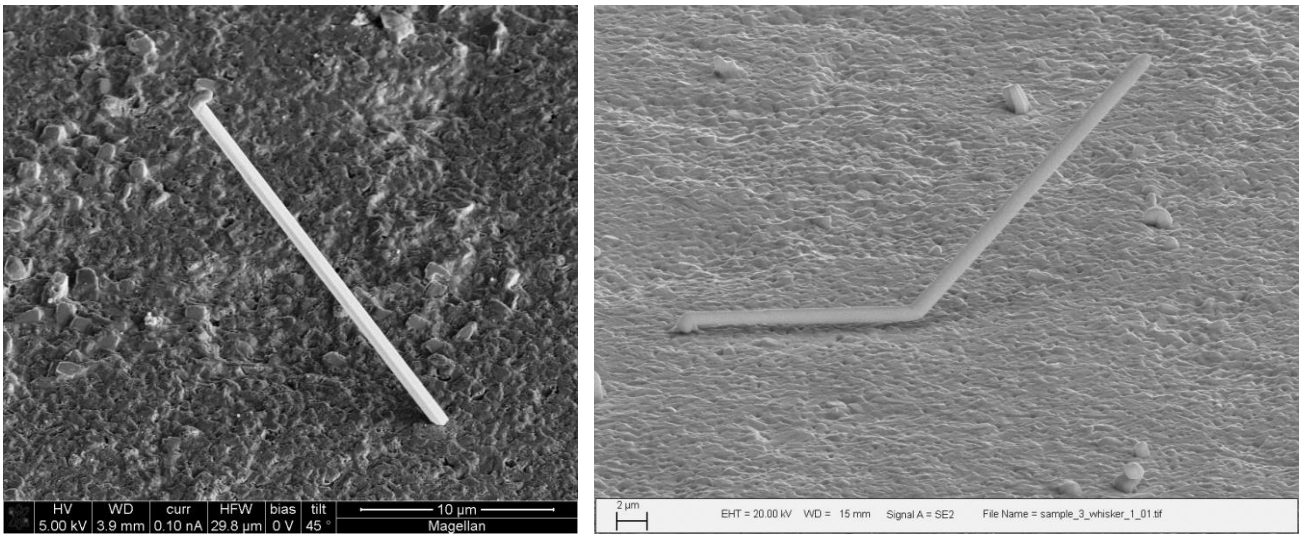

Figure 4.1. SEM photomicrographs of straight and kinked Sn whiskers.

4.4.1 The Crystallography of Straight Tin Whiskers

The crystallography results for straight whiskers will be described here. The first step in the characterization process is to rotate the sample so the apparent length of the whisker is aligned with the tilt axis of the SEM, in this case, the horizontal x-axis of the image. A schematic diagram of the situation is shown in Figure 4.2a for an intact whisker growing on the substrate. The sample is then tilted for EBSD pattern determination. On the correct stereographic projection, corresponding to the crystallographic growth direction of that whisker, the plotted growth axis from such a whisker will lie along the x-axis of the stereogram, as shown in Fig. 4.2b. The angle θ, measured from the center of the stereogram, represents the angle of the whisker with respect to the z-axis (SEM beam column). Using the EBSD software, inspection of stereograms for several orientations must be performed and the correct one is then chosen, i.e., the one in which the whisker growth axis lies along the x-axis.

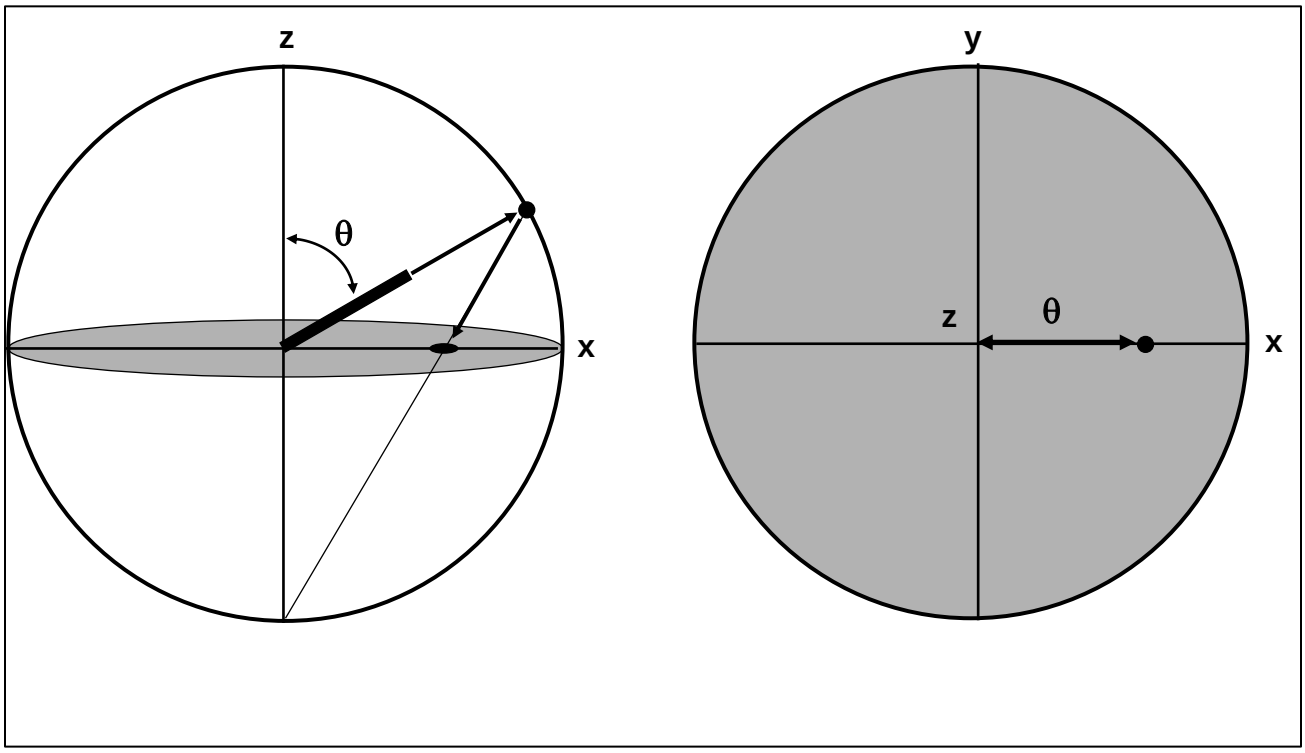

Figure 4.2. Schematic diagram of whisker orientation: a) geometry of whisker intact on the growth substrate, b) stereographic projection construction.

This SEM/EBSD procedure was repeated for many whiskers and typical sets of results are shown in Fig. 4.3. Figure 4.3 displays <001> and <100> stereograms constructed from the combined individual analyses of many whiskers using the procedure described above. The whisker axes found along the x-axis of the figures confirm the crystallographic growth directions of the whiskers. The many other points shown in Fig. 4.3 are from the other possible <001> and <100> directions (multiplicity) exhibited by the whisker grains. Note that β-Sn has a tetragonal crystal structure (a,b = 0.582 nm, c = 0.318 nm) so the <001> and <100> are not equivalent crystallographic directions.

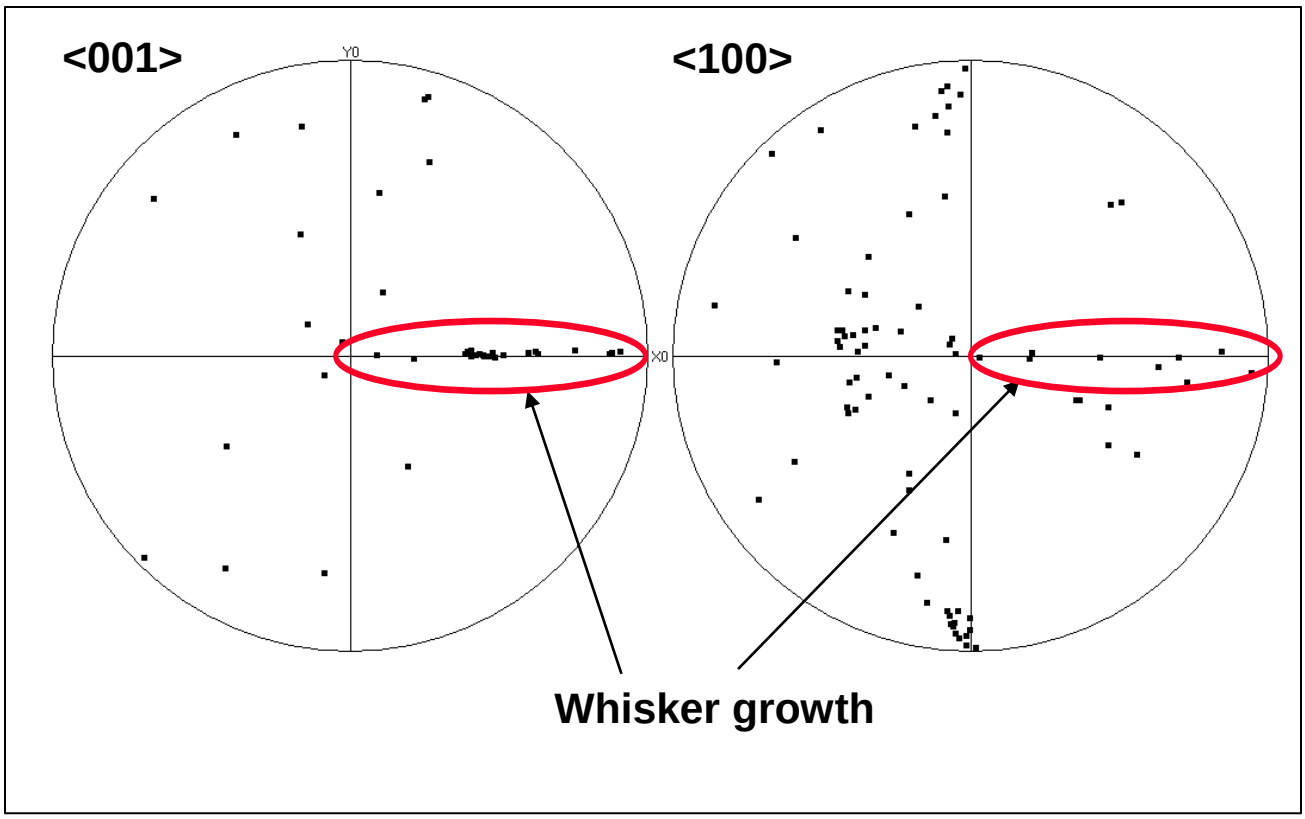

Figure 4.3. The <001> and <100> stereograms produced from the combined EBSD analyses of approximately 21 <001> whiskers and 7 <100> whiskers.

By using matrix operations to rotate the whisker orientation matrix about the y-axis, an inverse pole figure (with directions plotted, not poles) can be produced with respect to the z-axis frame of reference.[1] This type of construction allows for whiskers with many different orientations to be plotted on the standard triangle of the Sn stereographic projection as exhibited in Fig. 4.4. Figure 4.4 indicates that the majority of whiskers grow with <001>, <101>, <100>, and <111> orientations. Note the absence of the low-index <110> direction. There were also two <201> and one <102> whisker observed in these samples. One advantage of the inverse pole figure construction is that it can be compared directly to the parent grain orientations and the EBSD or XRD textural information from the Sn films, as discussed later.

Figure 4.5 shows a statistical summary of crystallographic growth directions obtained from 134 straight whiskers grown on four different Sn-plated samples. The Sn films were all deposited from an alkaline stannate bath but using slightly different plating parameters. The results indicate that the <001> growth direction (the c-axis in Sn) is the dominant growth axis for these whisker samples, followed by the <100> and <101> directions, and then the <111> direction. These results confirm that the low-index crystallographic directions are the preferred growth directions for whiskers, in agreement with several previous studies.[3-17] Note that the results for each individual sample differed slightly. For instance, in sample three the most-represented growth direction was <100>. This is most likely statistical scatter and not a consequence of the particular plating parameters used. However, as shown later, the Sn-plated samples display

different overall crystallographic textures, which could be influencing the actual statistical distribution of whisker growth axes.

Out of 134 whiskers represented in Fig. 4.5, only one was found with a <110> growth axis. This interesting result is in agreement with the early work done on Sn whisker crystallography. For the sixteen previous studies listed in Table 4.1, only two had found the <110> growth direction. In Table 4.1, the analyses of roughly 139 whiskers are represented -- with different plating baths, different substrate types, different Sn film thicknesses, etc. These previous results are remarkably consistent with the statistics of the present study. The reasons why whiskers do not grow in the <110> low-index direction are not known. It could be related to the A5 tetragonal crystal structure of Sn and the particular stacking of atoms in the <110> direction. However, as noted by previous authors, the other four low index directions also contain different atomic packing densities.[4] Perhaps the structure in the <110> direction is significantly different from the others. Further investigation of this topic is certainly warranted. The near absence of the <110> growth orientation could also be related to the easy glide directions for plastic deformation in Sn, as suggested by Ellis and coworkers.[5,7,8] More work is needed to understand the relationship between plastic deformation and the selection of whisker growth crystallographic directions. It would especially be of interest if the *relative* ease of plastic deformation of these low-index orientations agreed with the results shown in Fig. 4.5.

Very few whiskers were found with higher index growth directions, such as the <012> and <321> directions, as displayed in Fig. 4.5. Again, this is in good agreement with previous research, Table 4.1. If researchers come across whiskers with such higher-index growth axes, they should be regarded as anomalous, not representative of the general whisker growth phenomenon. However, while whiskers clearly prefer low-index directions, the inclusion of both the <110> and the higher index directions suggests that the whisker growth process is not governed solely by a single crystallographic parameter.

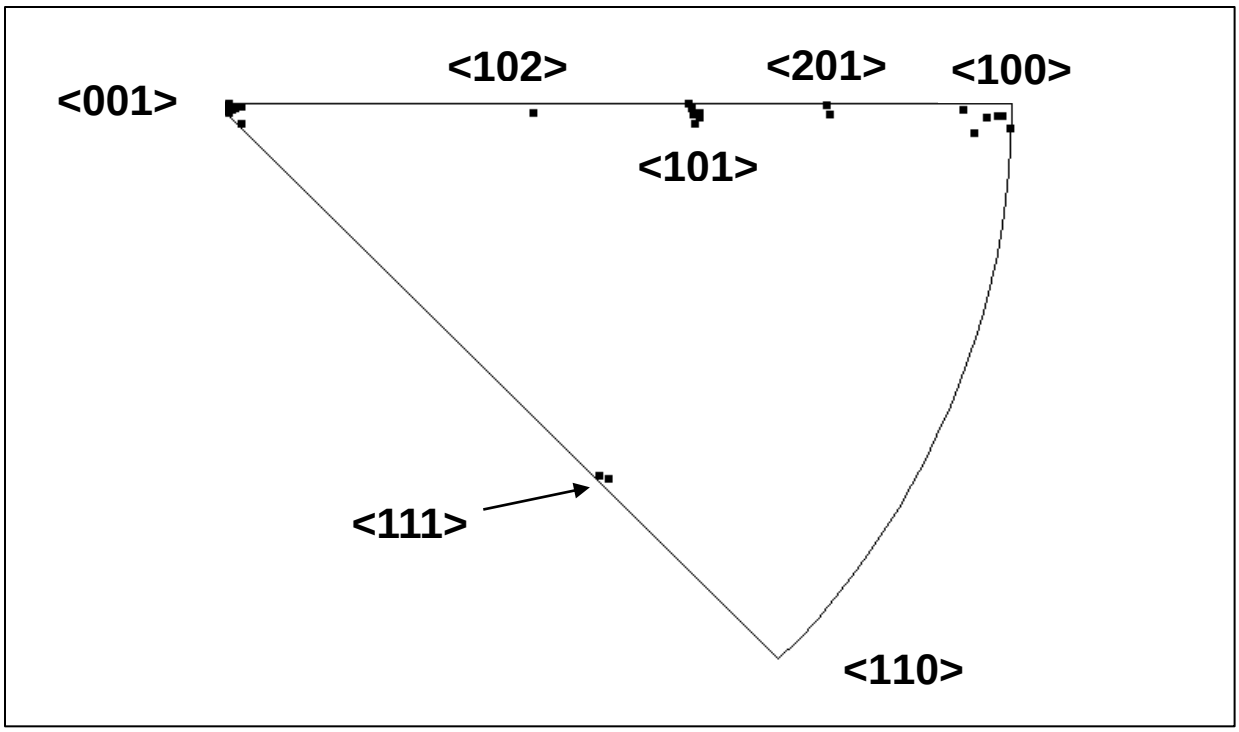

Figure 4.4. Inverse pole figure plot (with directions plotted, not poles) of whisker growth axes after rotation of the orientation matrices of several whiskers.

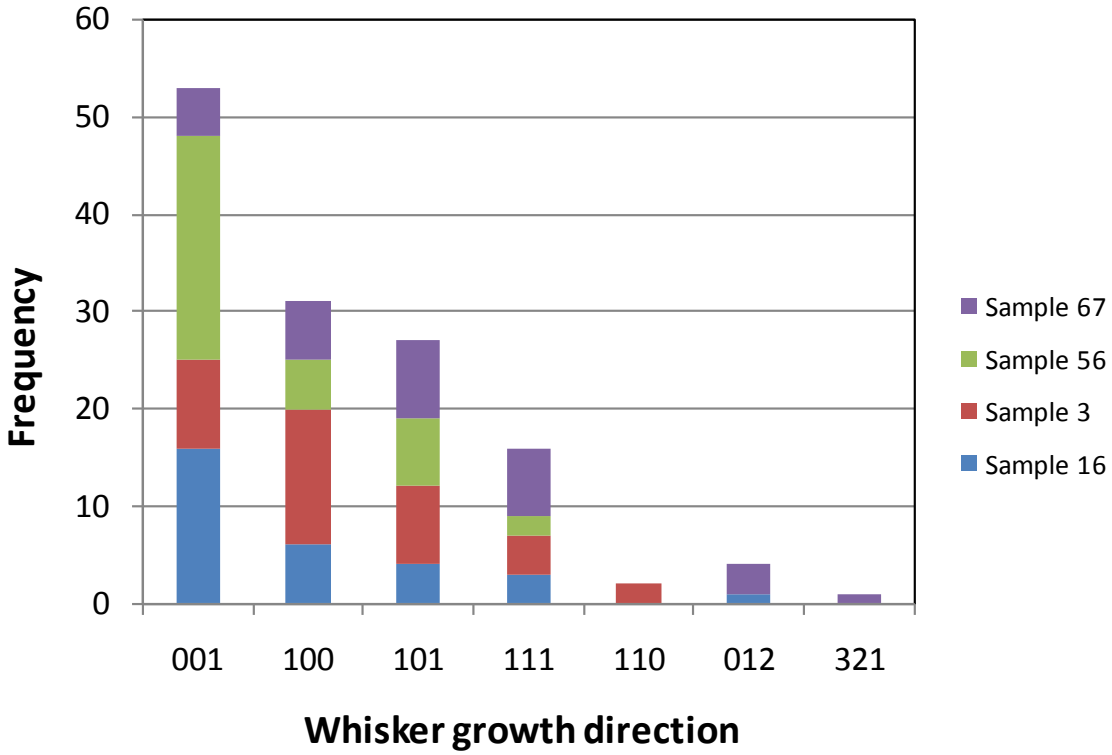

Figure 4.5. Summary histogram of the crystallographic growth axes of 134 whiskers grown on four different samples.

As discussed previously, by combining the EBSD technique with matrix rotation operations it is possible to determine the relationship between a whisker and its parent grain. The parent grain is actually the whisker grain embedded within the Sn film -- there is no grain boundary separating the external whisker growth from this "internal" grain. Figure 4.6a exhibits the standard triangle for Sn with the orientations of the parent grains plotted for a large number of whiskers from a single sample. The symbols on each plotted direction represent the crystallographic orientations of the whiskers that grew from those parent grains. The figure shows that the various whisker types can grow from grains with many different orientations. There is no simple relationship between the whisker growth axis and the orientation of the original Sn grain. This, in turn, implies that whiskers can grow with many different physical growth angles relative to the sample surface. The following examples illustrate the qualitative interpretation of the diagram. There is only one <001> whisker shown close to the <001> direction of the standard triangle. This particular whisker, therefore, was growing with a high angle relative to the substrate; if an <001> data point was exactly at the <001> corner of the diagram the whisker would be growing perfectly normal to the substrate. Similarly, there are three <001> whiskers growing from grains with orientations close to <100>. These whiskers were oriented nearly 90 degrees from the sample normal or almost parallel to the sample surface. Inspection of the diagram shows that many other growth angles are possible but, at least for <001> whiskers, the parent grain orientations do not seem to be completely random. For <001> whiskers, well represented in Fig. 4.6, there is some clustering of parent grains in one region of the diagram near the <102> orientation. All of these whiskers have physical growth angles in the vicinity of 45 degrees from normal. Whisker angle distributions were shown in a separate publication, without reference to their crystallography.[23]

At first glance, one might think that the whiskers orientations shown in Fig. 4.6a are related to the overall texture of the Sn film. However, as shown in Fig. 4.6b, the parent grains are generally not oriented in the major texture orientation, which happens to be near <110> for this sample. Furthermore, comparison to Fig. 4.4 above shows that the whisker orientations themselves also are dissimilar relative to the main texture. The lack of <110> whiskers was discussed above. The exceptions are the two higher-index <201> whiskers, which grew from parent grains oriented close to <110>. It should be noted that the film is not highly textured; the <110> grains are only found at about "six times random" frequency in this sample. This means that there are sufficiently large numbers of grains with other orientations to support whisker growth. This discussion brings up the concept of crystallographic engineering of Sn films. For example, if Sn films could be produced with a near-perfect texture, (almost all of the grains with a single orientation), it may be possible to suppress the growth of certain whiskers. If a perfectly textured <110> sample could be produced it would suppress any whiskers with orientations 90 degrees to <110>. The whiskers would not be able to grow "in the plane of the film". A perfect <110> film would, for example, suppress the growth of <001> whiskers. Unfortunately, due to the high number of available whisker orientations, it is not possible to suppress all whiskers from growing (e.g., <100> whiskers would still be possible at a growth angle of 45 degrees from <110> parent grains). More discussion about crystallographic texturing of films will be presented later.

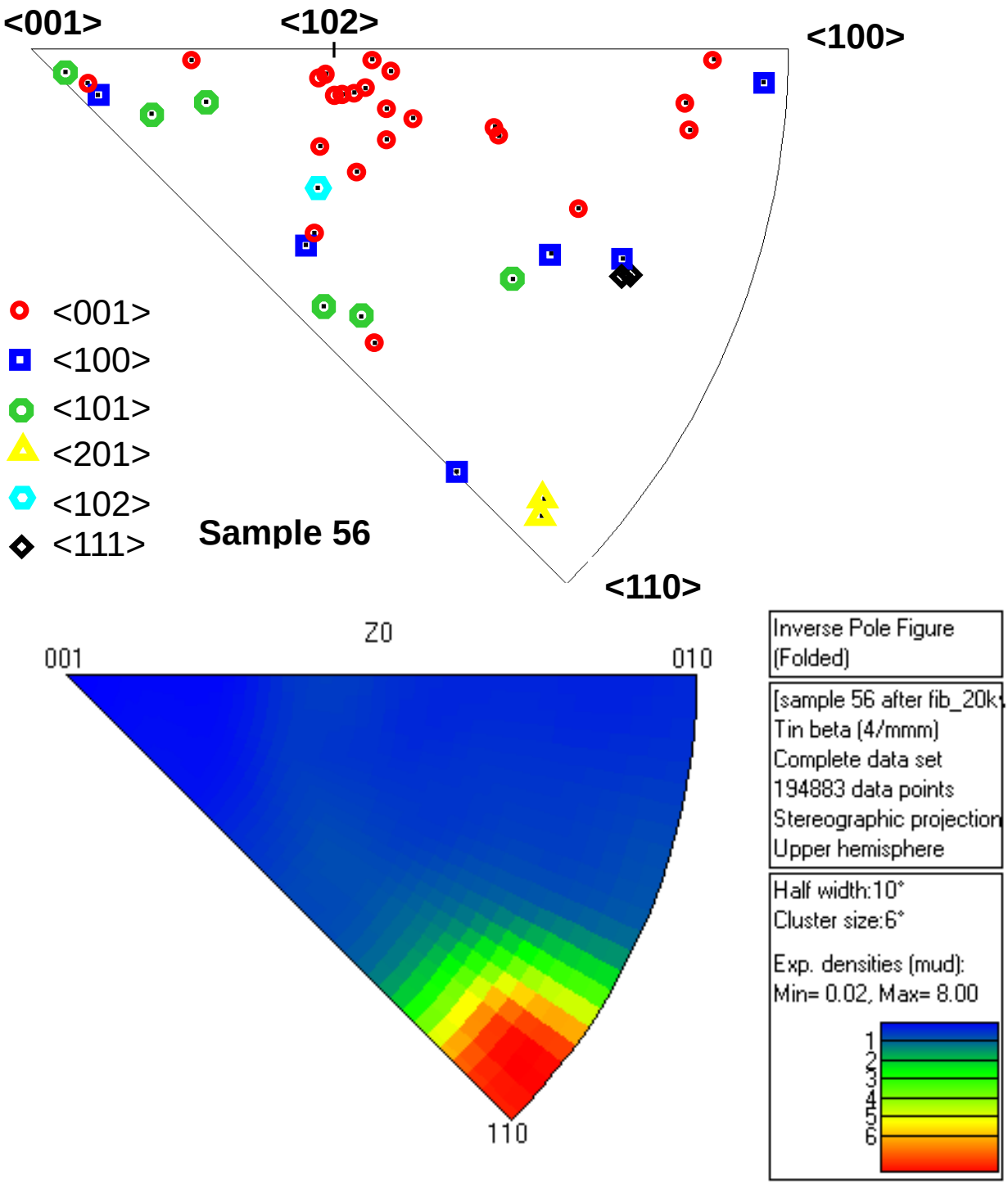

Figure 4.6 a) Standard triangle for Sn with orientations of the parent Sn grains plotted. The various symbols represent the growth axes of the whiskers growing from any given parent grain. b) Overall texture of the Sn film for same sample. Texture was determined by EBSD analysis of approximately 2000 grains.

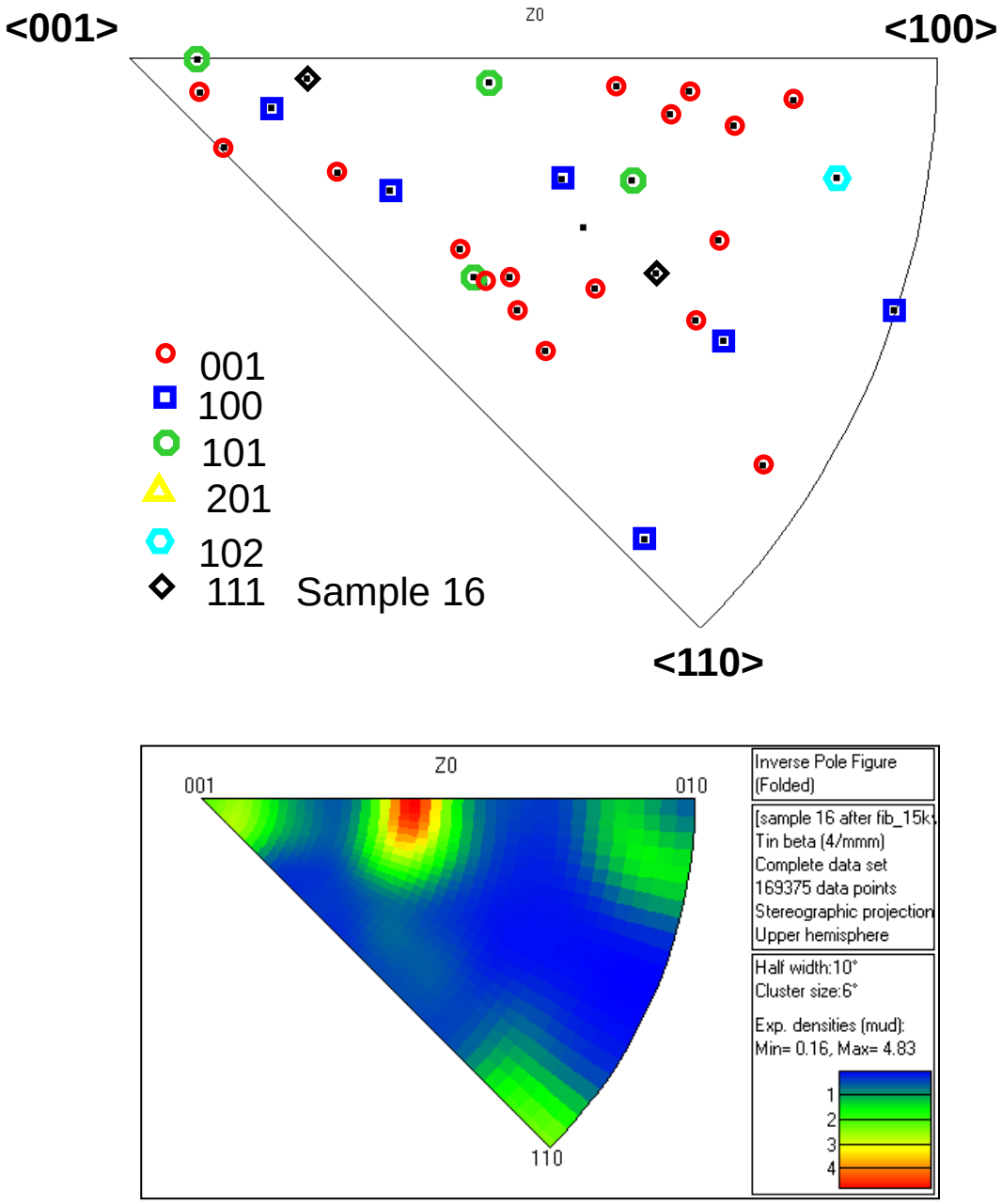

Figure 4.7. a) Standard triangle for Sn with orientations of the parent Sn grains plotted for sample 16. The colored symbols represent the growth axes of the whiskers growing from any given parent grain. b) Overall texture of the Sn film for same sample 16 determined by EBSD analysis of approximately 2000 grains.

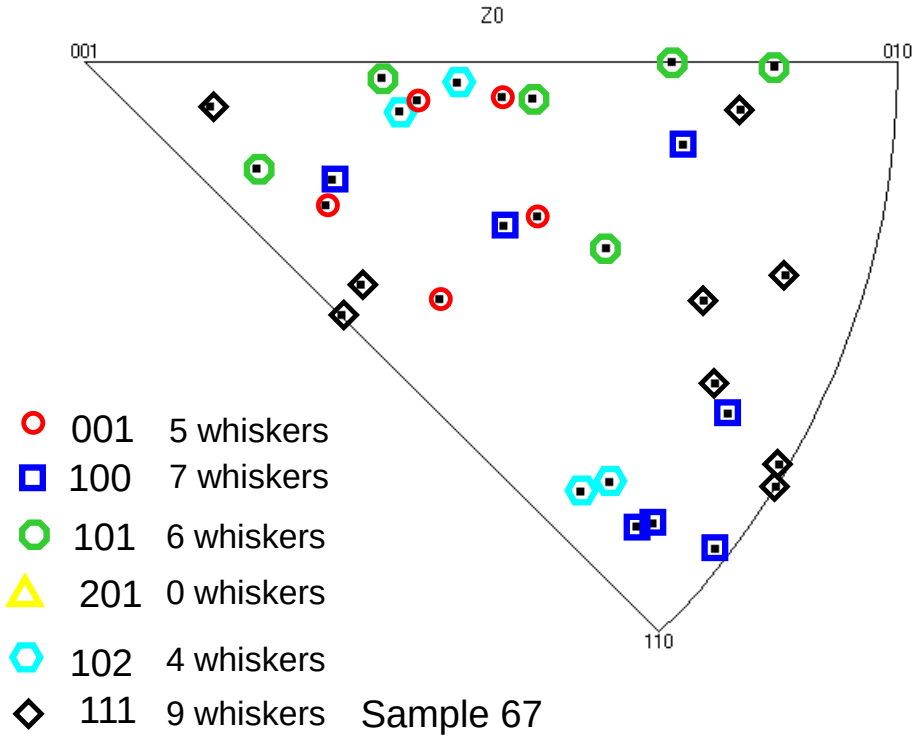

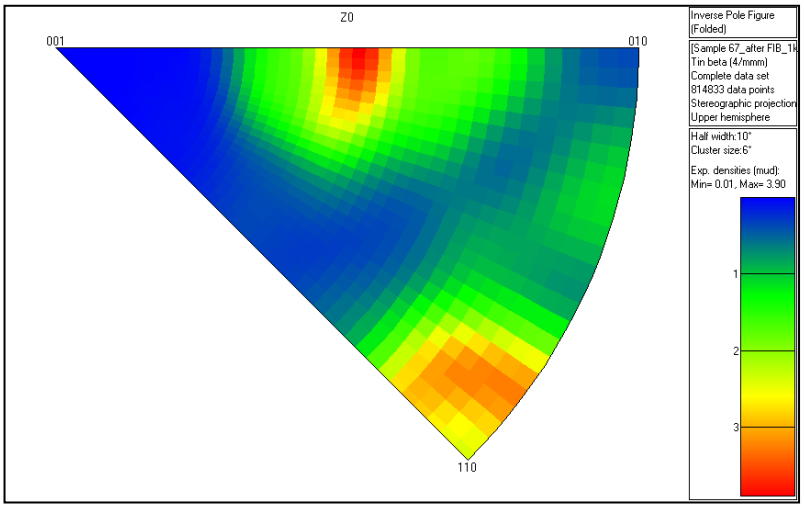

Figure 4.8. a) Standard triangle for Sn with orientations of the parent Sn grains plotted for sample 67. The colored symbols represent the growth axes of the whiskers growing from any given parent grain. b) Overall texture of the Sn film for same sample 67 determined by EBSD analysis of approximately 2000 grains.

The whisker grain/parent grain orientations and overall film textures are shown for two more samples in Figs. 4.7 and 4.8. In Fig. 4.7, sample 16 shows a similar distribution of whisker growth axes when compared to sample 56 discussed above (see also Fig. 4.5). However, the texture of the Sn film is different with slight clustering near <102>. Unlike sample 56 above, sample 16 does not show whiskers from these parent grains. These results reinforce the fact that whiskers generally do not grow from the main texture grains of the film, having already noted that these films are only slightly textured. In this sample, many <001> whiskers grow with orientations in a band across the diagram, corresponding to growth angles of about 60 degrees from normal. These results can be correlated to the whisker angles measured previously [23] and summarized below in Fig. 4.9.

Figure 4.8 displays a sample with yet another combination of whisker axes and parent grain orientations. The overall film texture in sample 67 shows clustering near the <101> ((301) pole) and <110> orientations. This film is probably the most lightly textured of the three analyzed here. The parent grains are distributed randomly, even to include grains near <101> and <110>. Note also that this sample exhibited a slightly different distribution of whisker types, with more <111> whiskers (see also Fig. 4.5).

All of the results in Figs. 4.6-4.8 show the complicated nature of the crystallography of whiskers, the relationship to parent grains, and the possible physical growth angles. While there appears to be no simple relationship between the texturing of the film and the crystallography of Sn whiskers, it may be important that these films are only slightly textured. The results also point to the fact that the Sn plating parameters can have a dramatic effect on film texturing.[24][other Purdue refs?] If very highly textured films could be produced, it may still be possible to influence the types of whiskers that grow and to suppress certain whisker types, as discussed above. Texturing in the <110> orientation may be a promising way to suppress <001> whiskers, which are the most common type. Even texturing the film in the <001> orientation could be helpful. An <001> textured film would suppress <100> whiskers (oriented 90 degrees to <001> or in the plane of the film). Such a film could also suppress <001> whiskers since they generally do not grow normal to the surface (Fig. 4.9). All of the foregoing discussion assumes that the Sn films do not recrystallize prior to whisker growth. If the parent grains reorient themselves prior to whisker growth, then any effects of texturing on whisker growth will be lost. Other researchers have been analyzing the recrystallization of Sn films, which, at room temperature are approximately sixty percent of their absolute melting temperature ($0.6T_m$). The effect of texturing may depend on the incubation time for whisker growth relative to the recrystallization time for the Sn film. Indeed, recrystallization within the film may be a prerequisite for some whiskers to grow. More research is needed on the effects of film texturing and recrystallization on Sn whisker susceptibility and our future work will include research to produce very highly textured films.

4.4.2 Analysis of Sn Whisker Crystallography, Growth Angles, and Lengths

Figure 4.9 displays histograms of the physical growth angles of whiskers relative to the surface normal. The technique for accurately measuring growth angles is described elsewhere.[23] The combined histogram from all whiskers is shown for the three samples analyzed above. A similar histogram was shown previously for a larger set of samples, some of which were not analyzed crystallographically.[23] In Fig. 4.9, the histogram is further broken down according to the crystallographic growth axes of the whiskers analyzed in the present work. The results indicate that many whiskers grow with angles between about 45 and 75 degrees from normal. The data summarize the relationships described in Figs. 4.6-4.8 above. There is no simple relationship between the crystallographic growth axis of the whiskers and their physical growth angles. Also, few whiskers grow normal to the surface of the film. This supports the evidence that whiskers with a given crystallography do not grow from parent grains with the same or nearly the same orientation (with respect to the surface normal).

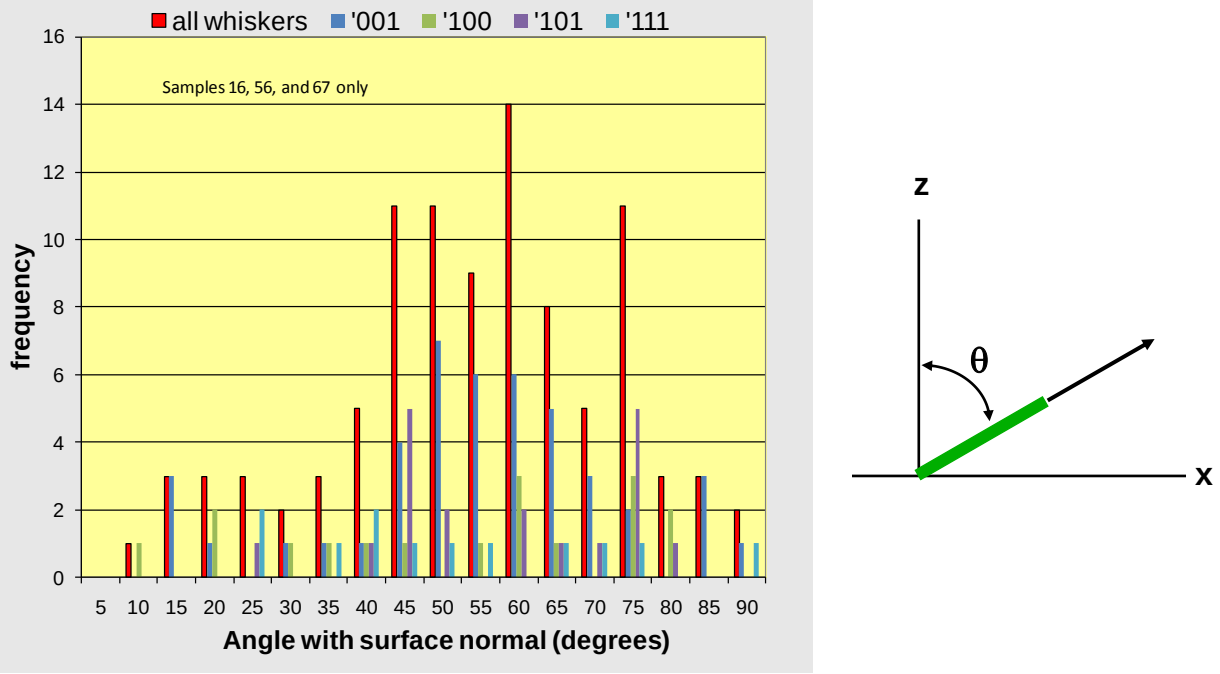

Figure 4.9. Summary histogram of whisker growth angles for 134 whiskers from 3 samples. The data was obtained from straight (non-kinked) whiskers only.

Another summary is presented in Figs. 4.10a and 4.10b, this time with regard to whisker lengths. The method for accurately measuring whisker lengths from SEM images is described elsewhere.[23] For the major low-index growth directions, there is no clear trend regarding whisker lengths. Each of the whisker orientations displays a similar broad length range. Some of the spread in the data is due to differences in the age of the samples at the time of analysis. All of the samples were analyzed roughly between one and two years after Sn plating, but not at exactly the same age. The results suggest that the various crystallographic growth directions have the

same whisker growth rates or, more likely, the same *distribution* of growth rates. Other sources of spread in whisker length measurements are differences in incubation time for whiskers and the possibility that some whiskers may have stopped growing, i.e., differences in actual "growth time" not necessarily related to absolute sample age. Some of these issues were discussed in the kinetic analysis in Reference [23]. Further understanding of the effects of whisker crystallography on growth kinetics will require time-lapse SEM analyses that include a concurrent crystallographic analysis as well.

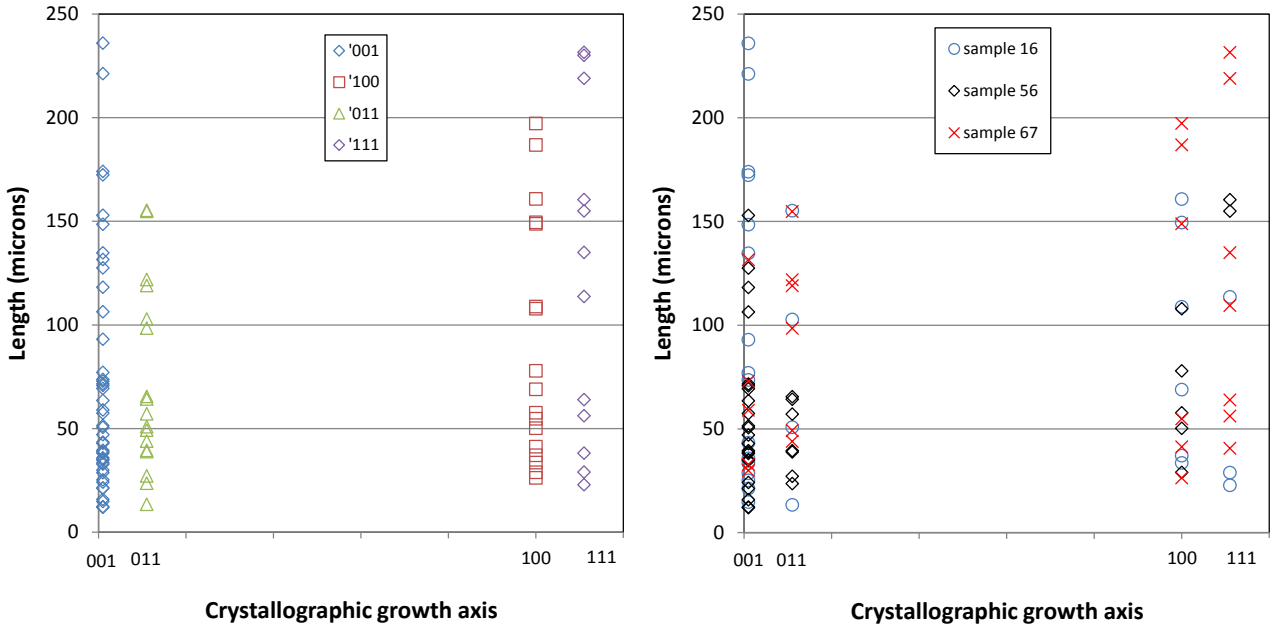

Figure 4.10. a) Summary of measured whisker lengths with respect to the crystallographic growth axes for the four major whisker types. Note that the samples were analyzed at different ages, all roughly between one and two years after Sn plating. b) Same data as in (a) showing the individual samples analyzed.

Figure 4.10b shows the same data set with the individual samples identified. There is no clear preference for longer whiskers of a given crystallographic type on the three samples analyzed. Therefore, the overall film texture does not affect the whisker growth rates appreciably. Sample 16 shows a few longer <001> whiskers, but this sample also displays the highest number of <001> whiskers. Similarly, sample 67 displays a few longer <111> whiskers, but this sample also contained the most <111> whiskers. In both samples, the longer whiskers likely result from simple statistical scatter. Further discussion about whisker lengths and growth angles can be found in Reference [23].

4.4.3 Crystallography of Kinked Sn Whiskers

The EBSD techniques described previously [1] were also utilized to characterize the individual segments of kinked whiskers. Kinked whiskers have been shown to be single crystals [23,25]. In an early investigation, Baker measured kink angles and correlated the angles to the various crystallographic directions in tetragonal Sn.[20] In the current study, the kink angles were measured and the crystallographic growth axes were determined independently. The results below indicate that the kink angles are indeed the angles between crystallographic directions, thus confirming Baker's angular correlations.

Kinked whiskers were analyzed with two techniques. In the first method, the whiskers were removed from the growth substrate and placed on a TEM sample grid (Fig. 4.11). In the second technique, the kinked whiskers were analyzed in-situ, still intact on the growth substrate (Figs. 12 and 13). In either case, for accurate angle measurement it is important that the segments of the whisker are lying in the same plane. It is more difficult to measure kink angles and determine the crystallography for kinked segments lying out-of-plane and analysis methods are currently being developed.

In Fig 4.11, a whisker with two kinks is shown lying flat on the support grid. Segments one, two, and three were determined to be <001>, <111>, and <001>, respectively. The <001>, <111>, and <001> stereograms obtained from the three segments are also shown. Prior to EBSD analysis, the sample is rotated so a segment is aligned with the tilt axis (x-axis) of the SEM and, therefore, the growth axis from the whisker is found close to the x-axis if the correct stereogram is produced (see Fig. 4.2 above). The procedure is repeated for each segment. The measured kink angle for both kinks was 68.8 degrees. Table 4.3 shows the angles between the crystallographic directions in Sn.[20,22] The measured angle agrees well with the 68.9° angle listed for the <001>/<111> crystallographic directions. The convention used here is to report acute angles.

Figure 4.12 displays a kinked whisker analyzed by the second technique -- still intact on the growth substrate. Again, the segments of the kinked whisker are lying flat upon the substrate. This situation is possible due to an additional kink very near the base of the whisker (arrow in Fig. 4.12). For the samples in this work, several whiskers were found lying flat on the surface due to these base kinks. The measured kink angle was 48.9° and the published angle between <111> and <100> is 48.7° as shown in Table 4.3. The EBSD analysis of each kink confirmed the <111> and <100> directions as indicated by the stereograms in Fig. 4.12. For intact whiskers, it is easier to distinguish between the tip and the base of the whisker. Thus the kinks can be characterized in terms of the growth sequence. In Fig. 4.12, segment 1 with the <111> orientation was growing first and then the whisker "kinked to" the <100> direction. This would be reported as a "<111>/<100>" kink.

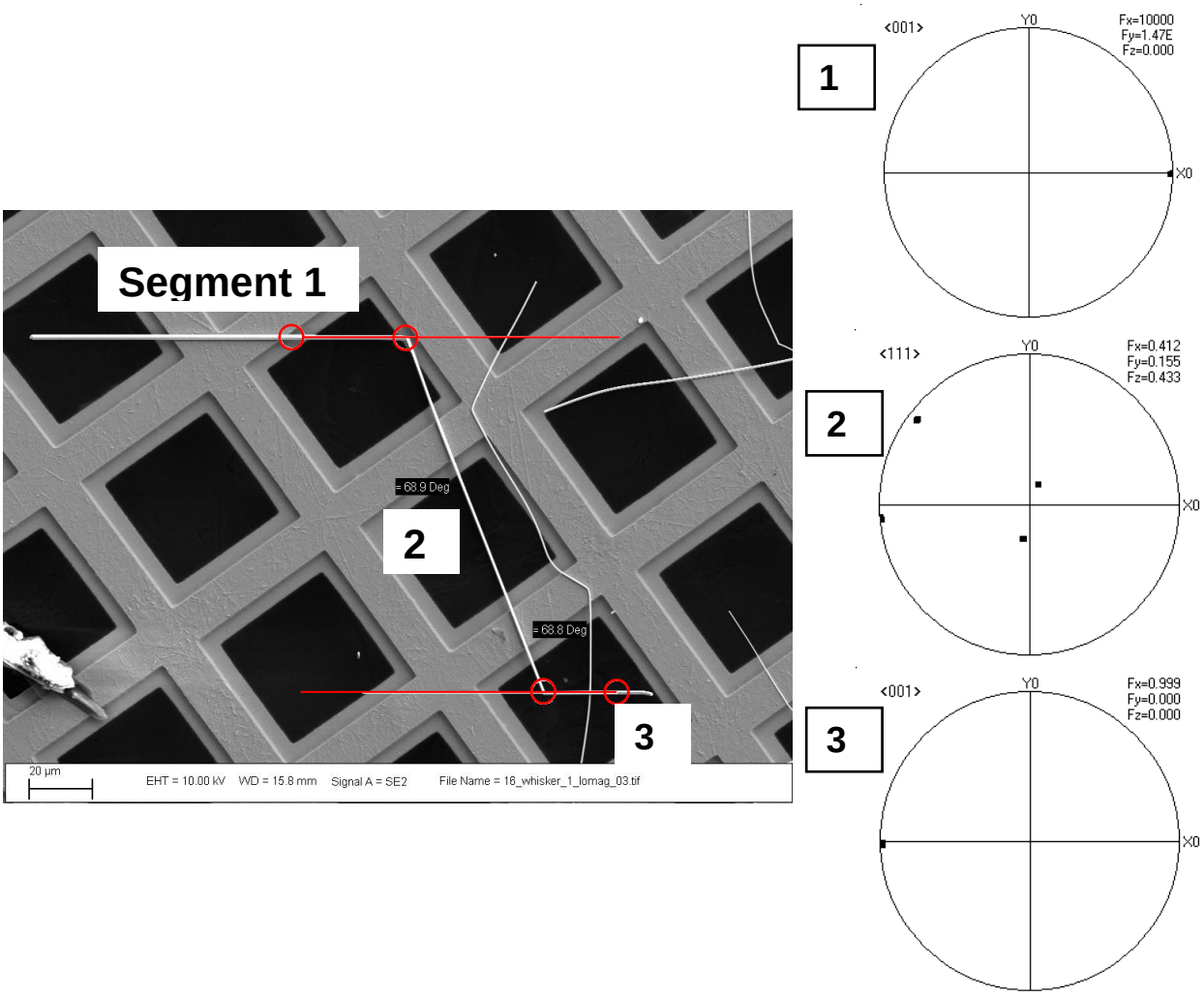

Figure 4.11. SEM photomicrograph of a kinked whisker extracted from a sample and lying flat on a grid support. The red circles and lines were used to measure the kink angles. Also shown are the <001>, <111>, and <001> stereograms obtained from EBSD analyses of each segment.

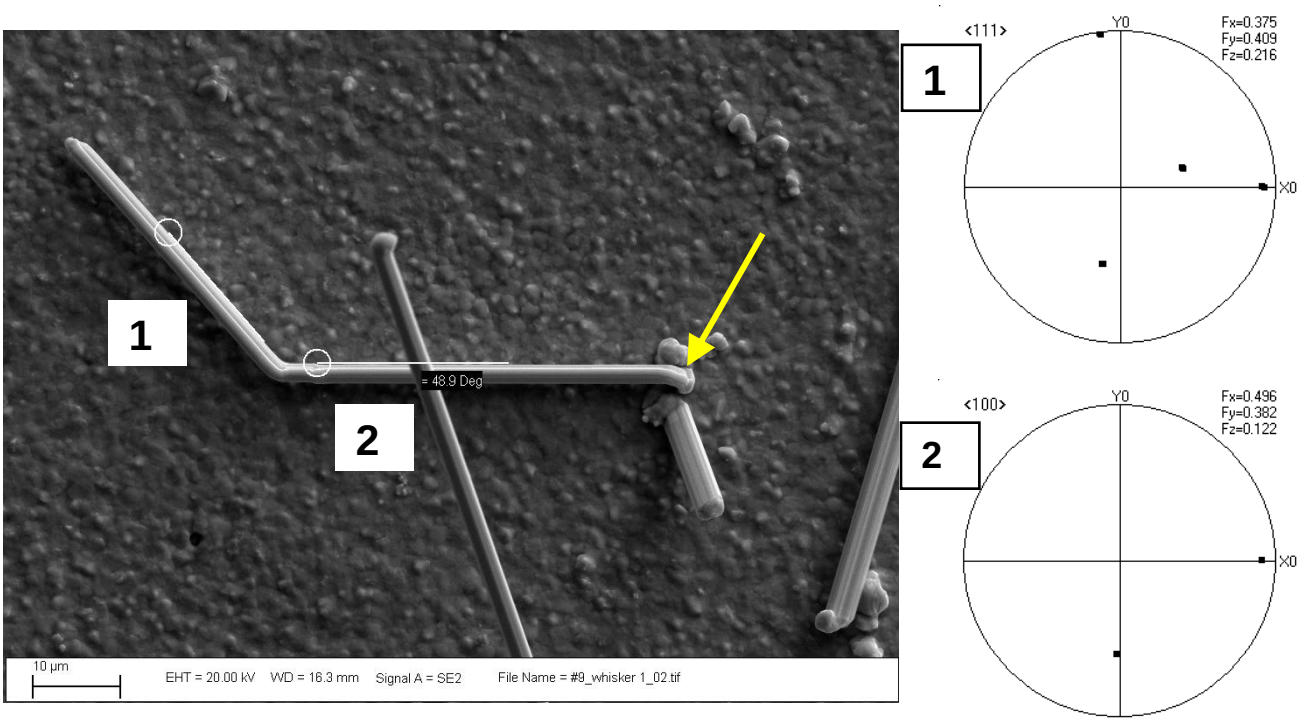

Figure 4.12. SEM photomicrograph of a kinked whisker intact on the growth substrate. The whisker had also kinked near the base and is now lying flat on the substrate. Also shown are the <111> and <100> pole figures for segments one and two, respectively.

The kinks exhibited in Figs. 4.11 and 4.12 all involved changes from one crystallographic direction to a different growth direction. This type of kink was called a "heterogeneous kink". It is also possible for a whisker to kink from one crystallographic direction to an equivalent direction, e.g., from a <101> direction to a different <101> direction within the Sn lattice. Such a "homogeneous kink" is shown in Fig. 4.13. Both segments two and three were determined to be <101> directions and the angle measurement was 77.7 degrees. These results agree well with the 76.7° angle between <101>/<101> directions shown in Table 4.3.

A few other kinks were analyzed in this work and Table 4.4 displays a summary of eight kinks from six different whiskers. All of the measured angles agree well with the predicted angles expected from the crystallography of the individual segments. Results from both the whisker extraction technique and the in-situ technique are indicated in the table. The fact that seven out of the eight kinks analyzed were the heterogeneous type suggests that this may be the preferred kink type. However, more statistical analyses of many kinks would be necessary to determine the preference for heterogeneous vs. homogeneous kinks. If it is assumed that segments of kinked whiskers follow the same statistical trends as straight un-kinked whiskers (Fig. 4.5), then the prevalent kinks can be surmised from Fig. 4.5 and Table 4.3.

The conditions that prompt whisker kinks are not fully understood. In reference [23], we schematically described the kink process. During whisker growth, the Sn atoms are accumulated into the whisker across the grain boundaries at the whisker base within the Sn film. During the

kink process, it appears that the dominant site for Sn accumulation abruptly changes from one grain boundary to a different boundary or set of boundaries. Other grain boundaries must be able to slide relative to each other if Sn accretion is not occurring there in order for the whisker to increase in length and remain "straight". For the sharp kinks analyzed in these studies, there does not appear to be appreciable motion of the grain boundaries at the base of the whisker. The whisker morphology and diameter remain the same before and after the kink. Other kinks/bends, such as those very near the whisker base (Figs. 12 and 13) do display changes in morphology and diameter. These types of kinks/bends have been associated with a stoppage in whisker growth.[23] In those cases, the kink/bend process involves grain boundary movement near the base and the conditions for sustained whisker growth are removed.[23] If kinks are found very near the base, it is likely that the whiskers are no longer growing (Figs. 12 and 13).

Based on the research by Baker [20] and the results shown here, it is possible to indirectly determine the crystallography of kinked whiskers simply by measuring the kink angles. However, it is important that the angles be measured carefully with the kink segments lying in the same plane and keeping in mind the projection effect associated with SEM images.

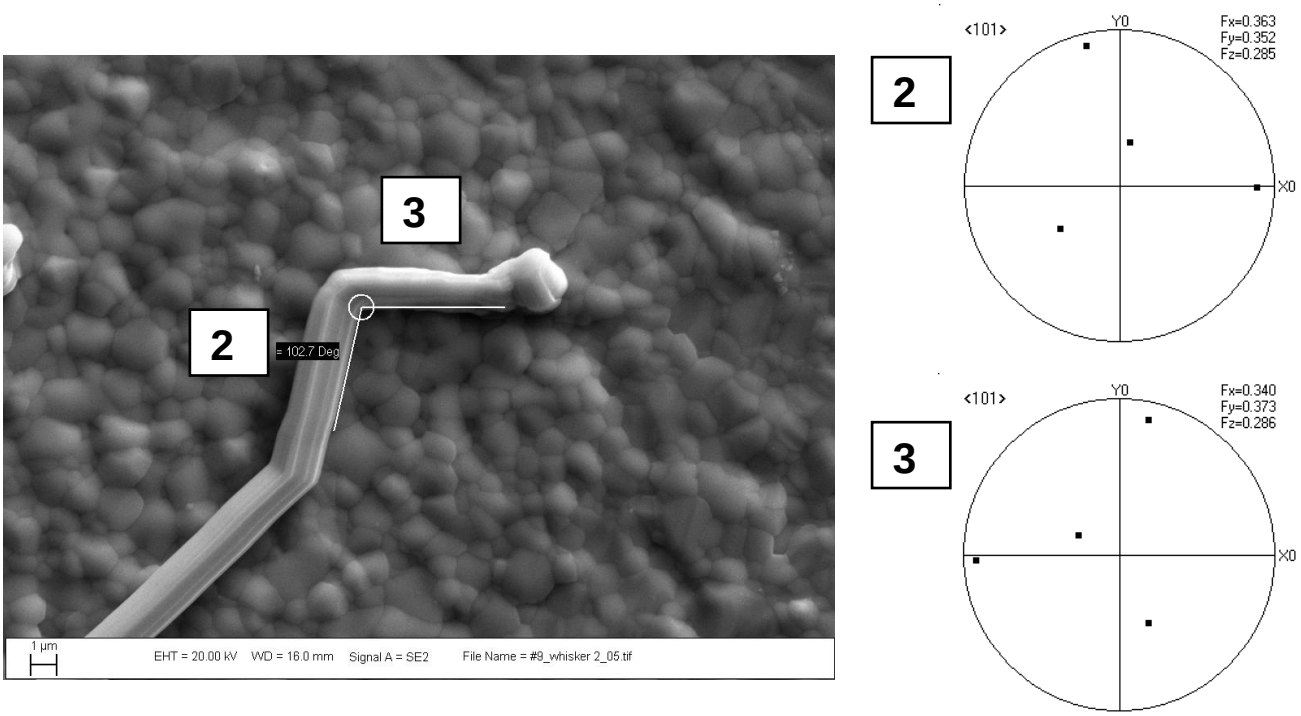

Figure 4.13. SEM photomicrograph of an intact whisker that kinked near its base and is lying flat on the substrate. Also shown are the <101> pole figures obtained by EBSD from segments 2 and 3.

Table 4.3. Angles between crystallographic directions in tetragonal Sn.[20,22]

Direction 1	Direction 2	Angle between directions (degrees)
<001>	<001> <100> <101> <111>	0 90 61.4 (118.6) 68.9 (111.1)
<100>	<100> <101> <111>	0, 90 28.6 (151.4), 90 48.7 (131.3)
<101>	<101> <111>	0, 57.2 (122.8), 76.7 (103.3) 41.3 (138.7), 66.0 (114.0)
<111>	<111>	0, 82.6 (97.4), 42.2 (137.8)

Table 4.4. Results from eight kinks obtained from six different whiskers.

Segment 1	Segment 2	Segment 3	Measured Kink Angle (degrees)	Calculated Angle (degrees)	Method
<111>	<100>		48.9	48.7	In-situ
<001>	<101>	<001>	60.1, 60.1	61.4	In-situ
	<101>	<101>	77.7	76.7	In-situ
<001>	<111>	<001>	68.8, 68.8	68.9	extracted
<001>	<101>		61.8	61.4	extracted
<101>	<100>		26.2	28.6	In-situ

4.4.4 Summary

Figure 4.14 summarizes the known whisker parameters based on the crystallographic analyses presented above. First, the whisker growth axes for both straight and kinked whiskers have been determined. Second, by employing matrix rotation operations [1], the orientation normal to the substrate, the so-called parent grain orientation, has been determined for many whiskers. These parent grain orientations may be important relative to the texture of the film. However, at least for weakly textured films, no simple correlation was found between whisker crystallographic types and the parent grain orientation. This lack of correlation implies that whiskers can grow in many physical growth angles with respect to the substrate (Fig. 4.9). In general, whiskers grow from grains that are not oriented in the major texture component. Third, through simple inspection of the orientation matrix (not discussed in this paper), the direction normal to the whisker can also be determined. This direction is shown schematically in Fig. 4.14 extending to grain boundary B at the base of a whisker. Fourth, both the growth angle with the substrate as well as the kink angles have been determined through SEM techniques.[23] The whisker growth angles were discussed in Fig. 4.9, the technique for measuring kink angles was also discussed above, and the kink angle data was compiled in Table 4.4.

It is difficult to obtain other information about the surrounding grains by external analysis -- without FIB cuts through the whisker base. As shown in red in Fig. 4.14, to further understand the whisker growth process, it will be necessary to characterize the surrounding grains and, in particular, the grain boundaries at the whisker base. Combined FIB/EBSD techniques are currently being developed to investigate these unknown microstructural parameters.

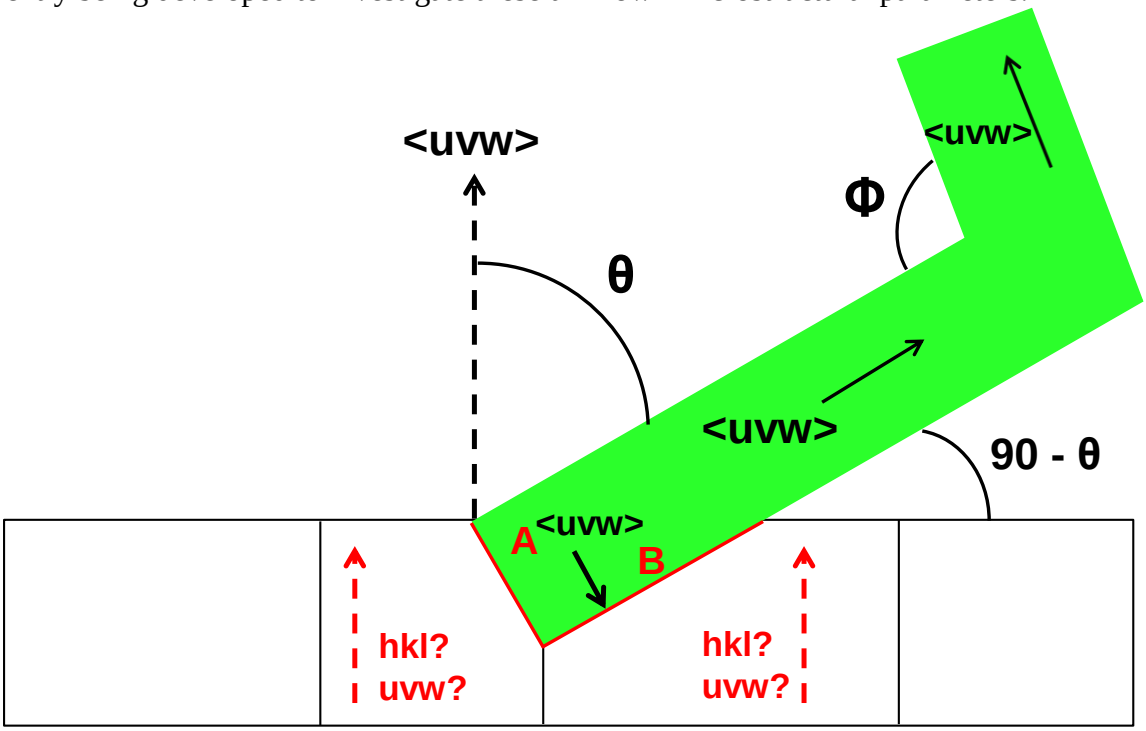

Figure 4.14. Schematic diagram of the various parameters obtained through SEM/EBSD analyses. The crystallography of the grain boundaries and surrounding grains, shown in red, have not yet been determined.

4.5 CONCLUSIONS

Based on SEM/EBSD techniques, the crystallography of straight and kinked whiskers has been determined. In all, approximately 150 whiskers were analyzed and the following conclusions were compiled.

1. The whisker growth axes for both straight and kinked whiskers have been determined. For the whiskers in this study, the prevalence of whisker growth directions was: <001>, <100>, <101>, and <111>. Only two <110> whiskers were found along with a few <321> and <012> whiskers.

2. By performing a rotation of the orientation matrix, the crystallographic direction normal to the substrate (parent grain orientation) has been determined for many whiskers. For the weakly textured films in this study, no simple correlation was found between whisker crystallographic types and the parent grain orientation. This lack of correlation implies that whiskers can grow with many physical growth angles with respect to the substrate. There is no simple correlation between a whisker's crystallographic growth direction and its growth angle.

3. In general, whiskers grow from grains that are not oriented in the major texture component of the film. The effect of film texture on the distribution of whisker types requires further study.

4. For kinked whiskers, both the growth angle with the substrate as well as the kink angles have been determined through SEM/EBSD techniques.[23] The kink angles correspond to the angles between directions in the Sn lattice. In this study, most kinks were of the heterogeneous type, with whiskers kinking to a different crystallographic direction. More work is needed to determine the statistics of kink crystallography and kink types.

4.6 ACKNOWLEDGEMENTS

Special thanks to W.G. Yelton and Jamin Pillars for Sn plating expertise and thanks to Mark Reece for substrate preparation. Mark Rodriguez is acknowledged for XRD analysis and helpful discussions. Thanks also to Dr. T.E. Buchheit for careful review of the manuscript.

* Sandia National Laboratories is a multi-program laboratory managed and operated by Sandia Corporation, a wholly owned subsidiary of Lockheed Martin Corporation, for the U.S. Department of Energy's National Nuclear Security Administration.

4.7 REFERENCES

[1] J.R. Michael, B.B. McKenzie, and D.F. Susan, *Microscopy and Microanalysis, Vol. 17, Suppl. 2*, pp 392-393, Cambridge University Press, 2011.
[2] NASA Goddard Space Flight Center Tin Whisker Homepage, website http://nepp.nasa.gov/whisker/
[3] R.G. Treuting and S.M. Arnold, *Acta Met.*, Vol. 5, pg. 598, 1957.
[4] H.G. Smith and R.E. Rundle, *J. Appl. Phys.*, 29, (4), pp 679-683, 1958.
[5] W.C. Ellis, D.F. Gibbons, and R.G. Treuting, Growth and Perfection of Crystals, John Wiley and Sons, New York, pg. 102, 1958.
[6] Powell and Skove, 1963
[7] W.C. Ellis, *Trans. Met. Soc. AIME*, Vol. 236, pp 872-875, 1966.
[8] W.C. Ellis, *J. Cryst. Crystall.*, Vol. 1, pp 204-206, 1967.
[9] R.B. Morris and W. Bonfield, *Scripta Met.*, Vol. 8, pp 231-236, 1974.
[10] B.-Z. Lee and D.N. Lee, *Acta Mat.*, 46, (10), pp 3701-3714, 1998.
[11] George T.T. Sheng, C.F. Hu, W.J. Choi, K.N. Tu, Y.Y. Bong, and Luu Nguyen, *J Appl. Phys.*, 92, (1), pp 64-69, 2002.
[12] W.J.Choi, T.Y. Lee, K.N. Tu, N. Tamura, R.S. Celestre, A.A. MacDowell, Y.Y. Bong, and Luu Nguyen, *Acta Mat.*, Vol. 51, pp 6253-6261, 2003.
[13] J.B. Lebret and M.G. Norton, *J. Mater. Res.*, 18, (3), pp 585-593, 2003.
[14] B. Hutchinson, J. Oliver, M. Nylen, and J. Hagstrom, *Mat. Sci. Forum*, Vols. 467-470, pp 465-470, 2004.
[15] A. Frye, G.T. Galyon, and L. Palmer, *IEEE Trans. Elec. Pack. Manuf.*, 30, (1), pp 2-10, 2007.
[16] T.-C. Chiu and K.-L. Lin, *Scripta Mat.*, Vol. 60, pp 1121-1124, 2009.
[17] J. Cheng, S. Chen, P.T. Vianco, and James C.M. Li, *J Appl. Phys.*, Vol. 107, 074902, 2010.
[18] G.T. Galyon, *IEEE Trans. Elec. Pack. Manuf.*, 28, (1), pp 94-122, 2005.
[19] P.W. Levy and O.F. Kammerer, *J. Appl. Phys.*, Vol. 26, pp 1182-1183, 1955.
[20] G.S. Baker, *Acta Met.*, Vol. 5, pp 353-357, 1957.
[21] N. Furuta, *Japan J. Appl. Phys.*, Vol. 4, pp 155-156, 1965.
[22] D. McKie and C. McKie, Essentials of Crystallography, Blackwell Scientific, Oxford, UK, pp 137-159, 1986.
[23] D.F. Susan, J.R. Michael, R.P. Grant, B.B. McKenzie, and W.G. Yelton, *Met. Mat. Trans. A*, to be submitted.
[24] P. Sarobol, A.E. Pedigo, P. Su, J.E. Blendell, and C.A. Handwerker, *IEEE Trans. Elect. Pack. Manuf.*, 33, (3), pp 159-164, 2010.
[25] D.F. Susan, J.R. Michael, R.P. Grant, and W.G. Yelton, *Microscopy and Microanalysis, Vol. 16, Suppl. 2*, pp 792-793, Cambridge Univ. Press, 2010.

5.0 SUMMARY, IMPLICATIONS, AND CURRENT RESEARCH

This report briefly summarized the process for plating our Sn films on Cu substrates. The bulk of the report then focused on characterization of Sn whiskers, techniques for evaluating whisker crystallography, and a detailed summary of the crystallography of many whiskers. The crystallographic results lead to the following implications and follow-on research.

Most importantly, the whisker growth process is complex in terms of the possible crystallographic growth directions, the physical growth angles, and the crystallography of the grains from which the whiskers grow. This complexity implies that it is likely not possible to suppress all whiskers by manipulation of the crystallography of the Sn film (as was hoped). However, there are classes of whiskers that *could* be suppressed by crystallographic engineering of the film. One example is the deposition of a very highly textured <100> or <110> film, either of which would suppress the formation of <001> whiskers, oriented 90 degrees from the main texture, i.e. within the film plane. Along these lines, single crystal Sn samples were recently purchased. By depositing Sn films on Sn substrates with preferred orientation, the objective is to control the crystallographic growth direction of the Sn film. Depositing Sn on Sn also removes the complicating Cu_6Sn_5 layer and removes any stresses due to mismatch of the Sn film lattice and the substrate structure. While these multiple changes make the system simpler, they may also make it more difficult to compare the results to the present work. It is anticipated that by controlling the crystallography of the Sn film, whiskers can be suppressed. Even if whiskers grow, it will be interesting if a different distribution of whisker crystallography is produced for these orientation-controlled films. To date, work has progressed on developing the parameters for depositing Sn on Sn substrates. Other methods of manipulating Sn film crystallography, including changing plating parameters (discussed previously) or the use of different Cu substrates (see Appendix A) are being investigated.

In addition to controlling Sn film crystallography, other work has progressed on manipulating the microstructure of the film. As shown in this report, the Sn films grow with a columnar structure with vertical grain boundaries extending from the film surface to the substrate. This microstructure, coupled with the compressive stresses within the film, can results in Sn whisker growth. By manipulating the Sn plating process, it is possible to alter the microstructure as well. Specifically, studies in Dept. 1725 have focused on pulse plating. Pulse plating typically produces a laminar morphology of fine grains. This layered morphology, with many grain boundaries oriented parallel to the film plane, is thought to be able to accommodate stresses better than the typical columnar Sn morphology. So far, pulse plating results have been promising as no whiskers have been observed in these samples. Again, it is difficult to determine at this point whether the whisker suppression is due to the morphology alone or if it is due to a change in the Sn crystallography or a change in stress within the coatings, or a combination of these. More work will continue on pulse-plating of Sn films. While pulse plating is important from a research standpoint, it may not be the most favorable approach for commercial plating applications because of the lower plating efficiency -- due to the “off time” of the pulsed deposition.

Finally, new techniques are being developed for characterization of Sn whiskers. Focused ion beam (FIB) cross-sectioning of whiskers was touched upon only briefly in this report. Several

FIB cuts have been performed to characterize the morphology of the Sn layer and the Cu_6Sn_5 interfacial layer. These FIB studies have included FIB serial sectioning as well, which allows for detailed understanding of the microstructure in-depth through the base of the whisker, as well as changes in the surrounding grains. A recent new capability in Org. 1800 is simultaneous FIB cross-sectioning with EBSD (and EDS) analysis. This new capability allows for detailed characterization of the morphology *and crystallography of the whisker as well as the surrounding grains*. The crystallography of the surrounding grains and grain boundaries remains unknown, as discussed in Section 4.4.4. The data obtained from this technique can be used to reconstruct a *three-dimensional view* of the microstructure and the crystallographic information. This powerful technique has already been applied to several straight and kinked whiskers and work will continue in this area in the future.

APPENDIX A: BRIEF DISCUSSION OF XRD RESULTS

A significant amount of X-ray diffraction analysis was performed on Sn-whisker samples as part of this LDRD research. This appendix will highlight examples of this work. The XRD results from sample 56 will be shown. Qualitatively similar results were obtained for Sample 67 as well. The EBSD results were shown in Figs. 4.6 and 4.8 within the report. The main objective here is to compare the crystallographic textures of the Sn films obtained from XRD with those obtained through EBSD, as outlined in Section 4 of the report.

There are other additional results from XRD that are important for understanding our particular system: Sn on Cu with a Cu_6Sn_5 intermetallic layer at the interface. For example, the underlying texture of the Cu substrate was determined. This information, in turn, can be used to investigate the orientation of the Sn grains relative to the Cu substrate grains. Some templating effects will be shown below, i.e., Sn grains with a certain orientation growing off of Cu grains with a certain orientation.

Figure A.1 shows the XRD spectrum from sample #56. Three phases were identified: Cu, Sn, and Cu_6Sn_5. Note that only one small peak can be definitively identified from the Cu_6Sn_5 phase in this sample. Other Cu_6Sn_5 peaks are overlapped behind other Cu or Sn peaks. The largest diffraction peak is from the Cu substrate material. The Cu substrate displays a preferred (200) orientation (out-of-plane texture). Note that this would correspond to the (100) plane for EBSD analysis. This texture is a result of the Cu sheet manufacturing process.

The second largest peak in the spectrum corresponds to the (220) orientation of Sn grains, indicating that the Sn film has a (220) out-of-plane texture, equivalent to (110) obtained by EBSD. Note that a randomly oriented Sn sample (powder diffraction sample) would show the following peaks in decreasing intensity: (200), (101), (211). So the presence of the large (220) Sn peak indicates that there is definitely a preferred orientation within the film. The results are consistent with those obtained by EBSD, which showed a (110) out-of-plane texture (Figure 4.6 in the report). The agreement between the two techniques shows that either method can be used to obtain the overall texture of the Sn film.

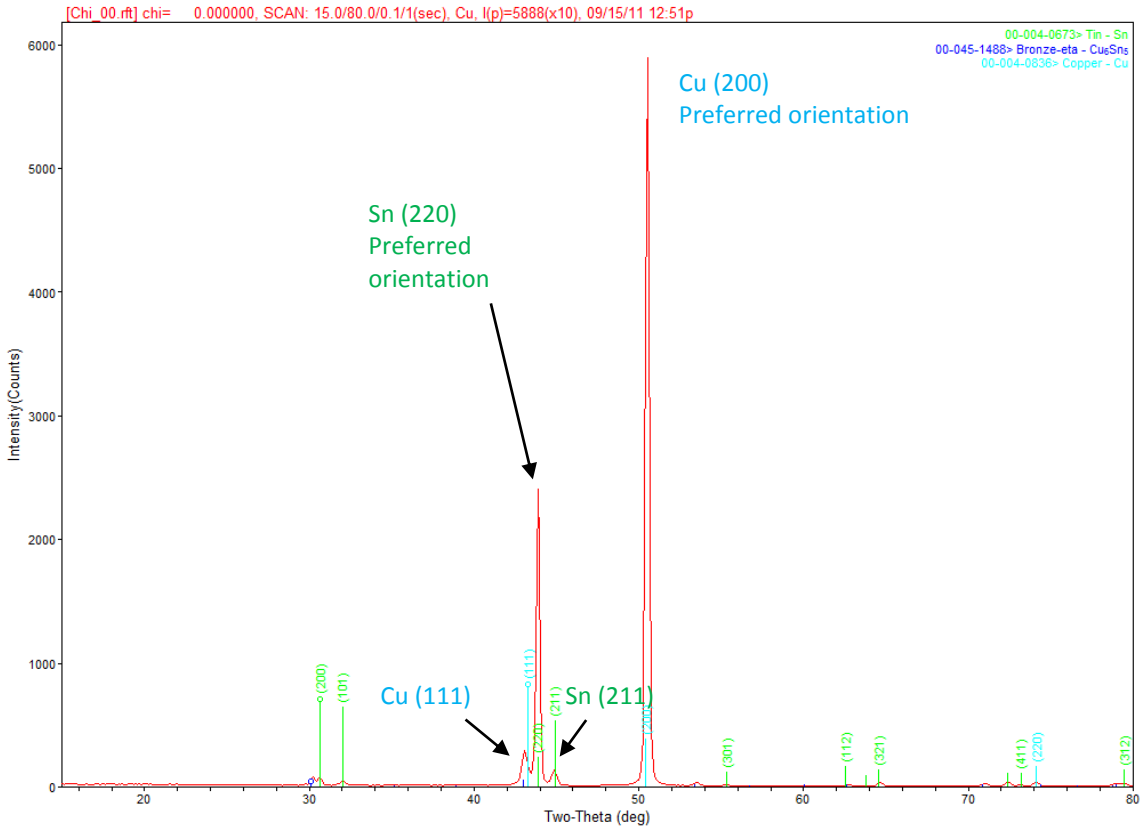

Figure A.1. XRD spectrum obtained from Sn plated Cu sample #56. The (220) preferred orientation of the Sn film agrees with the EBSD results in Figure 4.6 within the report ((110) EBSD orientation).

Other information can be obtained from the XRD analysis. Figure A.2 display the copper (200), (220), and (111) pole figures obtained by XRD. The Cu (200) pole figure shows a central spot, as expected, corresponding to the (200) out-of-plane texture discussed above in Figure A.1. The Cu (220) pole figure shows intensity spots located at a χ (chi) angle of 45° degrees from the center of the figure. This adds additional evidence for the out-of-plane (200) texture. The presence of four lobes in the Cu (220) pole figure indicates that there is also a biaxial in-plane texture within the Cu substrate. The Cu (111) pole figure shows similar lobes, again indicating a biaxial in-plane texture. The (111) intensity spots are located 45° in Φ relative to the (220) intensity spots.

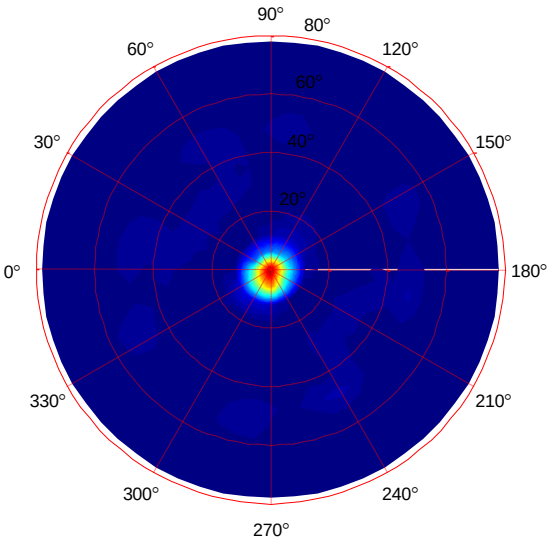

Linear data pole figure for 2-θ Angles 49.8 to 51.3 degrees.

Cu (200)

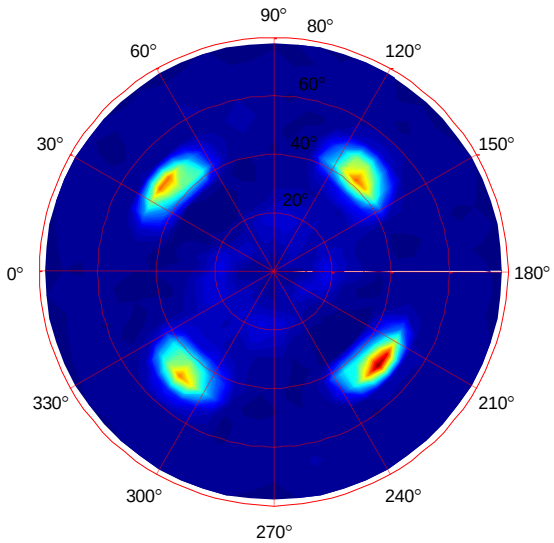

Linear data pole figure for 2-θ Angles 73.8 to 74.8 degrees.

Cu (220)

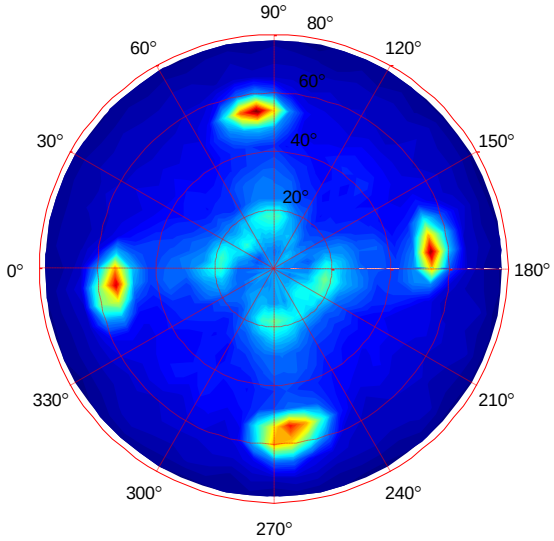

Linear data pole figure for 2-θ Angles 42.5 to 43.6 degrees.

Cu (111)

Figure A.2. Copper pole figures obtained from XRD analysis of the substrate. The pole figures indicate a (200) out-of-plane texture and a biaxial in-plane texture within the copper substrate.

A similar pole figure analysis was performed for the Sn film XRD data. Figure A.3 shows the Sn (220) pole figure with a central intensity spot corresponding to the main Sn peak discussed in Fig. A.1 above. The Sn film also shows an in-plane biaxial texture as shown by the Sn (200) and Sn (301) pole figures. (Note the (301) pole corresponds to the ~ <101> direction in Sn.)

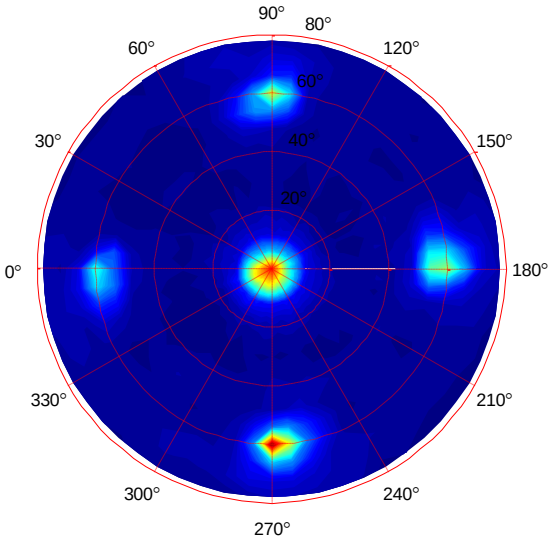

Linear data pole figure for 2-θ Angles 43.7 to 44.6 degrees.

Sn (220)

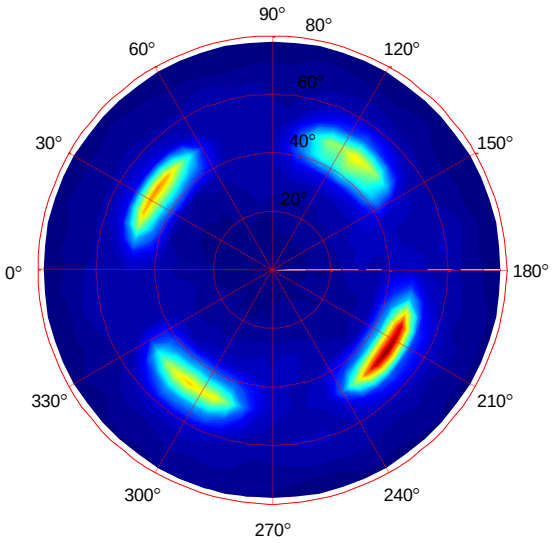

Linear data pole figure for 2-θ Angles 30.5 to 31.4 degrees.

Sn (200)

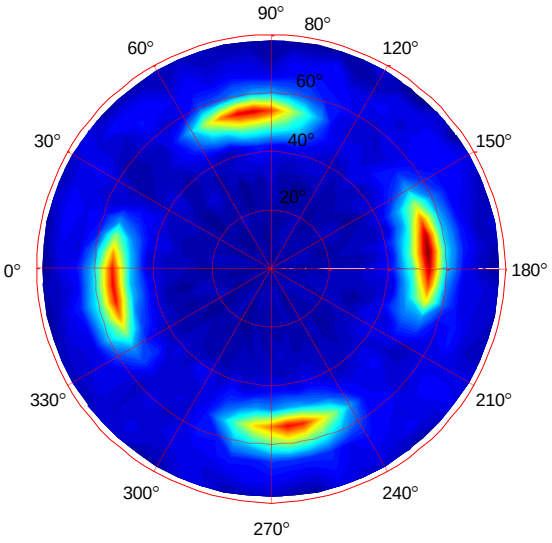

Linear data pole figure for 2-θ Angles 55 to 56.3 degrees.

Sn (301)

Figure A.3. Sn pole figures obtained from XRD analysis of the Sn film. The pole figures indicate a (220) out-of-plane texture and a biaxial in-plane texture within the Sn film.

The information in Figs. A.2 and A.3 can be combined to indicate that the Sn film is templating off of the Cu substrate. Figure A.4 shows the Cu (220) and the Sn (200) pole figures. Both pole figures show the biaxial in-plane texture as discussed above. The intensity lobes are located at approximately the same Φ angles suggesting this templating effect. Based on the pole figure analysis, the schematic diagram shows how the Sn (200) planes template off of the Cu (220)

planes of the Cu lattice. The orientation of the Sn lattice also confirms the significant out-of-plane orientation of the Sn (220) planes as discussed with Fig. A.1. The relatively strong preferred orientation of the Cu substrate likely encourages this biaxial alignment and templating of the Sn film. The schematic diagram also suggests that the c-axis of the Sn (<001>) lattice is forced to reside in the plane of the film. This would be a favorable orientation for suppression of <001> whiskers. However, as discussed within the report, the <110> out-of-plane (and hence, <001> in plane) texture is weak so there are many grains for which the <001> direction is not contained within the plane of the film. The Sn (301) pole figure is also shown in Fig. A.4 with its respective plane (light green) cutting through the Sn lattice to confirm the grain alignment and relative orientations.

The results from XRD analysis indicate that the Cu substrate could be influencing the Sn film growth. This seems to be the case for both samples 56 and 67 which showed weak (220) out-of-plane (<110> from EBSD) textures. It is possible that an annealing treatment could be performed on the Cu substrate to remove or change the crystallographic texture of the substrate. It is unknown how this might influence the Sn film growth. The application of substrate heat treatments or the use of other substrate materials to influence Sn film growth is part of on-going research on Sn whiskers. It should be noted that the major influence on Sn film crystallographic texture appears to be the electroplating parameters used to deposit the Sn. Changing the plating parameters produced several different textures (not shown here). However, the Cu substrate can also have an influence, as shown above, at least for the plating conditions employed for these particular samples.

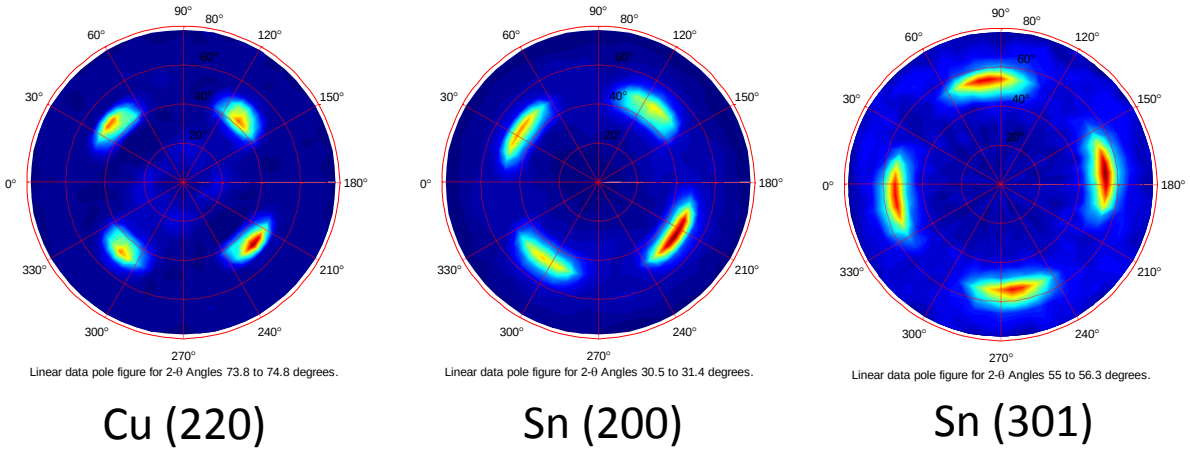

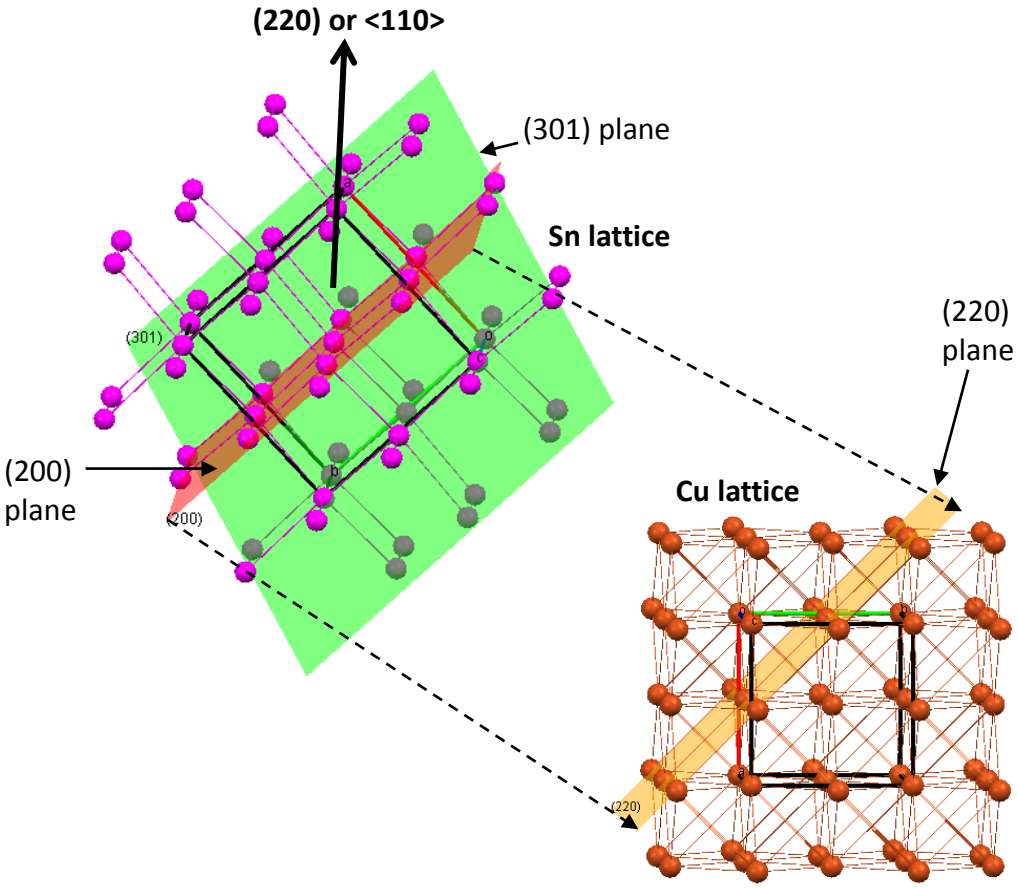

Figure A.4. (top) Cu and Sn pole figures indicating possible templating of Sn (200) off of the substrate Cu (220) planes. (bottom) Schematic diagram of the configuration of the Sn lattice templating off of the Cu substrate.

APPENDIX B: RECENT SANDIA PUBLICATIONS AND PRESENTATIONS ON Sn WHISKERS

1. J.R. Michael, B.B. McKenzie, and D.F. Susan, "Application of Electron Backscatter Diffraction to the Crystallographic Characterization of Whiskers", submitted *Microscopy and Microanalysis, 2011*.

2. D.F. Susan, J.R. Michael, R.P. Grant, B.B. McKenzie, and W.G. Yelton, "Morphology and Growth Kinetics of Straight and Kinked Sn Whiskers", to be submitted *Metallurgical and Materials Transactions A*.

3. J.R. Michael, D.F. Susan, and B.B. McKenzie, "The Crystallography of Sn Whiskers", to be submitted *Acta Materialia*.

4. J.R. Michael, D.F. Susan, and B.B. McKenzie, "2D and 3D EBSD Characterization of Tin Whiskers", *10th Asia-Pacific Microscopy Conference (APMC)*, Perth, Australia, Feb. 2012.

5. D.F. Susan, P.T. Vianco, W.G. Yelton, and J.R. Michael, "Recent Tin Whisker Research at Sandia*", 5th International Brazing and Soldering Conference (IBSC)*, April 2012, Las Vegas, NV.

6. J.R. Michael, B.B. McKenzie, and D.F. Susan, "Crystallographic Characterization of Whiskers Using EBSD", M&M 2011 Nashville, TN, published in *Microscopy and Microanalysis*, Vol. 17, Suppl. 2, pp 392-393, 2011, Cambridge University Press.

7. D.F. Susan, J.R. Michael, R.P. Grant, and W.G. Yelton, "Tin Whiskers: Electron Microscopy and EBSD Characterization", M&M 2010 Portland, OR, published in *Microscopy and Microanalysis*, Vol. 16, Suppl. 2, pp 792-793, 2010, Cambridge University Press.

8. J.R. Michael, B.B. McKenzie, and D.F. Susan, "Crystallographic Analysis of Tin Whiskers with SEM/EBSD", presented at *5th Annual Sn Whisker Symposium*, Univ. of Maryland, College Park, MD, Sept. 2011.

9. W.G. Yelton, D.F. Susan, J.R. Michael, P.T. Vianco, and J.R. Pillars, "Controlling Direction of Strain Energy Driving Forces Responsible for Whisker Growth, presented at *5th Annual Sn Whisker Symposium*, Univ. of Maryland, College Park, MD, Sept. 2011.

10. D.F. Susan, J.R. Michael, Edmund Webb III, R.P. Grant, B.B. McKenzie, and W.G. Yelton, "SEM Observation and EBSD Analysis of Straight and Kinked Sn Whiskers", presented at *4th Annual Sn Whisker Symposium*, Univ. of Maryland, College Park, MD, June 2010.

11. P.T. Vianco and J.A. Rejent, “Dynamic Recrystallization (DRX) as the Mechanism for Sn Whisker Development: Model and Experiments”, presented at *4th Annual Sn Whisker Symposium*, Univ. of Maryland, College Park, MD, June 2010.

12. W.G. Yelton, D.F. Susan, J.R. Michael, and Daniel Shore, “Understanding and Predicting Metallic Whisker Growth as a Function of Electrodeposited Morphology”, *217th Electrochemical Society Meeting*, Vancouver, Canada, April 2010.

13. J. Cheng, S. Chen, P.T. Vianco, and J.C.M. Li, “Quantitative Analysis for Hillocks Grown from Electroplated Sn Film”, *J. Applied Physics*, Vol. 107, pp 107-110, 2010.

14. P.T. Vianco and J.A. Rejent, “Dynamic Recrystallization (DRX) as the Mechanism for Sn Whisker Development. Part I: A Model”, *J. Electronic Materials*, Vol. 38, (9), pp 1815-1825, 2009.

15. P.T. Vianco and J.A. Rejent, “Dynamic Recrystallization (DRX) as the Mechanism for Sn Whisker Development. Part II: Experimental Study”, *J. Electronic Materials*, Vol. 38, (9), pp 1826-1837, 2009.

DISTRIBUTION

3	MS0886	D.F. Susan	1831 (Hard copy)
1	MS0886	J.R. Michael	1822 (Hard copy)
1	MS0886	B.B. McKenzie	1822 (Hard copy)
1	MS0886	R.P. Grant	1822 (Hard copy)
1	MS1425	W.G. Yelton	1725 (Hard copy)
1	MS1425	J.R. Pillars	1725 (Hard copy)
1	MS1411	M.A. Rodriguez	1822 (Hard copy)
1	MS0886	A.C. Kilgo	1822
1	MS0886	P.G. Kotula	1822
1	MS0889	S.J. Glass	1825
1	MS0959	D. Hirschfeld	1831
1	MS0889	M. Reece	1831
1	MS0889	C.V. Robino	1831
1	MS0889	P.T. Vianco	1831
1	MS0889	T.E. Buchheit	1814
1	MS0886	M.J. Rye	1822
1	MS0886	G.L. Bryant	1822
1	MS0886	L. Deibler	1822
1	MS1425	S.J. Limmer	1725
1	MS0885	M.F. Smith	1830
1	MS0869	P.H. Gorman	2732
1	MS0965	S.E. Garrett	5761
1	MS1425	L.E. Rohwer	1718
1	MS0888	E.M. Russick	1821
1	MS0889	J.A. Rejent	1831
1	MS0889	M.J. Grazier	1831
1	MS0888	L.M. Serna	1825
1	MS0889	N.R. Sorensen	1825
1	MS0889	Z. Ghanbari	1831
1	MS0899	RIM-Reports Management	9532 (electronic copy)
1	MS0359	D. Chavez, LDRD Office	1911

EXTERNAL DISTRIBUTION

1	E.B. Webb III	Lehigh University (electronic copy)
1	C.A. Handwerker	Purdue University (electronic copy)
1	L. Panashchenko	Univ. Maryland (electronic copy)

Sandia National Laboratories